



Thermal modeling of petroleum source rocks

Master Thesis

Presented to the School of Mineral Resources Engineering

Technical University of Crete

For the partial fulfilment of the requirements of the degree

Petroleum Engineering Master

By Koketso Ludwig

Supervisor: Professor Nikos Pasadakis

Abstract

Development of basin modeling programs began in the 1980s, initially by building just 1D models, with the main aim of heat flow simulation. Later model upgrades incorporated geochemical models enabling basin temperature history to be calculated and allowing source rock maturity evaluation. The models have since evolved to model up to 3D level or 4D if the time dimension is considered. Simulation of the maturation of kerogen is no easy task as the reactions formed from the thermal maturation of kerogen are complex and cannot easily be defined. Workers keep formulating new and improved kinetic models ever since the publication of the Lopatin (TTI method) in order to closer mimic the chemical reactions involved in kerogen degradation. As such there are several kinetic models available to-date to choose from. The aim of this study is to follow the processes and parameters involved in modeling the maturation of organic matter in source rocks.

This work includes a case study to scrutinize the hydrocarbon potential of the hypothetical F_well (.) petroleum system source rocks and related processes. This was carried out using the PetroMod (1D) version 2017.1 software. There is limited geological knowledge of the petroleum system except for the well log data and some inferred information on the erosional history and thrusting in the regional area of where the well was drilled. Measured values of vitrinite reflectance as well as vitrinite reflectance values calculated from Tmax (from pyrolysis data) were used to validate the model. The Easy%Ro as is default in the PetroMod version 2017.1 was applied for vitrinite reflectance calculations. Pepper and Corvi, (1995) model was chosen to calculate the kinetics. Geochemical analysis of the pyrolysis data from Rock_Eval measurements revealed the Layer 4 and Layer 5 sediments of the F_well (.) petroleum system have type II, type II/III and type III kerogens, and the TOC (%) range of the source rocks is from 0.19-3.83 with an average of 1.35% indicating poor to fair source rocks. The geochemical analysis allows better appropriation of petroleum system elements (at least the source rocks) in the PetroMod software. The combined effects of the burial and thermal history conditions were evaluated and the petroleum potential of the sediments surrounding F-well was calculated.

Μοντελοποίηση της της δημιουργίας πετρελαίουσεμητρικούςσηματισμούς – η επίδραση της θερμοκρασίας

Περίληψη

Η ανάπτυξη λογισμικού προσομοίωσης λεκανών δημιουργίας πετρελαίου ξεκίνησε τη δεκαετία του 1980, με στόχο κυρίως την περιγραφή των ροών θερμότητας σε μία διάσταση (1D). Στη συνέχεια αναπτύχθηκαν με την εισαγωγή γεωχημικών δεδομένων και χρησιμοποιήθηκαν για την περιγραφή της θερμικής ιστορίας των σχηματισμών και την αποτίμηση του βαθμού ωριμότητας του κηρογόνου. Σήμερα χρησιμοποιούνται μοντέλα τριών διαστάσεων (3D) ή και τεσσάρων (4D) με ενσωμάτωση και του χρόνου. Η προσομοίωση της ωρίμανσης του κηρογόνου αποτελεί και σήμερα ένα δύσκολο πρόβλημα δεδομένου ότι οι αντιδράσεις που λαμβάνουν χώρα είναι πολυάριθμες και εν πολλοίς μη περιγράψιμες. Η έρευνα στην κατεύθυνση αυτή ξεκίνησε από το γνωστό μοντέλο Lopatin (TTI) και συνεχίζεται με την δημιουργία νέων κινητικών μοντέλων των αντιδράσεων ωρίμανσης του κηρογόνου.

Η παρούσα εργασία εστιάζει στην μελέτη των διεργασιών και των παραμέτρων που υπεισέρχονται στην μοντελοποίηση της διαδικασίας ωρίμανσης της οργανικής ύλης σε μητρικούς σχηματισμούς πετρελαίου. Στην εργασία παρουσιάζεται η μοντελοποίηση της δημιουργίας πετρελαίου με βάση τα δεδομένα μίας υποθετικής γεώτρησης F_well. Η προσομοίωση πραγματοποιήθηκε χρησιμοποιώντας το εξειδικευμένο λογισμικό PetroMod 2017.1. Τα γεωλογικά δεδομένα του μοντέλου αντλήθηκαν από την βιβλιογραφία μίας συγκεκριμένης περιοχής και συμπληρώθηκαν με υποθετικά στοιχεία που αφορούν την διάβρωση των στρωμάτων. Για την βαθμονόμηση και έλεγχο του μοντέλου χρησιμοποιήθηκαν πειραματικές τιμές του δείκτη ανάκλασης του βιτρινίτη αλλά και τιμές που υπολογίστηκαν από τις θερμοκρασίες T_{max} , σε σχέση με τις τιμές που προκύπτουν από την μέθοδο Easy%Ro. Ως κινητικό μοντέλο χρησιμοποιήθηκε το Perrier and Corvi (1995). Η γεωχημική ανάλυση των στοιχείων πυρόλυσης από τις μετρήσεις Rock Eval έδειξε ότι το στρώμα ιζήματος 4 και 5 του σχηματισμού πετρελαίου F.Well έχουν τύπο κηρογόνου II, II/III και τύπο III, και το εύρος TOC (%) των πετρωμάτων είναι από 0.19-3.83 με μέσο όρο 1.35% που υποδεικνύει κακά (poor) έως μέτρια (fair) πετρώματα. Από την αξιολόγηση της επίδρασης της ιστορίας δημιουργίας των σχηματισμών αυτών (burialhistory) και της θερμικής διαδρομής τους (thermalhistory) υπολογίστηκε το πετρελαϊκό δυναμικό των σχηματισμών αυτών.

Table of Contents

Πίνακας περιεχομένων

1.0 Introduction	1
2.0 Developing a model.....	3
2.2 Burial History.....	4
2.3 Thermal History.....	13
3.0 Identification of Source Rock.....	27
4.0 Kinetics	40
5.0 Modeling in PetroMod	59
The F_well Petroleum System Case Study.....	75
6.0 Results Section	75
6.1 Analysis of vitrinite reflectance and pyrolysis data	75
Analysing Rock Eval Pyrolysis Data	76
6.2 Modeling F_well (.) Petroluem system in PetroMod 1-D	90
Model validation-Ro data	90
Geological constraints	91
Model Inputs	92
Model results	99
Conclusion.....	107
Recommendation	108
Acknowledgements.....	108
Appendices.....	109
References.....	113

List of Figures

Figure 2.1.1	5
Figure 2.1.2	7
Figure 2.1.3	9
Figure 2.1.4	12
Figure 2.3.1	21
Figure 2.3.2	26
Figure 3.1.1	28
Figure 3.1.2	29
Figure 3.1.3	32
Figure 3.2.1	35
Figure 3.2.2	38
Figure 3.2.3	39
Figure 4.2.1	45
Figure 4.2.2	46
Figure 4.2.3	48
Figure 4.3.1	52
Figure 4.3.2	54
Figure 4.3.3	56
Figure 4.3.4	58
Figure 5.1.1	60
Figure 5.1.2	66
Figure 5.1.3	69
Figure 5.1.4	70
Figure 6.1.1	76
Figure 6.1.2	77
Figure 6.1.3	78
Figure 6.1.4	78
Figure 6.1.5	79
Figure 6.1.6	80
Figure 6.1.7	81
Figure 6.1.8	82
Figure 6.1.9	83
Figure 6.1.10	84
Figure 6.1.11	86
Figure 6.1.12	87
Figure 6.1.13	90
Figure 6.2.1	93
Figure 6.2.2	94
Figure 6.2.3	95
Figure 6.2.4	100
Figure 6.2.5	102
Figure 6.2.6	103
Figure 6.2.7	103

Figure 6.2.8	105
Figure 6.2.9	106

List of Tables

Table 2.1.1 Some sediment accumulation rate examples	3
Table 2.3.1. Table shows some selected thermal conductivity values	16
Table 3.1.1 approximate equivalent names used to describe the organic matter types	30
Table 3.1.2 Geochemical parameters describing the petroleum potential quality	31
Table 3.1.3 Geochemical parameters that describe the approximate quality of immature source rocks	31
Table 3.1.4 geochemical parameters that describe the level of thermal maturation	31
Table 3.1.5 Division of thermal maturity modelling into thermal indicators and hydrocarbons	34
Table 3.2.1. Example data (after Waples, 1984) showing Ro% values	36
Table 5.1.1. Capabilities and required data for creating a 1D model	60
Table 5.1.2. Time, Equipment and Personal requirements	64
Table 5.1.3 Results that can be obtained from Petrorisk	74
Table 6.1.1 Vitrinite reflectance as a maturity Indicator	80
Table 6.2.1 Lithotype conductivities	91
Table 6.2.2 The values approximating the prevailing heat flow trend over time.	95
Table 6.2.3 shows the resulting differences that can be incurred when from a particular choice of models ..	97
Table 6.2.4 The resulting effects of erosion events presence or absence on changes to thermal maturity results	98
Table 6.2.5 Salt piercing for the F_well Petroleum system	99
Table 6.2.6 Lists the hydrocarbon balances for the two scenarios, no thrust and thrust model	104

1.0 Introduction

Progressively intensifying research into organic geochemistry started in the 1960s tied to a need of a better understanding of the origins of petroleum especially by exploration companies. Once it had been established that petroleum originated from temperature- and time-induced transformation of organic matter contained in fine grained sedimentary rocks (carbonates and shales), there was still need to define its formation mechanism. Work carried out on defining petroleum source rocks led to the discovery of similarities between petroleum formation and the coalification process. From the coalification process scientists discovered that they could use the different levels of vitrinite reflectance with increasing burial depths to identify stages of coalification and maturation levels in the petroleum process. This led to the development of the van Krevelen diagram. The process of thermal cracking of the kerogen as temperatures rise during burial is mainly effected by temperature and time with some pressure effect (Hunt et al. 2002). Expulsion of petroleum and water from source rocks occurs aided by pressure gradients in the subsurface (Dembicki, 2016). Primary migration is a capillary pressure driven process of fluids in the small pores of sedimentary rocks. Secondary migration takes effect in micro-fractures induced by overpressures in low permeability rocks. The experiments carried out by (Dueppenbecker, 1991) on the Posidonia Oil shale rock mechanical behaviour concluded that expulsion of petroleum has a greater effect on the tendency of petroleum to concentrate in mature oil prone source rocks than its generation due to temperature.

The available geological assessment tools have limitations that disable their precision when assessing hydrocarbon generation and maturation processes. Seismic interpretation can delineate closed structures and identify potential subsurface traps, but it does not reliably predict trap content. A petroleum system comprises geologic elements and processes needed for oil and gas to accumulate. The elements include an effective source rock, reservoir, seal and overburden rock for burial of the elements. In order for a petroleum system to be viable or successful the elements and processes have to occur in the order that ensures conversion of organic matter in a source rock into petroleum that will be stored and preserved. Basin and petroleum system modeling is carried out to reduce the risk that is introduced by the uncertainties typical of oil and gas exploration and exploitation by firstly ascertaining if the requirements for generation and accumulation have occurred. By using mathematical algorithms basin modeling combines, manipulates and transforms geologic, geophysical, geochemical, hydrodynamic and thermodynamic data to simulate the interrelated effects of deposition and erosion of sediments and organic matter, compaction, pressure, heat flow, temperature effects, petroleum generation and multiphase fluid flow. The model geometry in basin modeling is dynamic throughout the simulation. Conversely, static geometry models dynamic flow in reservoir simulators.

The process of basin and petroleum system modelling is carried out in order to estimate the volume of hydrocarbons that can be generated by the available organic matter and assess the combined effects of the processes that lead to its expulsion, migration, entrapment and accumulation. The timing of the processes responsible is determined by assigning each layer in the basin and petroleum system model its absolute age in order (Al-Hajeri & Al Saeed, 2009). Basin modelling is also able to calculate the timing of hydrocarbon migration thus making it a very useful risk assessment tool for the exploration companies.

Basin modelling is done in order to achieve the best approximation of the real situation in the subsurface to aid interpretations for exploration purposes. This is a continuous process that allows additions of new data and updates on interpretation. Accuracy of interpretation is subject to geologic interpretation, equation manipulations, amount of data available, who is modelling the data and with which model. Compaction calculations allow for estimation of porosity depending on the lithology being compacted and the overburden. Incorporating the transport equation (Darcy's Law) allows accounting for phase flow in the permeable system from source rocks, through the drainage rocks to reservoir rocks where the hydrocarbons are stored and preserved. The model geometry during Basin and petroleum system modelling is dynamic through the millions of years being modelled (Makhous and Galushkin (2005), (Hantschel & Kauerauf, 2009), (Dembicki, 2016). The changes in depth and time affects heat conductivity, heat capacity, unfrozen water, salt content and porosity of rocks and these have an effect on modelling. Thermal history is also affected by surface temperatures thus requiring that the climate influences be considered. The burial history of a single point is modelled in a 1D model. Hydrocarbon generation is simulated in a two-dimensional model using maps or seismic sections. A three-dimensional model has the capability to rebuild petroleum systems at reservoir and basin scales. The results can then be displayed in 1D, 2D or 3D and through time. Considering the time dimension models 4D (Higley et al., 2006).

Development of Basin modelling programs began in the 1980s, initially by building just 1D models. Their main aim was heat flow simulation and then later geochemical models were incorporated enabling basin temperature history to be calculated and allowing source rock maturity evaluation. This model could only simulate single phase flow. A 1D model combines chemical kinetics equations, transport equations for single phase flow and calculations of pore fluid pressures, sedimentary compaction equations and temperature profile information. Compaction and porosity are used to calculate thermal conductivities to be used in heat flow calculations. In time improvements were made to the 1D concept to model migration of multiphase flow in a 2D system. This is a more complex simulation of the hydrocarbon generation, migration and accumulation along a cross section or a map allowing distribution of volumes along the reservoir-seal boundaries. The 3D model is the advancement to three phase fluid models capable of modelling horizontal petroleum migration in the third dimension representing the whole reservoir or basin. 3D models focus on

pressure and GOR predictions (Telnaes et al.2000). 3D models however have high computational and development requirements and their simplification yields oversimplified geometries. (Hantschel & Kauerauf, 2009) gives alternative means for modelling migration as flow path or ray path models, hybrid flow simulators and the invasion percolation method.

This work was carried out to follow the processes and mechanisms considered when modelling the thermal maturation processes of petroleum source rocks. A case study was carried out to model a hypothetical petroleum system in PetroMod 1D.

2.0 Developing a model

2.1 Introduction

Modeling petroleum generation requires time; a parameter that is given by geologic age, and temperature obtained from the geologic history of the section, (Barker, 1996). The combination of burial history and thermal history yields the temperature ranges over in time. Temperature is found through the use of the geothermal gradient combined with depth, or rock thickness combined with thermal conductivity and heat flow. Lithologies influence compaction rates, thermal conductivities and heat capacities. Unfortunately eroded lithologies can only be inferred or estimated to enter into the software thus introducing uncertainties (Waples in Magoon & Dow, 1994). The shorter the accumulation rate the longer the time span for the period over which the accumulation rate is being determined. Indications offered by short term rates cannot be relied on when assessing long term accumulation regimes (Sadler 1981 in (Barker, 1996). Estimating sedimentation rates from burial history plots of present day values after accounting for compaction produces reduced vertical thickness of the same interval. These values have to be uncompacted in order to be representative. The actual high rates obtained due to near surface sediment accumulation are regulated by lithology and degree of compaction. Some sediment accumulation rates recorded or suggested for some common rock types are shown in Table 2.1.1.

Table 2.1.1 Some sediment accumulation rate examples

Sediments types	Sediments Accumulation rates or comments
Poorly sorted clastic sequences and sands	have higher accumulation rates than clays
Pelagic sediments	Low; 25-45m/m.y
Carbonates	Extremely variable (an average of 1000m/m.y is suggested by Schalager 1981)

Evaporites	Range between 5-10000 m/m.y
------------	-----------------------------

Tectonic influences on the way basins fill must also be considered when estimating original rock thickness from present day thickness that will have reduced uncertainties. The rate of basin subsidence and availability of sediment supply from adjacent uplift and erosion are controlled by tectonics. According to Schwab (1976) in Barker, 1996) intracratonic basins accumulate sediments at 1-24 m/m.y and rates are much higher on plate margins.

2.2 Burial History

Introduction

Burial History simulates the sedimentation events as captured in a stratigraphic column. Important input data is obtained from well samples complimented by well logs, seismic data or outcrop data represented on a depth-time plot. Each segment of a burial history curve represents either deposition, erosion or a period of no deposition (hiatus). A sedimentation history chart or graph of sedimentation plotted against age is useful when constructing a burial history curve. It depicts thicknesses or their absence for every depositional event over an interval. The age in million years is labelled with zero on the right and plotting will start from the left. The last stratigraphic event (oldest) plots first in the sedimentation history plot. The burial history based on the stratigraphic column is then plotted moving towards the right, one depositional interval for each successive curve. Although this gives a profile of the sedimentation events in the stratigraphic column it is inaccurate, (Dembicki, 2016). Mechanical compaction and corrections must be done to represent the loss of porosity with increasing burial that results due to increasing amounts of overburden. The thicknesses of existing rock units specified by the modeler are present-day thicknesses after compaction. Original depositional thicknesses are greater than present-day thicknesses by an amount equal to the amount of porosity reduction due to compaction, (Waples In Magoon and Dow, 1994).

Constructing burial history curves

Shown in Figure 2.1.1(a) are 5 depositional events, for each thickness deposited over a certain period in time with 2 unconformities. The first unconformity is a depositional unconformity at 2000 ft, with a time gap from 2 to 3 MYBP. The second unconformity is an erosional unconformity at 6000 (ft), that has a time gap from 8 to 12 MYBP. From 12 to 10 MYBP, 2000 ft of sediment was deposited followed by 2000 ft of erosion from 10 to 8 MYBP. Figure 10 (b) shows how the sedimentation history is broken down to represent this stratigraphic column in a burial history.

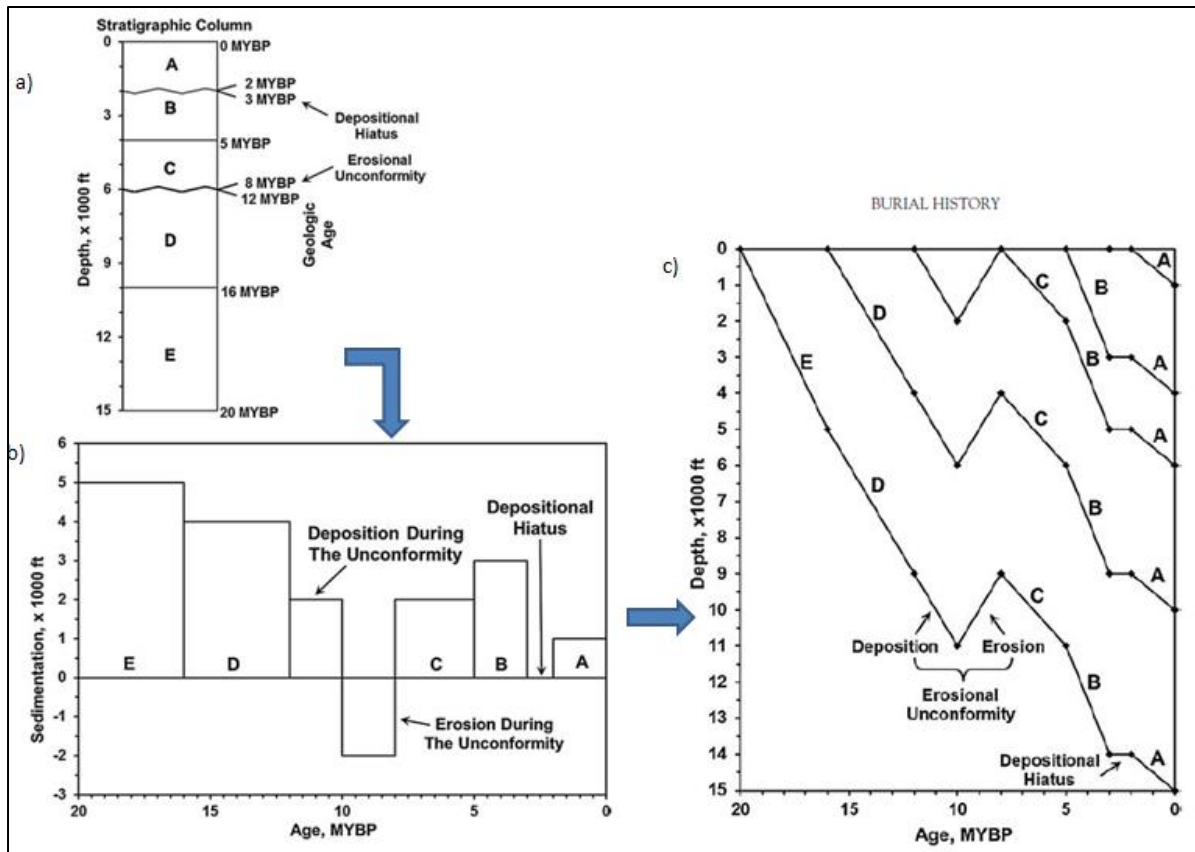


Figure 2.1.1 Edited from Hatchel and Kaurauf, (2006), a) is a hypothetical stratigraphic column containing both a depositional hiatus and an erosional unconformity to be used in the construction of a burial history. b) is a sedimentation history for the stratigraphic column shown in Fig. 8.1 to be used in the construction of a burial history. c) The burial history based on the stratigraphic column in (a) and the sedimentation history in (b).

Erosional events are negative sedimentation events and depositional hiatus events plot along the zero line. A burial history diagram is built from the left side of the sedimentation history plot and to the right, one step at a time. First, interval E is deposited at the 0 depth and 20 MYBP on the burial history diagram in (c). Interval E deposits 5000 ft of sediment in 4 million years with the burial history curve segment ending a depth of 5000 ft at 16 MYBP. Then 4000 ft of sediment in 4 million years was deposited in interval. The next interval of the burial history curve ends at a depth 9000 ft at 12 MYBP. The erosional unconformity occurs between intervals D and C. Deposition of 2000 ft of sediment occurs between 12 MYBP and 10 MYBP, so that the third segment of the burial history curve ends at a depth of 11,000 ft at 10 MYBP. Next follows the erosional phase of the unconformity that removed 2000 ft of sediment between 10 MYBP and 8 MYBP. It follows that the end of the fourth segment of the burial history curve goes to a depth of 9000 ft at 8 MYBP. Next is the deposition of intervals C and B so that the burial history curve arrives to 11,000 ft at 5 MYBP and 14,000 ft at 3 MYBP, respectively. Following the deposition of interval B, hiatus occurs between 3 and 2 MYBP. As such this interval of the burial history curve stays at 14,000 ft for this time period. At last interval A deposits 1000 ft of sediment between 2 MYBP and the present day thus completing the burial history curve at a depth of 15,000

ft at 0 MYBP. To draw the other burial history curves in (c), are drawn in a similar manner moving to the right one depositional interval for each successive curve. To account for compaction that occurs as more and more sediments are deposited atop already deposited layers, compaction corrections are carried out.

Compaction and erosion effects

The rock units have to be decompacted from the present day thickness so as to closely represent the original thickness of the units before they underwent burial by overlying units. Decompacted units are deeper and occur at higher temperatures and so petroleum generation would have commenced earlier. The oil window is shorter for deeper units as there is more temperature effect. The temperature increases exponentially with depth (Barker, 1996). The exponential model of Sclater and Christie (1980), the reciprocal model of Falvey and Middleton (1981) and the argillaceous sediment model of Butler and Baldwin (1985) are lithology dependent equations incorporated in the software to help predict changes in porosity in different lithologies (Waples in Magoon and Dow, (1994), and Dembicki, (2016)). The effects of decompaction are exhibited in Figure 2.1.2 (a & b). The respective equations are as follows;

The Exponential Model of Sclater and Christie;

$$\Phi = \varphi_o \exp(-bz) \quad (1)$$

The Reciprocal Model of Falvey and Middleton (1981);

$$1/\varphi = 1/\varphi_o + kz \quad (2)$$

and the Argillaceous Sediment of Baldwin and Butler (1985);

$$Z = (1 - \varphi)^b \quad (3)$$

where φ is porosity, z is depth and the constants are lithology dependent (**A**).

Also considered are the maturity dependent compaction equations as follows;

$$\varphi = A (TTI)^B, \quad \varphi = A (R_o)^B \quad (4)$$

and

$$\varphi = A (R_o) + B \quad (5)$$

TTI or **R_o** represent thermal maturity.

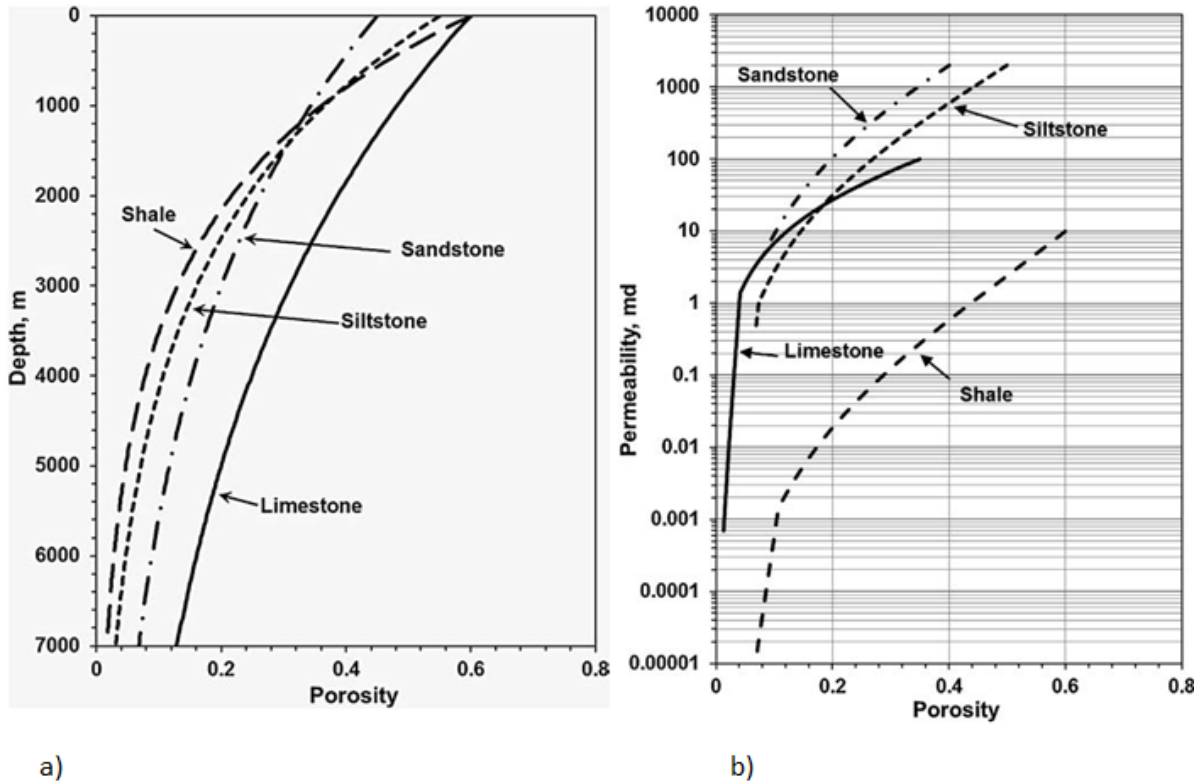


Figure 2.1.2 Depth versus porosity plot for a series of lithologies based on the Sclater and Christie (1980) exponential model using empirically determined initial porosities and compaction factors.

To correct for varying rates of compaction with burial in over-pressured zones the constants of the equations are reduced to give less compaction. Another way is to find porosity reduction as a function of effective stress (Waples in Magoon & Dow, 1994). To account for under-compaction in over-pressured zones by the effective stress approach, the rate of porosity reduction is directly carried out. The effective stress method is not applicable in one dimensional modeling because it requires significant vertical fluid flow (Schneider et al. 1993 in Magoon & Dow, 1994). Over-pressurized zones result from water expulsion in low permeability, under compacted sediments due to rapid sedimentation. The high amounts of water result in low thermal conductivity and thus high geothermal gradients. The rate of loss of vertical thickness for under compacted sediments is then also different to normally compacted sections. Abnormal pressures can also arise as a consequence of thermal maturation of organic matter. Low geothermal gradients are expected in sediments that had not reached thermal equilibrium such as zones of rapid sediment accumulation. Erosion targets higher porosity sediments so that the rocks remaining have higher average conductivities and thus lower geothermal gradients for a constant heat flow. Overpressuring (undercompaction) could be considered to some degree in the depth-dependent equations by merely changing the equations' constants to yield less compaction. The effective stress approach can directly decrease the rate of porosity reduction during overpressuring. However, Schneider et al. (1993) have concluded that pressure (and therefore also effective stress) cannot be predicted

using one-dimensional modeling (that is, z dimension plus time) since in their opinion most fluid flow is horizontal rather than vertical (England et al., 1987) (Waples in Magoon & Dow, 1994).

Creating a 1D model requires that the start and end of the event which gives the thickness of the layer are input. It is impossible to represent all lithologies found in a layer especially those of small thicknesses. Mixed lithologies are thus created by lumping several lithologies together with some geologic reasoning to formulate a unit. This allows porosity reduction for the entire unit to be calculated based on the lithologic make-up of the stratigraphic interval. (Hatchel and Kauerauf, 2009) elaborate on an optimizing procedure involving back stripping of the layers from present day thickness or imported from structural restoration programs having taken into account the effects of igneous intrusion and salt movement. Simulation of the resulting difference between present day thickness and present day geometry yields a more accurate thickness. Correction is also made for fluids that leave the sediment during compaction which are determined by the permeability of the sediment (Figure 2.1.2 and Figure 2.1.3).

A porosity-permeability relationship described by the Kozeny-Carman equation is commonly used in most compaction models combined with the application of Darcy's Law for fluid flow predictions. Due to its mathematical complexity, compaction correction is usually carried out by basin modeling software. As temperature increases with depth the corrected burial history curve is always deeper than the uncorrected. This is due to the temperature that is being experienced by the corrected curve always being more than that experienced by the uncorrected curve. Additional factors influencing porosity loss and volume reduction in sediments include overpressures experienced in low-permeability sediments such as in shales that could not lose fluids fast enough and the resulting higher porosities. Cementation results in less compaction due to a tougher structure. "Compaction is said to be increased by expulsion due to an increase in porosity resulting from the conversion of solid kerogen to mobile petroleum which affects overall rock compressibility", (Dueppenbecker, 1991). Other responsible processes include clay diagenesis and authigenic mineral growth fill pores and stylonization that can eliminate pore space and reduce rock volume. However, these processes are hard to predict and simulate in basin modeling and so are usually ignored. Rock expansion resulting from release of pressure after erosion is sometimes modeled by allocating a small percentage increase to porosity otherwise it is ignored (Waples in (Magoon & Dow, 1994). The resulting effects on the layer thickness due to these factors have also to be considered. Among them are effects from Igneous intrusions or the presence or withdrawal of a salt dome.

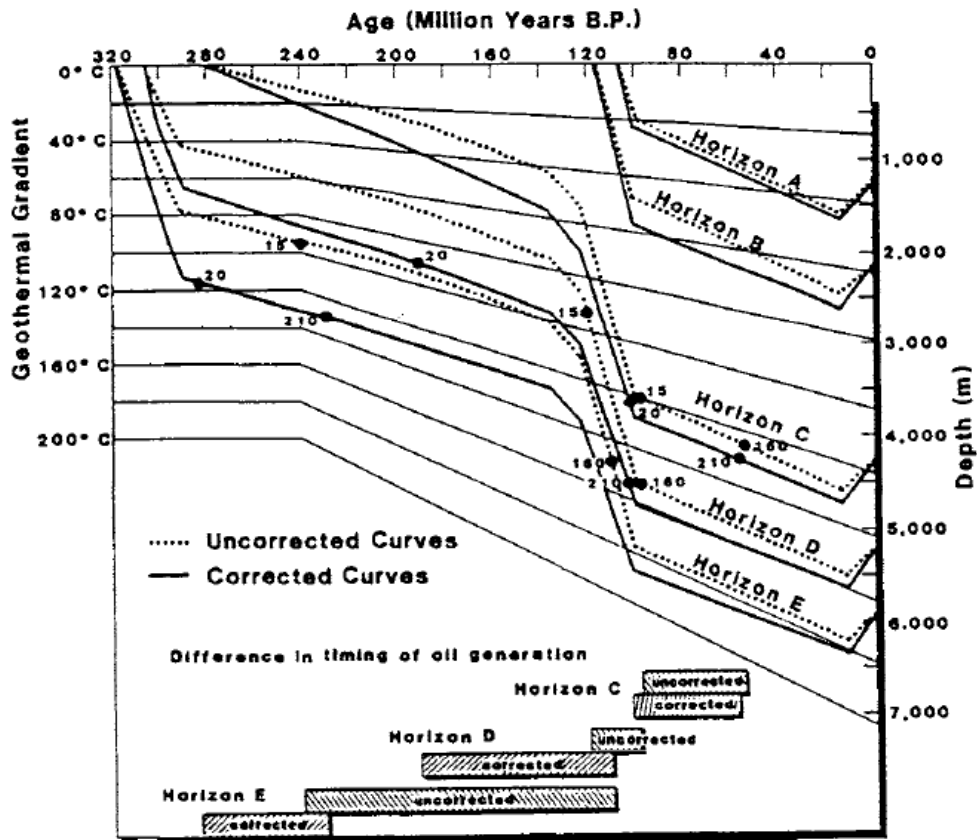


Figure 2.1.3 Adapted from Dykstra, (1987) shows the burial history for several units in the Inigok No.1 well, Alaska. The diagram shows curves corrected and uncorrected for compaction, and the effects on the timing of the oil window

One indicator for unconformities is the difference measured in sonic transit times in shales before and after deposition following a hiatus. This difference is dependent on the amount of erosion that occurred, (Waples in Magoon and Dow, 1994). To model unconformities the program must be provided with the period and thickness of the units lost (Barker, 1996). More care is given to the rebuilding of unconformities that occur at deeper and higher temperature zones where temperature effects are more prevalent. Unconformity zones typically show sudden high vitrinite reflectance stemming from high oxidation effects. “Vitrinite reflectance profiles typically show abrupt increase in reflectivity at unconformities”, (Barker, 1996). There is a method that allows the estimation of the amount lost to erosion provided there is enough reflectance data and there has been limited reburial. According to Dow (1977) in Barker (1996) the vertical distance covered when extrapolating the trend from below an unconformity to the unconformity reflects the amount of rock lost to erosion. Vitrinite reflectance values for erosional present day surfaces can be extrapolated to a typical surface value or the commonly used 0.2% which gives an eroded rock thickness of 2196m. Some researchers have used coalification to estimate the rock lost to erosion. Another way is the use of biomarkers to establish the

loss of section due to reduced reaction rates resulting from decreased temperatures. Methods simulating thermal history also estimate the amounts of erosion. Under or overestimated porosities from erosional data affects thereafter calculated permeabilities and thermal conductivities.

Petrophysical properties are calculated by the program from the entered lithology as per the already existing lithology library in the software. Some softwares are set to accept the user overriding the library inputs to enter their own lithologies or giving combined lithologies (Waples in Magoon and Dow, 1994). The petrophysical properties are then calculated by the software using averaging techniques such as the harmonic, geometric or arithmetic. The assumption that deposition and erosion are known allows paleo times to be assigned to each layer, (Hatchel and Kauerauf, 2009).

Pressure calculations

Pressure calculations mainly consider pressure due to overburden weight resulting from sedimentation. This includes pressure from processes such as mineral conversions, quartz cementation and gas generation. Pressure calculation and compaction change the geometry of the basin and are thus carried out prior to heat flow analysis at every time step in simulators. The heat emanating from Igneous intrusions induce thermal phase transitions in sediments in their vicinity. The heat entering the base of the sediments must be incorporated into thermal boundary condition formulations. “These basal heat flow values are often predicted with crustal models in separate pre-processing programs or are interactively calculated for each geological event,” (Hantchel and Kauerauf, 2009).

Workers have observed a ‘slow down’ of the overpressures due to the difference between formation fluid pressure and the hydrostatic pressure in the vitrinite maturation process. The laboratory work of Le Bayon *et al.* (2011) of pressures on vitrinite maturation revealed a dependence on pressure of the vitrinite maturation process. This assessment work revealed pressure retardation effects at high pressures corresponding to a least depth of 8.7km. As this depth is out of the usual vertical drill depth by a kilometre, it was concluded that the measured vitrinite reflectance data does not usually experience pressure retardation unless if measured from metamorphic terrains (Nielson et al., 2015). This was interpreted to mean that sedimentary basins of pressures of 200MPa and lower would not be expected to experience pressure retardation. Teichmuller (1979) in Nielson et al., (2015) observed that “vitrinite reflectance initially rises at a low rate until c. 1% R_o after which it increases at a higher rate. The measured vitrinite reflectance was found to be too high for the present-day borehole temperatures in some cases. This led him to suggest that the thermal gradient and therefore heat flow was probably higher in the past than at present.

The Petroleum System Elements

(Magoon and Dow, 1994) define a petroleum system as a natural system that includes a pod of active source rock that may be inactive or depleted and all related oil and gas incorporating all the geologic elements and processes that are essential if a petroleum accumulation is to exist. The term elements was used in (Magoon, 1987 in Magoon and Dow, 1994) to refer to source rock, migration path, reservoir rock, seal and trap. It was explained that the elements have to be placed in time and space that will enable a petroleum deposit to occur.

Figure 2.1.4 shows a burial history chart that shows the essential elements at specific location in time and the critical moment for the petroleum system being modeled. The petroleum system history chart shows how the essential elements relate spatially with processes and the preservation time. The critical moment is chosen by the modeller as the point in time that best represents the generation to migration to accumulation in a trap of most hydrocarbons in a petroleum system. The generation, migration and accumulation of hydrocarbons in a single location is said to occur in a geologically short time span. The burial history chart can be combined with a burial history curve to show the functions of the lithological units in the petroleum system as overburden, source, reservoir, seal or under-burden rock and their time of deposition. The role of the overburden rock is to provide the weight required to thermally mature the source rock and it has an effect on the geometry of the migration path and trap in the units below it. This depicts the time the petroleum system elements occurred. Stratigraphic and petroleum geochemical studies as well as the burial history chart provide a means to investigate the generation, migration and accumulation of the hydrocarbons or age of the petroleum system. During the subsequently process of preservation, the hydrocarbons are preserved, altered or biodegraded unless the generation, migration and accumulation processes extend to the present day. Choosing the critical moment is carried out after all the above processes (Magoon and Dow, 1994).

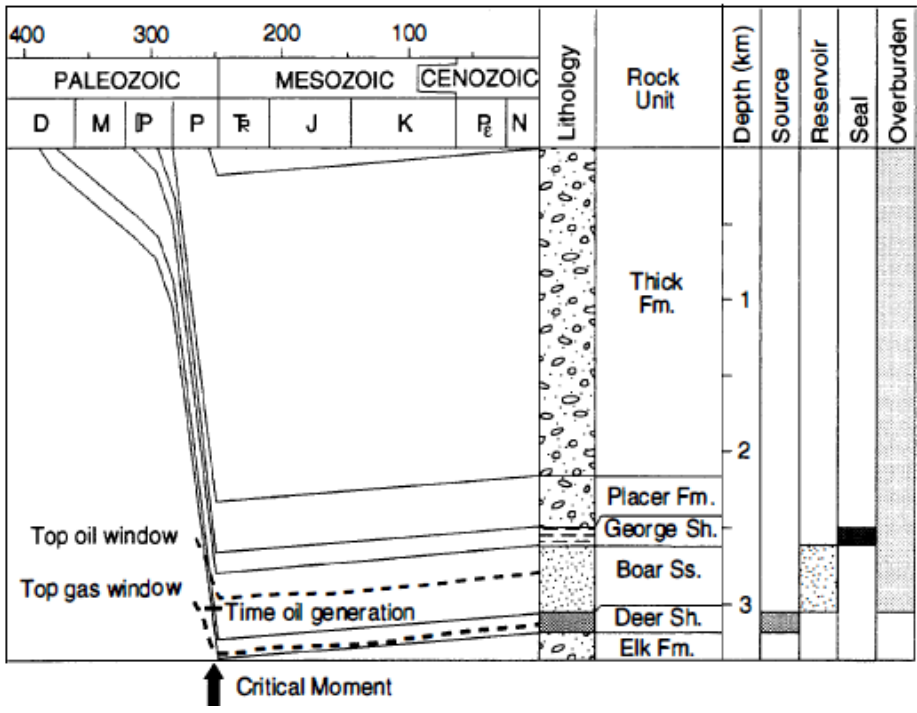


Figure 2.1.4 shows a burial history chart inclusive of a burial history curve showing the functions of the lithological units in the petroleum system as either over-burden, source, reservoir, seal or under-burden rock. The burial history chart shows the critical moment and the time of petroleum generation of a fictitious petroleum system in Magoon and Dow, (1994).

Magoon and Dow, (1994) describe three levels of certainty for a petroleum system as; known, hypothetical or speculative. These are symbolically expressed as a (!), (.) or (?) respectively. In a known system and hypothetical system the source rocks are characterized by geochemical analysis although there is no identified hydrocarbon accumulation in a hypothetical system. In a speculative system the correlation of a source rock to petroleum is merely postulated based on geologic inference. A depth-based structural model of the area of interest is firstly created. The model may encompass a single petroleum system in a small basin or multiple petroleum systems in one basin or many basins across a region. Input is typically in the form of formation tops and layer thicknesses and can be imported from a separate model-building program. A petroleum system events chart depicts geologic processes of a time during which deposition, non-deposition or erosion occurred including structural and tectonic events. The critical moment is manually chosen by the modeller to represent the time when most of the hydrocarbons in a petroleum system would have generated, migrated and accumulated.

2.3 Thermal History

Introduction

In order to model maturation and generation, kinetic processes that are controlled by temperature and time represented as time-depth in the burial history are converted to time-temperature so as to have a thermal history. Temperature is necessary for the geochemical reactions. This simulates the heat flow and temperatures that affect the sediments during burial. This requires the consideration of effects from surface temperature, heat flow, thermal properties of the sediments and any igneous bodies including effects of circulating fluids. One simple way of approximating the thermal history involves finding a linear relationship of temperature with depth. The geothermal gradient is calculated as Bottomhole temperature (BHT) minus surface temperature divided by depth less elevation of Rotary Kelly bushing, usually expressed in °F/100ft or °C/km. Present day rock temperatures are affected by fluids circulated from the surface during drilling and testing so that the readings normally measured are some significant degrees lower than the subsurface rock temperatures. Gas expansion inside the pipe also results in lower measured temperatures. The Horner plot is one of the ways used to correct the BHT for the temperature effects experienced during drilling. Other documented examples include finding the temperature using the Total Depth (TD) and gradient minus the surface temperature to calculate the temperature. Alternatively rock temperatures are given time to equilibrate, but this can take years. Some researchers find the current temperature by subtracting 10 to 15° from the measured temperatures. Others have used empirical correction curves such as those used by Harrison et al. 1983 and Jones (1975) in their works using data from well-studied geological zones to correct other wells. The quality of industrial borehole temperatures is questionable and they tend to be biased towards too low temperatures, (Nielson et al., 2015).

Surface temperatures are affected by climate conditions, solar heating and changes in thermal properties according to types of sediments. Near surface groundwater or cave temperature can be used to correct for this variations. Higher temperature variations are experienced in high latitude zones while equatorial zones only show minor changes. The onshore starting temperature is usually set at 10°C, while the set temperature at the water-sediment interface is the offshore surface temperature. This offshore surface temperature will vary with depth and latitude but it is usually approximated at 4°C. Heat transfer mechanisms are considered in order to establish their effect on the subsurface temperatures of sediments. Most heat transfer in the crust is by conduction (Barker, 1996) while some is contributed by radiation from the earth's interior to outer space. Temperature increases with depth into the subsurface.

By Fourier's law, given that heat transfer is by conduction having neglected convection and radiation, then the gradient is obtained from;

$$Q = -K dT/dz \quad (6)$$

Q is the heat flow in the z direction. T is the temperature and K is the thermal conductivity. When the equation is evaluated for some temperature and depth range and constant heat flow then the temperature range divided by the depth range gives the geothermal gradient. Then heat flow (mW/m^2) equals thermal conductivity multiplied by geothermal gradient. Barker gives the average geothermal gradient to be 25°C/km . High average geothermal values are experienced at geologically active areas and so are high heat flow values. Corrections for contributions from crustal radiogenic heat flow are made using the equation;

$$Q = AD + Q_r \quad (7)$$

where A is the radiogenic heat production, D is the radioactive crust thickness and Q_r is the reduced heat flow. When heat from radiogenic elements is factored in, petroleum generation has been shown to occur earlier and/or at shallower depths.

Porosity decreases with burial and so does the low conductivity fluids that are filling the pores and so thermal conductivity increases with burial. Thermal conductivity values of minerals decrease as temperatures increase. Conductivity is affected by anisotropy which is found to increase with increasing depth. This results in greater anisotropy values along the grains and less across them. Although minerals have high conductivity values at lower temperatures and lower values at higher temperatures, the mineral conductivity values eventually equilibrate as high thermal conductivities decrease faster, resulting in similar conductivities at depth (Barker, 1996). Rocks containing high quartz content are bound to have high thermal conductivity as quartz has the highest temperature coefficient of thermal conductivity of all of the common rock-forming minerals (Barker, 1996). Salt has high thermal conductivity thus will produce low geothermal gradient. Some researchers have noticed that although the geothermal gradient increases below the salt dome, the temperature is lower than would usually be expected. Over-pressured zones usually have high water contents thus lower thermal conductivities and higher geothermal gradients. Some sedimentary layers are documented to be insulators. Coal was observed to have a blanketing effect thus causing increased temperatures in layers occurring below it. The equation;

$$K_r = (K_w/K_m)^\phi * K_m = (K_w^\phi / K_m^{1-\phi}) \quad (8)$$

relates thermal conductivities of the mineral grains and water conductivities to porosity to find the rock conductivity. The equations' validity is limited to smaller values of K_w/K_m (Barker, 1996).

FACTORS CONTROLLING TEMPERATURE (EFFECTS) IN SEDIMENTARY BASINS

Thermal conductivity

The thermal conductivity of rocks and sediments depends on mineralogy, porosity, and temperature. The bulk thermal conductivity of the sedimentary rocks depends on both the solid rock component and the pore fluid as saline water partially or fully saturates the sedimentary rock pores. Mixing models such as the geometric mean model below is available to estimate the thermal conductivities of an aggregate according to its individual components (Woodside and Messmer, 1961);

$$K_{pr} = k_m^{(1-\phi)} k_w^\phi \quad (9)$$

where ϕ is the fractional porosity, k_{pr} is the thermal conductivity of a porous rock, k_m is the thermal conductivity of the matrix, and k_w is the thermal conductivity of the pore fluid (usually water). Matrix thermal conductivity in sedimentary basins is found to predominantly decrease with increasing temperature. Usually measurements are made in the laboratory at -25°C before being corrected for in situ temperature estimates. The empirical corrections include the one below calibrated from the data of Birch and Clark (1940):

$$k(0) = k(25)[1.007 + 25(0.0037 - 0.0074/k(25))]k(D = k(0) / [1.007 + T(0.0036 - 0.0072/k(0))]) \quad (10)$$

$k(25)$ is the laboratory measured thermal conductivity at 25°C , $k(0)$ is the inferred thermal conductivity at 0°C , and $k(T)$ is the estimated thermal conductivity at in situ temperature T . The dependency of the thermal conductivity of water on temperature is presented by (Touloukian et al., 1970) as;

$$k_w = a + bT + cT^2 \quad (11)$$

where k_w is the thermal conductivity of pure water in W /m K (watts per meter degrees Kelvin). For $0 \leq T \leq 137^\circ\text{C}$, $a = 5.65 \times 10^{-1}$, $b = 1.88 \times 10^{-3}$, $c = -7.23 \times 10^{-6}$; for $137 \leq T \leq 300^\circ\text{C}$, $a = 6.02 \times 10^{-1}$, $b = 1.31 \times 10^{-3}$, and $c = -5.14 \times 10^{-6}$. Compared to the rock matrix, the thermal conductivity of water is relatively low. At 0°C , $k_w = 0.56 \text{ W /m K}$, at 100°C , $k_w = 0.68 \text{ W /m K}$. The bulk thermal conductivity of a porous rock increases as porosity and temperature decrease.

Common lithologies can have significantly large differences in thermal conductivities. Table 2.3.1 lists some thermal conductivity values for some common minerals and rocks. The in situ thermal conductivity of most sedimentary rocks is in the range of about $1.0 - 4.5 \text{ W /m K}$. The lithological thermal conductivities are all estimates and are thus not accurate to every situation. The associated average error of these estimates is usually between $\pm 30-40\%$, with possibilities for more than 100% maximum error (Magoon & Dow, 1994).

Porosity and temperature affect laboratory measurements so that they become higher than the in situ measurements. Large deviations mainly occur due to changes in lithology and mineralogy with fewer due to errors in measurement. Lithologic heterogeneity determines the number of measurements that are required to find the thermal conductivity of a geologic unit to an acceptable error. Most sedimentary rocks typically have both vertical and lateral facies changes resulting in large spatial variations in thermal conductivity. The effect of juxtapositional lithologies, having different thermal conductivities also has to be accounted for. These lithologies (salt) are capable of focussing and defocussing heat, and thus will create local enhanced and depressed vertical temperature gradients (Yu et al., 1995). “Relative to sedimentary rocks (roughly a factor of 2-3 prevails between salt and sediments) (Yu et al., 1995). The effect of all these changes typically creates difficulties to collect adequate data for estimating the variation of thermal conductivity individual geologic units of a basin (Magoon & Dow, 1994). Geophysical well logs are often used to overcome the difficulty introduced by the facies changes and limited sampling possibilities. Calibrated laboratory parameters enable the use of well logs for interpolating between measurements sites. Thermal conductivity data has been found to correlate with resistivity, seismic velocity and density. As well as estimating mineralogy from well logs, bulk rock thermal conductivity for different lithologies can be estimated from laboratory derived values. This is only possible when there is an accurate mineralogy log. This method is specific to certain mineralogic compositions or lithologies as such it cannot be generalized (Magoon & Dow, 1994).

Table 2.3.1. Table shows some selected thermal conductivity values (adapted from Barker, 1996)

MATERIAL	W/m/°K	ROCK	W/m/°K
Quartz	7.8	Sandstone	1.9 - 7.4
Feldspar	2.3	Quartzite	3.7 - 7.5
Calcite	3.4	Clay	1.8
Halite	5.9	Mudstone	1.5 - 2.3
Anhydrite	5.1	Shale	0.6 - 2.9
Gypsum	1.1	Chalk	2.9
Analcime	1.3	Marl	0.9 - 2.8
Mica	2.3	Limestone	1.9 - 3.0
Siderite/ankerite	3.0	Dolomite	1.9 - 5.4
Pyrite	19.2	Granite	2.2 - 3.4
Rutile	5.1	Rhyolite	2.5
Ice	2.1	Diabase	1.9 - 2.2
Water	0.6	Dunite	4.0 - 5.6
Oil	0.2	Basalt	1.5
Gas	0.1		

Heat Flow

Heat transport in the crust is mainly by conduction. Both heat flow and thermal conductivity are first order properties. Heat flow is inversely correlated to tectonic age (Vitarello and Pollack, 1980; Morgan, 1984), the

greater the heat flow, the younger the tectonic age but it decreases with increasing age depressed by sedimentation. Foreland basins are associated with post-PreCambrian orogenic belts, intracratonic basins is located in old, stable cratons and pull apart or back arc basins have potentially young tectonic ages. Their respective heat flows are in the ranges 50-70mW/m², 30-50mW/m² and high heat flows for the young tectonic ages. Heat flow has been recorded to be as high as 90- 120 mW / m² or higher in young (<25 Ma) rift basins. High sedimentation rates exceeding 100m / m.y. as experienced in passive margins largely depress heat flow (Magoon and Dow, 1994). The variation in lithologies of relatively thick stratigraphic section means that they will have varying thermal conductivities ranging between relatively high and relatively low. A value of about 2.5W/mK is typically allocated as the average thermal conductivity of a section containing diverse lithologies. A lateral heat component becomes significant around salt domes and in the event the asthenosphere elevates to shallow depths during crustal thinning and extension. Significant lateral heat transfer is referred to as thermal refraction. Salt diapirs conduct heat from the deep subsurface up into shallower levels. Due to its high thermal conductivity, it may lead to higher temperatures immediately above the diapirs, but lateral heat conduction or heat refraction is also significant. It is expected that the convection perturbed by the high temperatures adjacent to the diapirs due to thermal refraction can create isotherms that become sub-vertical close to the salt diapirs and will affect the local thermal regime (Magoon & Dow, 1994). Convection can redistribute heat resulting in much reduced geothermal gradients due to temperatures that have been balanced by circulating fluids. The effect of convection is expected to be felt locally and not in the whole basin (Ludvigsen et al, 1993). Temperature data from oil and gas fields provide a good idea of temperatures in the subsurface. The high temperature anomalies associated with the well data resulting from vertical and lateral high temperature fluids transport in structures have to be taken into account (Barker, 1996). However, many seals especially over-pressured shales are good insulators with low thermal conductivities.

Calculating Heat Flow

Steady-state conductive heat transport estimates the deviation of sedimentary basins from their complete initial thermal equilibrium. The variation in temperatures is largely influenced by ground water flow. To calculate heat flow (Q), thermal conductivity (k) is multiplied by the thermal gradient (g), so that;

$$Q = kg \tag{12}$$

When the surface temperature and thickness of the overburden Δz are incorporated, the following equation can be applied to find the surface temperature (T) in the basin;

$$T = T_o + (q/k) * \Delta z \tag{13}$$

T_0 is the mean annual surface temperature. Geothermal gradient varies according to conductivity and thus heat flow is more reliably used for analysing basin temperatures. The following equation that defines the change of temperature with respect to time (dT/dt) is reached when temperature effects caused by heat advection due to moving fluids are factored in;

$$\rho C(dT/dt) = d/dz[k_z(dT/dz)] - v_z \rho_w C_w(dT/dz) + A^* \quad (14)$$

Depth is defined as z while p and C respectively define the bulk density and heat capacity of a porous rock. ρ_w is fluid density, C_w is fluid heat capacity, V_z is the Darcy velocity of a fluid moving through a porous medium, k_z defines the thermal conductivity while A^* is the radioactive heat generation per unit volume per unit time. The above equation can be directly applied to two or three dimensions but as the variation of temperature with respect to depth (dT/dz) is significantly higher than lateral variations in most geologic settings, a one-dimensional approximation is justified.

The present-day thermal state is important as a starting point to trace back to the possible thermal state at the time of oil and/or gas formation millions of years ago. Radiogenic material in the continents contributes 40% to surface heat flow and 60% to reduced heat flow. Heat flow contribution from the radioactive materials K, Th and U has a half-life in the order of millions thus resulting in an almost constant contribution whereas large heat flow variations occur at the base of the lithosphere due to fluctuations in heat flow, volcanism, and continents passing over hotspots. Lachenbruch and Sass (1977) gives the equation;

$$t = y^2 / 4\alpha \quad (15)$$

The equation calculates the time (t) taken for thermal disturbances to travel a distance (y) through a material of thermal diffusivity (α).

The approximate thermal diffusivity of the lithosphere of $32 \text{ km}^2/\text{m.y}$ results in lifetimes of between 50-100 m.y for 100km average lithospheric thickness, an indication that the lithosphere has a high thermal inertia. The lengths of time that the background thermal states tend to remain active are similar to the lifetime of a petroleum system.

Surface temperature

Surface temperature (T_0) is a requirement in maturation modelling as it is a boundary condition on geothermal conditions. Thermal disequilibrium is common at near-surface environments which often have rapid fluctuations due to activities such as deforestation, tunnelling and paving. Surface changes include diurnal and seasonal fluctuations as well as reduced temperatures due to retreating and advancing glaciations, (Magoon

and Dow, 1994). The magnitude of the change and the specific heat of the rock units determine the resulting changes on the thermal regime. Extensive permafrost developments also contribute to the local thermal variations. Some cool near-surface sediments are pulled into the subsurface at subduction zones too fast to have reached thermal equilibrium resulting in below average geothermal gradients. Conversely, extremely high near-surface temperatures may be experienced where there was rapid uplift and erosion. Using equation (15) reveals that the annual variation of temperature propagates only up to about 10m into the subsurface. The long term mean is a fictional quantity that is usually estimated by the linear extrapolation of a borehole temperature log to the surface. The long term mean has greater interest in geothermal analysis (T_0). Due to the insulating effect of snow cover in winter it has been shown that extrapolated borehole temperatures are closely related to mean annual air temperatures compared to the ground temperatures that are always higher by about 2°-3°C. Areas of low latitudes exhibit differences between the mean annual ground temperatures and air temperatures. The earth surface has a mean annual air temperature of -16°C, ranging from -25°C at the equator, to -22°C at the poles. Air temperatures get cooler with elevation. Any indications of global climate changes especially those affecting surface temperatures must be taken into account when modelling the thermal evolution of sedimentary basins. The global cooling that results in reduced air and ground temperatures must especially be taken into account when modeling the thermal history of sedimentary basins. Retreating and advancing glaciers experienced in the last 1 m.y. (Folland et al., 1990), are examples of short term climate variations that affects the subsurface temperatures. Recent silicate melt intrusions may induce temperatures above local equilibrium values causing variations which will be reflected on thermal indicators such as vitrinite reflectance (Magoon & Dow, 1994). Extrapolation of subsurface temperatures to the surface will include anomalous temperatures from the silicate melt intrusions if drilling had not penetrated the igneous material and its occurrence had not been taken into account. Calibration wells have maximum temperatures at the present day. Nielson et al., (2015) suggests that recent sedimentation is not an adequate enough condition to reach maximum temperature at the present day. They cite the observed general cooling of surface temperatures during the Cenozoic, and the low average surface temperature experienced during the Quaternary with an interval of significant heating as their bases.

McKenzie, (1978) stretching lithosphere model is applicable for estimation of timing of hydrocarbon generation. A sedimentary basin fill is “backstripped” so that tectonic subsidence is excluded from the total subsidence by applying the principle of isostasy and factoring in sediment compaction and changes in sea level (Dembicki, 2016). This allows creation of a tectonic subsidence curve which will be compared to McKenzie's theoretical predictions to find a "best" value for the stretching factor. The stretching factor value is used for estimation of the heat flow, calculation of the temperature, and prediction of the source rock maturity for a known source rock location in the basin fill. Estimating the thermal history of a basin takes into account the depression of heat flow by sedimentation, the thermal conductivity of rocks within the basin, the surface temperature, and the possible influence of groundwater flow. The relative importance of these intra-

basin factors increases with passing time while the influence of the initial basin-forming event decreases. Deming in Magoon and Dow, (1994) lists the factors determining temperature in basin fill as overburden thickness, heat flow, thermal conductivity, surface temperature and sedimentation. Groundwater and initial thermal event are the other factors of ranging importance.

The importance of the groundwater flow depends on if it is gravity driven, compaction driven or by free convection (Deming in Magoon and Dow, 1994). The initial thermal event importance is divided according to the age of the event, the youngest of up to 20Ma having the highest importance. Extrapolation of temperatures at depths below the drilled depths in the subsurface by geothermal gradient is not as accurate as it changes with depth as thermal conductivities change. Temperature and thermal conductivity measurements give conductive heat flow estimates. In such calculations advective heat transport by groundwater flow is assumed absent. Temperature is usually obtained from bottom-hole temperatures (BHTs) measured during the geophysical logging of oil and gas wells up to the depths of 6 km. This method has the advantage of avoiding near surface effects accounted when extrapolating from shallow holes. BHTs have the disadvantage of being noisy and need to be corrected as they are lower than the subsurface formation temperatures due to the cooling of BHTs by circulating drilling fluids. The basin temperature reconstruction process from analysis of BHT data is first extraction and screening of raw data from well log headers excluding inconsistent or implausible data. The raw BHTs data is then corrected for drilling disturbances through several schemes available correction schemes. This is provided there is enough data to allow for the corrections otherwise there is just the option of reducing bias from drilling inconsistencies. The interpretative stage involves averaging the corrected data by an interpretive model reducing the random error in individual measurements. Averaging data unfortunately reduces resolution but reduces the noise. The Horner plot correction scheme (Waples, 1991) includes making several temperature measurements in one well, thus it results in corrected temperatures that have less errors than those corrected with empirical schemes. Deming in Magoon and Dow (1994) found that modelling temperatures by just a single average gradient model was inadequate to define the temperature histories of the North Slope basin as the model did not incorporate lateral variation in the basin. Methods of estimating subsurface temperature from BHTs that can accommodate lateral and vertical variations in thermal gradients include kriging, inversion for thermal gradients in individual geologic formations, stochastic inversion and the method of variable bias.

Heat flow causes variations in thermal gradients as well as fluctuations in thermal conductivity due to variations of lithologies. Groundwater flow has also been found to influence thermal variations. A combination of heat flow analysis and oil and gas BHTs analysis was used by Deming (in Magoon and Dow, 1994) at the North Slope basin to explain thermal variations in the basin and make estimations on the oil migration mechanisms. Often in addition to thermal conductivities, the changes in thermal gradients can also

be due to heat flows that can also be affected by ground water flow systems. Both heat flows and BHTs estimations can be used to determine present-day boundary conditions on thermal history and maturation studies.

Heat flow Models

Recent and continuing extension has a small thermal contribution to subsidence. In older basins the large thicknesses accumulated over time have to be considered as well as the tectonic evolution in the basin. The simple model of McKenzie., (1978) assumes a constant temperature at depth corresponding to the original thickness of the lithosphere. The model incorporates subsidence calculations, heat flow, thermal diffusivity, new level above which the lithosphere sinks, the effects of extension on heat flux for certain times. The model assumes a constant thickness of the plate so that the approximately constant heat flux background observed in older ocean basins can be maintained. The heat flux as a function of time for different values of β as used in McKenzie's lithosphere stretching model for the evolution of sedimentary basins are shown in Figure 2.3.1.

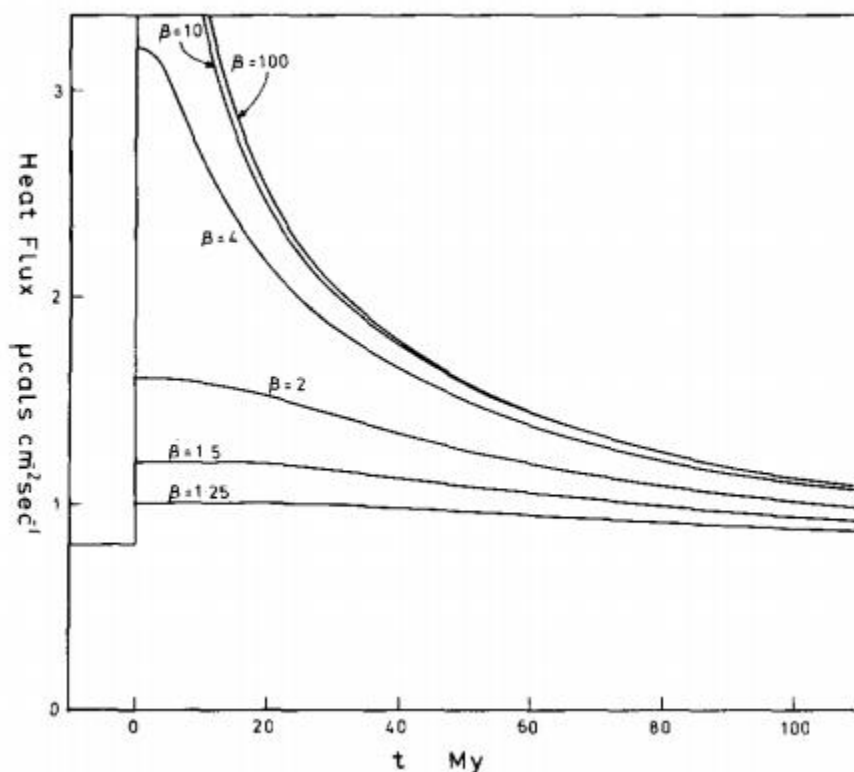


Figure 2.3.1 Adapted from McKenzie, 1978 to show the heat flux as a function of time for different values of β as used in McKenzie's lithosphere stretching model for the evolution of sedimentary basins.

McKenzie (1978) claims that the proposed model for the development and evolution of a sedimentary basin can account for the major evolution events of the Great Basin, The Aegean, the North Sea and the Michigan basin. The modeled events are inclusive of rapid stretching of continental lithosphere and associated block

faulting and subsidence, followed by thickening of the lithosphere by heat conduction to the surface. The slow subsidence and heat flow depend only on amount of stretching. McKenzie (1978) realized that there was a strong dependence on β when β is between 1 and 4 for time below 50M.y. and that large values of β had no effect on heat flux. McKenzie found that extension increased the heat flux by a factor β . Figure 2.3.1 shows the heat flux as a function of time for different values of β as used in McKenzie's lithosphere stretching model for the evolution of sedimentary basins.

Continental radioactivity has a greater effect on the heat flux more than temperature distribution (McKenzie, 1978). Evidence has shown the involved radioactive elements to be largely found towards the surface resulting in a small influence on the temperature distribution throughout majority of the continental lithosphere. McKenzie's simple model for extensions ignores the thickness of this generating layer in order to more simply determine the contribution to the heat flux. The McKenzie equations do not account for the large thicknesses of sediment in the majority of the basins that have a continental crust basement and thus make calculations for subsidence of an empty basin. However, by investigating further the McKenzie's rifting model through the evolution of rift basins and variations of heat flow, Sheplev and Reverdatto (1998) found that the old model is still valid today. They studied and compared the consequences of an instantaneous finite extension of the lithosphere, an accelerated extension of the lithosphere and the effects of a constant spreading rate. For the same values of initial parameters and extension duration, the subsidence dynamics for the accelerating and constant-rate solutions are closely similar although seemingly more intensely manifested at the end of spreading period. They reached similar conclusions regarding evolution of heat flow.

Parsons and Sclater (1977) used a simple cooling model and a plate model to explain the variation in depth and heat flow as the age of the ocean floor increases. Davis and Lister (1974); Lubimova and Nikitina, (1975) found that they can eliminate the singularity in the heat flux at the ridge crest by editing the boundary condition on the vertical boundary of the original McKenzie (1967) model. Parker and Oldenburg (1973) found that the plate thickness increased as $t^{1/2}$ everywhere but near the ridge crest, resulting in a heat flow that varies asymptotically as $t^{-1/2}$, with a linearly increasing depth as $t^{1/2}$. Davis and Lister, (1974) found a linear relationship within the age range of 0-80m.y. when plotting the 1-D heat flow equation data against original topographic data of Sclater et al. (1971). When investigating these findings, they found that the dependence of $t^{1/2}$ in the solution required to be treated as explicit. Their findings show that for ages that are adequately large, the depth increases slower than predicted by a linear $t^{1/2}$ dependence. They suggested that it is necessary to provide heat from the mantle to the base of the plate although for ages larger than 80m.y. there is a dependence of the 'flattening' of layers and probably of the thermal structure on the time scales which have differences that will induce errors. They suggest there is no influence from this as there is not enough evidence to suggest increase in crustal thickness with age. And anyway crustal thickness would incur significant effects for ages older than 70 m.y.B.P. and not where the linear $t^{1/2}$ dependence is valid. Additionally, the use of non-exact estimates of the mean depths at certain ages of the ocean floor induces bias. The uncertainties stems from large disturbances in the depth, inferred to stem from crustal variation and

mantle convection. In scrutinizing the plate model and earlier findings, Parsons and Sclater, (1977) found that there is a real deviation of the variation of depth with age from a linear $t^{1/2}$ dependence and that this requires an input of heat flux at the base of the lithosphere.

Geological contributions to heat flow

Sedimentation

Sedimentation depresses heat flow. The effect of depressed heat flow induced by sedimentation carries on long after sedimentation has stopped, provided no erosion has taken place. The underburden rock deposited prior to deposition of source rock can influence the maturation of organic material in the source rock. The thermal conductivity of the deposited sediments, the rate and the length of time taken for sedimentation to take place all affect the resulting depression on heat flow. The magnitude by which heat flow is reduced increases as the thermal conductivity of the sediments decreases. Increase in thermal conductivity of deposited sediments will favour an increase in heat flow if sedimentation rate remains constant, although the heat flow will still remain depressed.

Groundwater Flow

Groundwater is able to redistribute heat in the subsurface due to the high heat capacity of water (-4200J/kg K) enables significant perturbations to the background thermal regime with Darcy velocities as low as a millimetre per year, with depth of circulation considered. Vertical fluid flow mainly contributes to heat flow transport with little or no contribution from the horizontal groundwater flow. This results as the direction of isotherms is almost always parallel to the ground surface. Darcy (volumetric) velocity and depth of fluid circulation dictate the direction of influence of the upward or downward movement of groundwater on heat flow (or the geothermal gradient). Lachenbruch and Sass (1977) have shown that under steady state conditions, the following formulation is realized;

$$q(z_1)/q(z_2) = e^{\Delta z/s} \quad (16)$$

$q(z_1)$ is the conductive heat flow at the top of a layer of thickness Δz , $q(z_2)$ is the conductive heat flow at the bottom of the layer, and;

$$s = k/\rho_w C_w v \quad (17)$$

where k is the bulk thermal conductivity of the fluid-rock aggregate, ρ_w and C_w are the density and heat capacity, respectively, of the fluid moving with Darcy velocity v , and v is negative for downward flow.

Thermal measurements are possible in areas with permeabilities below 10 to 14m² but are not easily attainable in locations with high relief and rugged topography where groundwater seems to always be present. Groundwater is driven by potential gradients (Hubbert, 1940) and due to free convection. Hydraulic potential for variable density fluids is unattainable thus hydraulic potential or pseudo-potential are used instead for understanding of geological problems which would otherwise have no solution. Sediment compaction and elevation gradients are the usual geologic mechanisms used for creating potential gradients. In order for sediment compaction and pore collapse to be efficient heat and mass transport mechanisms, pore fluids have to be focussed spatially and temporally (Magoon & Dow, 1994). This is due to the usually low velocities and the low total water quantities that are contained in the original sediments. Potential gradients arising from elevation differences cause regional groundwater flow over distances of hundreds to thousands of kilometres. The influence or control on the thermal regime due to the groundwater flow depends on the depth and velocity of groundwater flow.

A typical flow system has been recognised in several foreland basins such as in the United States, Alaska, Canada and Australia. Groundwater advects heat downwards depressing surface heat flow and geothermal gradients due to the water that infiltrates the bases of the mountain range. Horizontal flow occurs at the midpoint of the basin effecting minimal basin temperature. A high geothermal gradient and high surface heat flow occurs at the distal edge of the basin due to flow that is forced upward by the basin geometry. Such flow systems are believed to have a strong effect on the “temperature-dependent generation of oil and gas and its migration. Density gradients can contribute to free convection in sedimentary basins resulting from thermal expansion or the presence of solutes. Free convection requires sufficiently high permeability of the porous medium and the presence of existing density inversion, provided that the higher density fluid overlies the less dense. However free convection probably seldom occurs in sedimentary basins as salinity and density increases with depth so that the decrease in density due to temperature and its eventual thermal expansion become less significant.

While there is still inadequate understanding of the free convection concept and its significance in thermal regimes, it has been offered as an explanation of extensive quartz cementation in an over-pressured zone in the Gulf Coast basin and subsidence of the Michigan basin of the United States (Magoon & Dow, 1994). The conductive heat transfer assumption may lose validity near the surface as gravity driven groundwater migration converts the heat transfer mechanism to forced convective heat transfer. This has the effect of decreased geothermal gradients and temperatures below the regional groundwater recharge areas and those that had been undisturbed under locations of lateral groundwater flow, with an opposite effect under regional groundwater discharge areas (Baker, 1996). Salinity patterns, tilted oil water contacts, sloping potentiometric surfaces, and the presence of biodegraded oils are distinguishing features for active recharge over long distances, (Magoon & Dow, 1994). The Rhine Graben studied by Person and Garven (1992) is an instance where the regional topography-driven groundwater flow was established as the reason for a more than a kilometre shift of the oil window between recharge and discharge areas.

Tectonics and Faults

Faults act as seals when closed or conduits for cold surface waters and hot subsurface waters when open. Places near faults are also typical of petroleum reservoirs and have been found to be the hosts of great temperature anomalies. Hot fluids percolate and move up to the surface through faults and cold surface waters reach depths into the subsurface through faults. Sealing faults are an important part to the structural setting that is necessary for petroleum reservoirs. Temperature anomalies are typical in the vicinity of faults. Some significantly higher values than average geothermal gradient values of 55 - 100 °C/km have been documented along some faults. Sealed petroleum reservoirs or those in rollover anticlines are typically found near temperature anomalies. Frictional heating has been documented to occur along faults. This is heat produced when rocks on each side of a fault move against the other. However, this heat source has been described as a minor heat source. Caution has to be taken when interpreting temperature anomalies near faults as small particles that are formed during shearing can be oxidized by hot waters and will produce very high vitrinite reflectance values near faults. Barker (1996) suggests that the resulting thermal effects if any, occurs locally in very small areas in the vicinity of the faults so that there are minimal effects on large source rock volumes maturation. The prevailing initial heat flow of an area before shortening establishes the thermal regime of the local thrust sheets, (Nemcok, Schamen and Gayer, 2009).

Figure 2.3.2 below presents the variety of basins capable of being later incorporated in thrust belts. These were reviewed according to their tectonic setting or geothermal signatures. The coolest thermal regimes are found in regions formed by old continental shield or old oceanic crust. Old passive margins such as Atlantic margins can be described as having near-normal geothermal gradients (Robert, 1988). They have present day geothermal gradients of about 25-30°C per km and the typical reflectance profiles for these gradients have an Ro of about 0.5% at depths of about 3km. Basins which are cooler than normal (Robert, 1988) include oceanic trenches (cold with surface heat flows of 40mW/m), outer fore-arcs and foreland basins.

“The presence of a graben or half-graben in a sedimentary basin in which the heat is being continuously supplied at a steady rate through the base of the basement rock underlying the sediments may cause considerable heat flux and/or temperature variation in a basin (Lerche, 1990)” “On the other hand, there is also a major structural geometry effect caused by the presence of the graben itself, with the flanks of the graben being elevated relative to the graben centre,” (Yu et al., 1995).

The syn-tectonic sediments of long lasting orogenic belts such as the Andes or the Great Caucasus are deposited under the thermal regimes of the orogenic belts and subsequently incorporated into the orogenic belt. The geothermal conditions of zones directly in front of the indenter will be higher, some such as in front of the Arabian plate which show heat flow values of 80-90mW/m² and the values lower to 50mW/m² indicating a cooling along the orogenic zone. “The zone in front of the indenter experiences high temperatures because the crust undergoes the greatest thickening by burial of radiogenic-enriched crustal rocks.” (Nemcok, Schamel and Gayer, 2009).

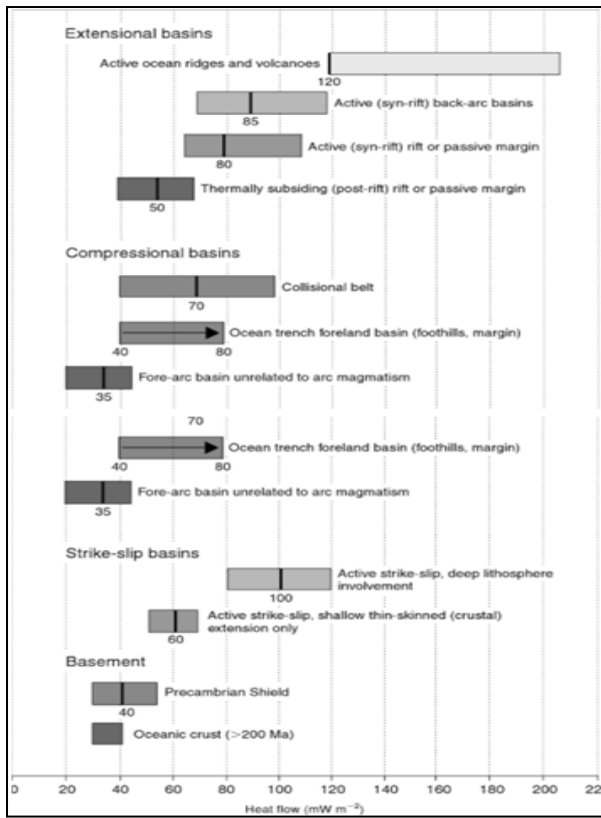


Figure 2.3.2 Adapted from Nemcok, Schamel and Gayer, 2009.

Evaporites

Evaporitic rocks affect source rock formation mechanisms, control migration pathways, generate traps and seal reservoirs. These rocks also affect sedimentation and sediment accumulation processes (Lerche and Peterson, (1995) in Barker, (1996). The extremely high biological productivity of evaporites affects the formation of potential source rocks in area surrounding the evaporites. Conversely, the evaporitic section itself will have low organic contents as a result of rapid accumulation rates of salt that are typically more than 1000m/m.y. (Hofmann et al, 1993 in Barker 2006). “Associated carbonates and shales accumulate much more slowly and develop high values for TOC,” (Evans and Kirkland, 1988; Benali, 1995) in Barker 2006). The ability of salt to flow and re-heal small fractures important for reservoirs, as well as regionally controlling migration pathways by creating laterally extensive permeability barriers makes salt an excellent seal. Conversely, salt movements can be destructive to adjacent sediments and the possibility of formation of traps (Barker, 1996).

Rapid salt accumulations will result in fast burial of the underlying sediments. The unique characteristic of salt is its dramatic variations in its thickness (either reducing or increasing in thickness) in a relatively short period of time. As it is very mobile and has a low density (only 2.2g/cm³), it has a tendency to float upwards forming diapirs. The eventual post-diapiric movement can induce more deformation to the sediments nearby

(Halbouty, 1979). Lateral salt movements can also be induced by varying overburden pressure from place to place. Salt intrusion can cause the deformation of overlying sediments and layers that were initially uniform above a diapir can be internally deformed resulting in large variations in layer thickness. “Flanks of piercement salt domes or diapirs commonly have adjacent strata tipped against them and most petroleum production associated with salt domes is from the flanks rather than the cap rocks,” (Barker, 1996). The salt that is removed from the original salt layer causes the formation of a rim syncline and subsequent accumulation of additional thickness of sediments.

Salt has high thermal conductivity that results in low geothermal gradients through salt beds. The salt diapirs that pierce through overlying sediments conducting heat upwards so that shallow sedimentary zones will have locally higher temperatures than usual. The resulting effect of the heat withdrawal is depressed deeper sediment temperatures near the diapir (Petersen and Lerche, 1995). “A comparison of the local and higher regional maturity profiles showed that near the diapir maturities were higher at shallow depths, but lower at greater depths. (this could be used to induce higher temps to match the Tmax Ro% model the goes higher in L2). “This effect can only be expected when the height of the diapir is less than about 5km because the thermal conductivity of salt decreases with increasing temperature.”

3.0 Identification of Source Rock

3.1 Kerogen transformation processes to generate hydrocarbons

Three main zones in [Figure 3.1.1 and Figure 3.1.2] describe the hydrocarbon formation stages; diagenesis, catagenesis and metagenesis. The Diagenesis stage occurs at shallow levels where the initial make-up of the organic matter is the controlling factor on the composition of kerogen is the initial make-up of the organic matter and the type and extent of microbial activity, forming methane.

During the immature zone shown in Figure 3.1.2 below of little transformation of kerogen and hydrocarbons occurs as there has not been sufficient temperatures and time for more effect. Transformation in this zone will result in high molecular weight compounds such as asphaltenes and resins and some gas from Type III kerogen.

Catagenesis is the main zone of oil generation and is coupled with significant generation of gas. Temperatures become elevated with increasing burial and so manage to break more bonds producing hydrocarbon molecules from kerogen and cracking of N,S,O compounds from the earlier stages, producing increased amounts of methane. This stage completes with residual kerogen of depleted in hydrogen with an atomic H/C ratio of about 0.5 (Tissot and Welte, 1984). A structural re-ordering of residual kerogen occurs in the metagenesis stage. The hydrocarbons generated from kerogen in this stage are mainly methane, with possibilities of large amounts of methane being formed from “cracking of source rock and of reservoired liquid petroleum”.

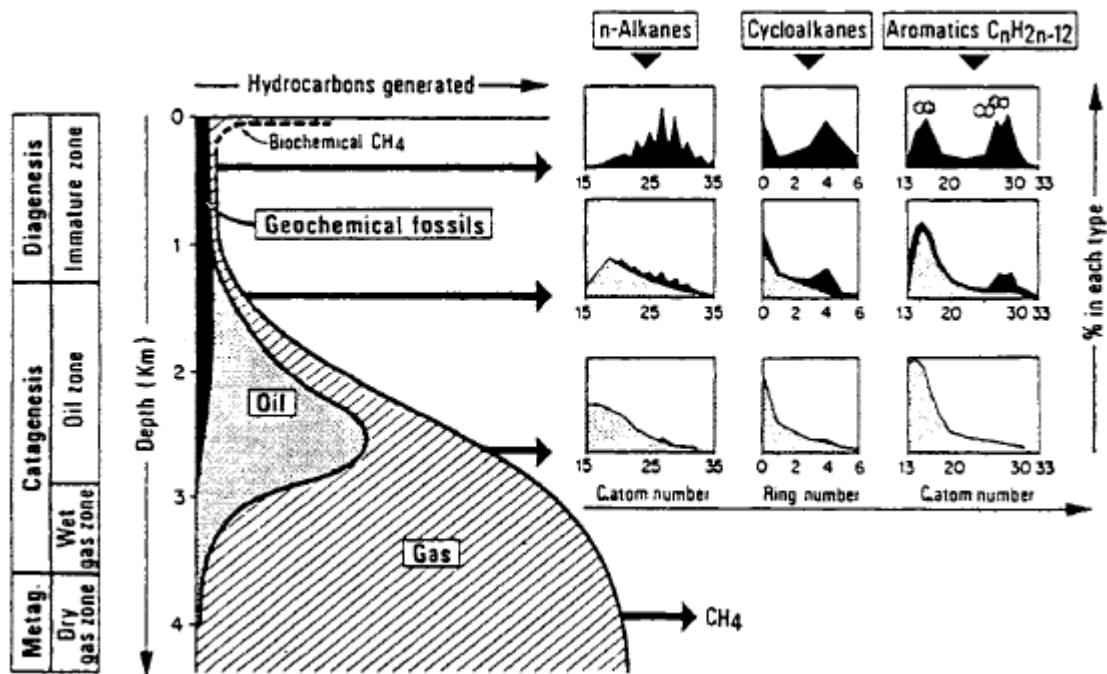


Figure 3.1.1. Edited from Tissot and Welte, 1984. The figure shows the evolution of hydrocarbon formation with increasing burial depth. They based the depth scale represented here on Mesozoic and Paleozoic source rocks. ‘Actual depth will vary depending on the kerogen type, burial history and geothermal gradient’.

The kerogen types responsible for generating the hydrocarbons with increasing depth and temperature are shown in Figure 2 and described below;

Type – I Kerogen is mainly derived from algal lipids or organic matter enriched in lipids by microbial activity. Type- I Kerogen is characteristic of an originally high H/C ratio and a high potential for oil and gas generation.

Type – II Kerogen mainly has marine originated organic matter deposited in a reducing environment containing medium to high sulphur. Type – II Kerogen has H/C ratio lower than that found in Type – I.

Type – III Kerogen is derived from terrestrial higher plants. It has a low H/C ratio, with a moderate oil generating potential and a greater potential to generate lots of gas deeper in the subsurface. It also has a higher O/C ratio than the Type I and Type II kerogens.

“Residual kerogen may consist of reworked, oxidized organic material, or inertinite material stemming from sub-aerial weathering or biological oxidation. It is one form of “dead carbon” and has no potential for oil and gas,” (Tissot and Welte, 1984).

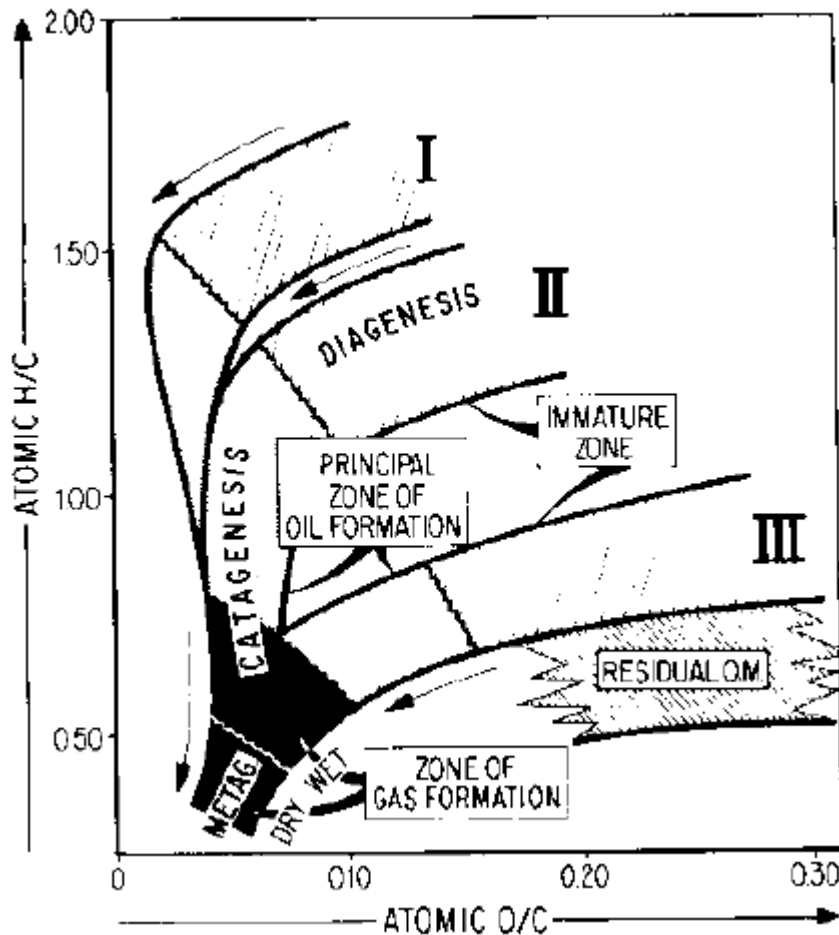


Figure 3.1.2. Adapted from Tissot and Welte, 1984. A general Kerogen evolution scheme imposed on a Van Krevelen's diagram to show the principal zones of formation of kerogen and the main products during that time. "Residual organic matter does not exhibit an evolution path," (Tissot and Welte, 1984).

Table 3.1.1 below by Cornford, (1977) in Tissot and Welte, (1984) gives the approximate equivalent names used to describe the organic matter types relating to the main groups of macerals in coal eg liptinite, vitrinite and inertinite;

Table 3.1.1 approximate equivalent names used to describe the organic matter types

Provenance	Terminologies			
Aquatic	Algal	Liptinite	Amorph.	Type I
	Amorphous			Type II
Sub-aerial (Terrestrial)	Herbaceous (fibrous)	Vitrinite	Humic	Type III
	Woody (plant structure)			Residual
	Coaly (angular to sub-angular fragments)	Inertinite		

Identifying the source rocks present, the hydrocarbon potential of each source rock in time and space with relation to the geological evolution of the basin allows the identification of the most favourable zones for petroleum accumulation by relating the hydrocarbon generation of a source rock at any given time during basin evolution to the most likely paths of petroleum migration. Geochemical studies, [Tables 3.1.2, 3.1.3 and 3.1.4] are combined with geological information in a scheme as presented by Tissot and Welte, (1984) (Figure 3), to aid in petroleum exploration.

Table 3.1.2 adapted from Magoon and Dow, (1994) gives the geochemical parameters that describe the petroleum potential (Quantity) of an immature source rock.

Table 3.1.2 Geochemical parameters describing the petroleum potential quality

Petroleum Potential	Organic Matter			Bitumen ^c		Hydrocarbons (ppm)
	TOC (wt. %)	Rock-Eval Pyrolysis S ₁ ^a	S ₂ ^b	(wt. %)	(ppm)	
Poor	0–0.5	0–0.5	0–2.5	0–0.05	0–500	0–300
Fair	0.5–1	0.5–1	2.5–5	0.05–0.10	500–1000	300–600
Good	1–2	1–2	5–10	0.10–0.20	1000–2000	600–1200
Very Good	2–4	2–4	10–20	0.20–0.40	2000–4000	1200–2400
Excellent	>4	>4	>20	>0.40	>4000	>2400

^amg HC/g dry rock distilled by pyrolysis.

^bmg HC/g dry rock cracked from kerogen by pyrolysis.

^cEvaporation of the solvent used to extract bitumen from a source rock or oil from a reservoir rock causes loss of the volatile hydrocarbons below about *n*-C₁₅. Thus, most extracts are described as "C₁₅₊ hydrocarbons." Lighter hydrocarbons can be at least partially retained by avoiding complete evaporation of the solvent (e.g., C₁₀₊).

Table 3.1.3 below adapted from Magoon and Dow, (1994) gives the geochemical parameters that describe the approximate Kerogen type (quality) and the character of expelled products, based on thermally immature source rock.

Table 3.1.3 Geochemical parameters that describe the approximate quality of immature source rocks

Kerogen Type	HI (mg HC/g TOC)	S ₂ /S ₃	Atomic H/C	Main Expelled Product at Peak Maturity
I	>600	>15	>1.5	Oil
II	300–600	10–15	1.2–1.5	Oil
II/III ^b	200–300	5–10	1.0–1.2	Mixed oil and gas
III	50–200	1–5	0.7–1.0	Gas
IV	<50	<1	<0.7	None

^aBased on a thermally immature source rock. Ranges are approximate.

^bType II/III designates kerogens with compositions between type II and III pathways (e.g., Figure 5.1) that show intermediate HI (see Figures 5.4–5.11).

Table 3.1.4 below adapted from Magoon and Dow, (1994) provides geochemical parameters that describe the level of thermal maturation.

Table 3.1.4 geochemical parameters that describe the level of thermal maturation.

Stage of Thermal Maturity for Oil	Maturation			Generation		
	R _o (%)	T _{max} (°C)	TAI ^a	Bitumen/TOC ^b	Bitumen (mg/g rock)	PI ^c [S ₁ /(S ₁ + S ₂)]
Immature	0.2–0.6	<435	1.5–2.6	<0.05	<50	<0.10
Mature						
Early	0.6–0.65	435–445	2.6–2.7	0.05–0.10	50–100	0.10–0.15
Peak	0.65–0.9	445–450	2.7–2.9	0.15–0.25	150–250	0.25–0.40
Late	0.9–1.35	450–470	2.9–3.3	—	—	>0.40
Postmature	>1.35	>470	>3.3	—	—	—

^aTAI, thermal alteration index.

^bMature oil-prone source rocks with type I or II kerogen commonly show bitumen/TOC ratios in the range 0.05–0.25. Caution should be applied when interpreting extract yields from coals. For example, many gas-prone coals show high extract yields suggesting oil-prone character, but extract yield normalized to TOC is low (<30 mg HC/g TOC).

Bitumen/TOC ratios over 0.25 can indicate contamination or migrated oil or can be artifacts caused by ratios of small, inaccurate numbers.

^cPI, production index.

**A decisive exploration philosophy incorporating geochemical data:
Determination of most favourable zones of petroleum accumulation**

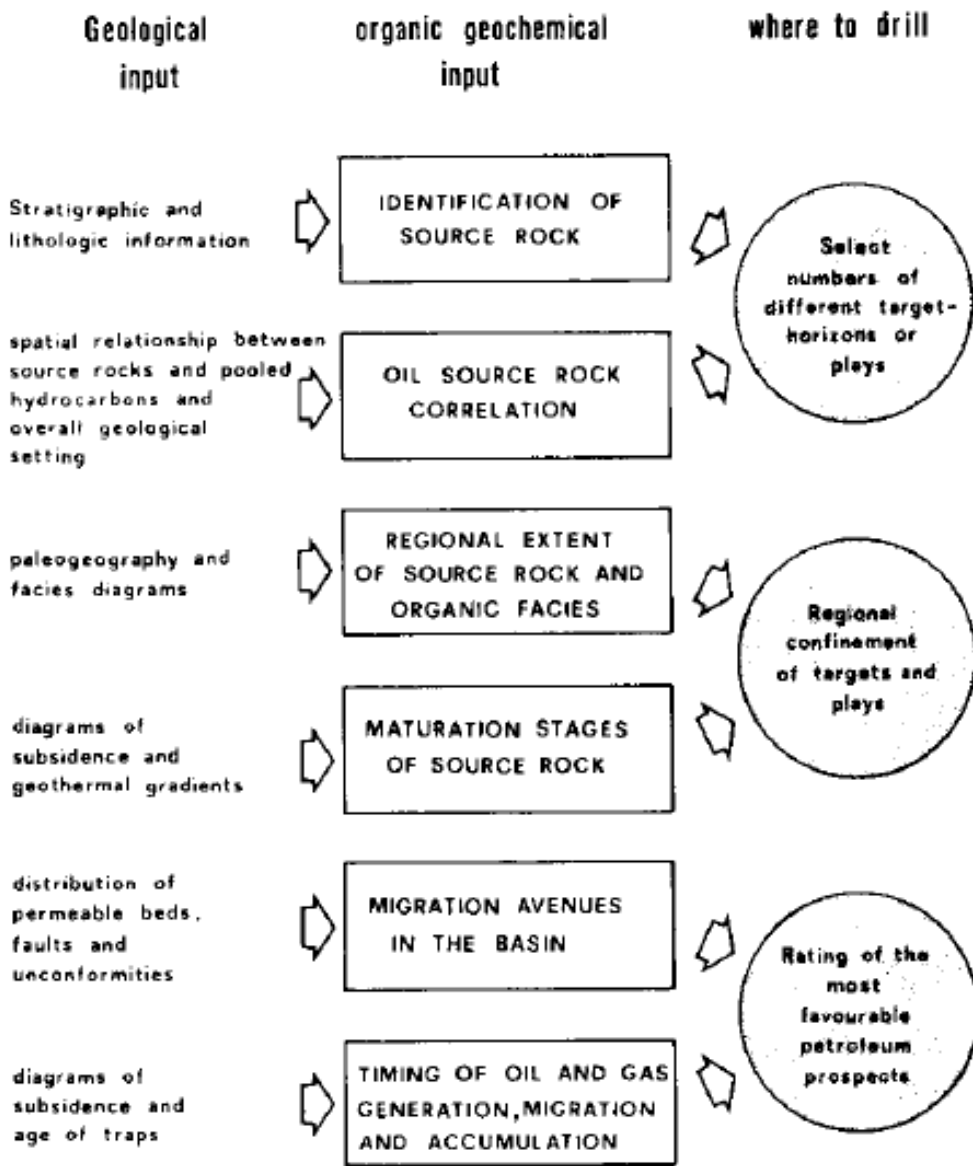


Figure 3.1.3 Adapted from Tissot and Welte, 1984, who summarized the steps that lead to the determination of the locations with high possibilities of petroleum accumulation in a basin.

Identifying source rocks and locating the main zones of oil and gas formation can be “introduced into an exploration campaign at any stage. However, it is of paramount importance that “maximum amount of information” can be gained prior to commencement of drilling, which will be verified by drilling the well(s). Indices such as vitrinite reflectance, fluorescence etc “characterize the quality and evolution stage of organic matter, they can be used as a first approach, in a semi-empirical manner for ranking of exploration targets” (Tissot and Welte, 1984). The indices do not allow for a truly quantitative evaluation of hydrocarbon

generation as a function of time, as most of them do not account for the respective kinetics of degradation of the various types of organic matter and also complex burial histories.” A more quantitative approach is achieved by using mathematical models based on kinetics of kerogen degradation and multiphase fluid flows and using computer simulation (Tissot and Welte, 1984), mainly relying on vitrinite reflectance. The relation between age and heating time of source rocks and temperature threshold of the main zone of oil generation can also be used. For a given type of organic matter, the threshold generally decreases with increasing age or heating time (Connan, 1974, 1976) of the source rock, according to an Arrhenius-type relationship.

Makhous and Galushkin (2005), listed some of the maturity level indicators currently under investigation in the industry as clay mineral assemblage (especially smectite – to illite transition features) and their crystalline polytypes, fluid inclusions, oxygen isotopic analysis, analysis of the $^{40}\text{Ar}/^{39}\text{Ar}$ age spectrum, zeolites, laumontite and mineral water indicators. Molecular transformations including biomarkers have gained some popularity, (Waples in Magoon and Dow (1994)). “The biomarker ratios most commonly used are $205/(20R + 205)$ for C₂₉ regular steranes, $225/(22R + 225)$ for homohopanes, and tri- and monoaromatic steranes,” Waples in Magoon and Dow,” (1994)). Makhous and Galushkin, (2005) mention that the using transformation ratios in minerals or biological markers are limited by the fact that the kinetic parameters are not accurately known to represent their chemical reactions.

“The combination of vitrinite reflectance, apatite fission track and present-day borehole temperature data is very useful when performing tectonic and thermal reconstructions in sedimentary basins” (Nielson, 2015). “Apatite fission track analysis is based on the annealing of fission tracks in detrital apatite crystals as a function of time and temperature. In principle, fission track data can yield detailed information on the timing and temperature of thermal events in a rock's history below about 100°-1 70°C, depending on the effective heating time (e.g., Naeser et al., 1989). The technique is thus different from other thermal indicators that simply represent the total effects of heating. In practice, however, some of the mathematical framework crucial to the interpretation of fission track data is in dispute (see Crowley et al., 1991; Naeser, 1993), and unraveling thermal histories, particularly quantitative paleotemperatures, from fission track data can be tricky. Because Rock-Eval Tmax data are abundant, much effort has been expended trying to develop a kinetic model for Tmax change. Although such models have now been published (e.g., Sweeney, 1 989, 1 990), many unsolved problems remain, largely as a result of the dependence of T max on kerogen type as well as on maturity,” Waples in Magoon and Dow,” 1994). Tmax obtained from Rock-Eval pyrolysis has also been used for modelling thermal maturation (eg. Peters, 1986). General consensus is that the maturation of organic matter depends on temperature and time, and that the process is irreversible, (Tissot and Welte, 1984). Vitrinite reflectance remains a widely accepted and commonly used thermal maturity indicator (Espitalie et al., 1988; Ungerer et al., 1990, Wood., 1988).

Table 3.1.5 lists some maturity indicators used in the industry.

Table 3.1.5 Division of thermal maturity modelling into thermal indicators and hydrocarbons. Adapted from Waples in Magoon and Dow, (1994).

Maturation of Thermal Indicators			Hydrocarbons	
Time-Temperature	Max. Temperature	Integrated Time-Temperature	Generation	Cracking
Fission track annealing	Fluid inclusions	R_o T_{max} 20S/(20R + 20S) steranes 22S/(22R + 22S) hopanes Sterane aromatization Methylphenanthrene index (MPI) Biphenyls pollen translucency Fraction of aromatic protons (FAP or PAP) ^a C-factor (IR spectrum) ^a W_{min} (IR spectrum) ^a Fraction of aromatic protons (NMR) ^a	Oil Gas	Oil to gas

3.2 Vitrinite reflectance as a thermal Indicator

Vitrinite reflectance is a commonly (Waples, 1980) used tool in quantitatively indicating thermal maturation and thus invaluable in basin modelling analysis (Hunt, 1979; Waples, 1981; Tissot et al. 1987). Initially reflected light measured from coal macerals was used for coal rank evaluation and vitrinite reflectance was used to define coalification stages (Tissot and Welte, 1984). Vitrinite reflectance has since been extended to measure reflectance of organic matter in petroleum exploration. Waples (1980) was the first to popularize Lopatin 1971's time - temperature index (TTI) method that uses vitrinite reflectance to calculate the maximum temperature attainable by sedimentary rocks in geothermal areas (Barker et al, 1986; Barker, 1989) and near igneous intrusions by Bostick and Pawlewicz (1984). Vitrinite reflectance is a method to evaluate maturation (Tissot and Welte, 1984 that is more accurate than the TTI method (Waples et al., 1992). Interpreting the thermal evolution of vitrinite depends on understanding the vitrinite formation and maturation processes that are time dependent and are vulnerable to environmental conditions such as temperature and pressure, (Sweeney and Burnham, 1987).

Vitrinite reflectance also depends on the corresponding residence time at a certain temperature which may be influenced by time-varying heating rates. Burnham and Sweeney, (1989) disagree with the findings Yukler and Kokesh (1984) that suggest that the relationship between vitrinite reflectance and oil generation is determined by heating rates. Vitrinite reflectance of "geologically simple settings start at about 0.2% near surface and increases steadily with depth" (Barker et al., (1986). According to Robert, 1988, "below about 0.4% vitrinite reflectance becomes a poor measure of thermal maturity". Vitrinite becomes increasingly anisotropic at high maturities, resulting in decreased resolution and thus exclusion of some populations from analysis. Dow, (1977) observed that the rate at which the reflectivity increases with depth, and plots of $\log R_o$ against depth are close to straight lines. According to Barker et al. (1986), vitrinite reflectance is more

sensitive as a temperature indicator because temperatures that correspond to vitrinite reflectance values of 0.1% or more coincides with the temperatures of low grade metamorphic minerals. Geological processes including thrust or normal faults, igneous intrusions, changes in Paleogeothermal gradient and unconformities have been shown by Barker et al. (1986) to affect the vitrinite reflectance profile as shown in Figure 4 below.

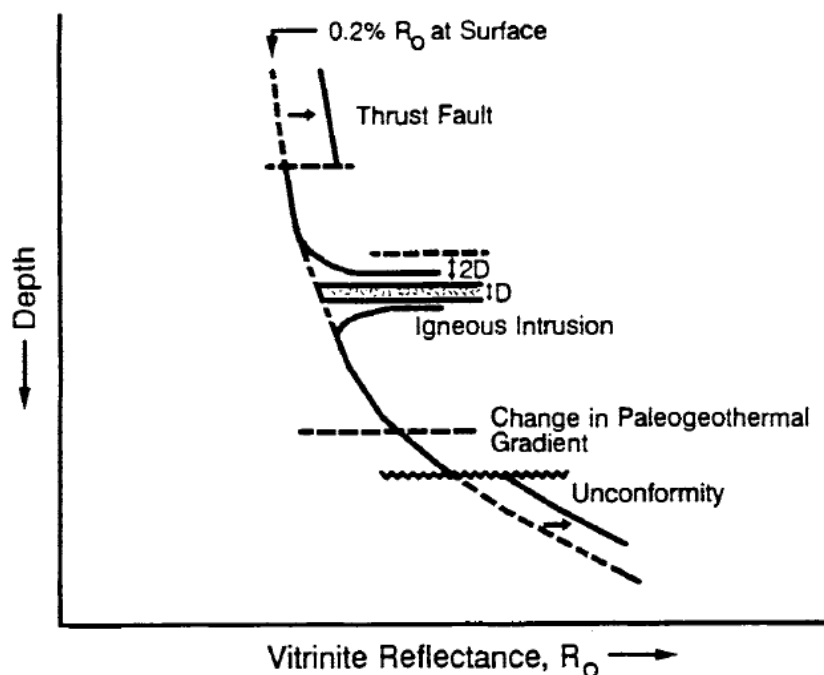


Figure 3.2.1 Adapted from Barker (1996) Geological processes that have an effect on the vitrinite reflectance profile.

Thrust faulting and normal faulting juxtapose rocks which in turn juxtaposes vitrinite reflectance data. Thrust faulting lifts the thrust zone to higher elevation shifting more mature samples from higher temperatures to shallower depths. Such an effect will be evident in a well that crosses a thrust zone when the usual trend of high values with increasing depth is broken by lower values. Normal faulting will lower the low values to high reflectivity zones. Vitrinite anomaly data shifted to deeper depths may also be induced by material that caves from shallower zones, contaminating the reflectance at the higher reflectivity zone. Erosion removes the lower range of R_o values of the lost surface and so the next sediments to be deposited on the erosional surface will show values starting with 0.2% (Barker, 1996). The profile will thus show an abrupt increase in R_o values at the unconformity. The effect of Igneous Intrusions is to induce locally, short duration, high temperature anomalies resulting in higher R_o values near dykes and sills. Barker also mentions the effect of bitumen soaking of suppressed R_o values that occurs in rocks that have elevated organic contents and hydrogen-rich organic matter. This will yield high pyrolysis values, (Barker, 1996). The vitrinite reflectance versus burial depth profile will also be strongly affected by the presence of salt, (Yu et al. 1995).

The popular method of estimating the level of maturity of organic sediments by measurement of vitrinite reflectance $R_o\%$ bases on the vitrinite ability to change its reflectance during the coalification process (Makhous and Galushkin, 2005). Maturation is approximated upon the knowledge that vitrinite reflectance is lower at the heat stage giving $R_o = 0.25\%$ and goes to $R_o = 4.0\%$ at the anthracite stage. Table 6 shows the approximate correspondence of R_o and TTI values to maturation stages. The Type of organic matter and impurities contaminating the organic material can cause the R_o values shown in Table 6 below to deviate from measured values.

Table 3.2.1. Example data (after Waples, 1984) showing $R_o\%$ values calculated by Waples (1980) then corrected by Dykstra (1987) for sediment compaction effects. This shows the relationship of the maturation stages of organic matter with the values of $R_o\%$ and TTI.

Maturation stages	Start of liquid HC generation	50% Maturation of kerogen	Maximum of liquid HC generation	End of liquid HC generation	Condensate generation	Start of dry gas generation
$R_o\%$	0.50–0.65	0.80	0.90–1.00	1.30	1.75	2.00–2.30
TTI	3–15	35	50–75	160	500	900–1600

Using vitrinite reflectance to correlate maturation is reliable only for vitrinite from coal layers and not for vitrinite sourced from terrestrial organic matter in clays with $TOC < 0.5\%$ and must be avoided for sandstones where the organic matter can be reworked or altered. (Makhous and Galushkin, 2005) warns even for terrestrial zones with R_o values over 2% where there might be influence of anisotropy throwing off the thermal history interpretation and also because there might be influence of pressure in addition to temperature and time. Also particles in lacustrine and marine rocks rarely have vitrinite of high plants and these high plants were nonexistent in pre-Devonian rocks. (Waples et al.1992) warns of low reliability of R_o values less than 0.30 – 0.40%. Vitrinite reflectance under burial conditions is influenced by more factors than just temperature and time, up to atleast the peak of oil generation from oil-prone kerogen ($R_o = 1.0$). The chemical composition of vitrinite strongly influences $R_o\%$ values (Durand et al., 1986 in Makhous and Galushkin, 2005). “Basins most likely to have oil have a greater potential of experiencing a shift of up to 0.35% in the reflectance of vitrinite,” (McCulloh, 1979c Makhous and Galushkin, 2005).

Calculating Vitrinite Reflectance (The TTI method)

Using calculated Time-temperature Index (TTI) to estimate vitrinite reflectance was proposed by Lopatin (1971). It is assumed an effective reaction with a rate doubling at every 10°C increase replaces all chemical

reactions describing the vitrinite maturation process. “TTI value is determined by the temperature T(t) in °C of a rock during its burial (Lopatin, 1971; Waples, 1980);

$$TTI = \int_{t_0}^{t_1} 2^{F(T)} \cdot dt \quad (18)$$

T is the time expressed in Ma, $t = t_0$ is the time when the rock was deposited at the surface, $F(T) = n - 10$ for $10 \cdot n \leq T \leq 10 \cdot (n + 1)$ °C so that $F(T) = n - 10$, and then TTI can be expressed as;

$$\frac{1}{2^{10}} \int_0^t 2^{(T(t')/10)} \cdot dt \quad (19)$$

where n is an integer part of (T/10). For the equation above to be usable in maturation estimation it has to be calibrated with measured data such as vitrinite reflectance. Using Waples (1980; 1984) correlation of TTI values with Ro data for more than 300 wells in different zones of the world, Kalkreuth and McMechan (1984) and Kalkareauth and Macauley (1984) made the following formulation to show the relationship between TTI and Ro values;

$$Lg(Ro\%) = -0.4769 + 0.2801 \times Lg(TTI) - 0.007472 \times (Lg(TTI))^2 \quad (20)$$

Lg is a decimal logarithm.

The above equations are commonly used despite inaccurate assumptions used by Waples in his calculations.

Thermal decomposition of the chemical complex kerogen material forms many by-products, each due to different activation energies. Rocks have different types of organic matter including vitrinite. Distinct kinetic parameters E and A characterise the vitrinite in a particular rock. The cracking reactions that occur are mainly affected by temperature in time, which determines the temperature at the initialization of catagenesis although it has a lesser effect on the start of the gas formation stage (Tissot and Welte, 1984).

Rock Eval Pyrolysis method applied to evaluating the genetic potential of source rocks

Rock-eval pyrolysis method developed by Espitalie (1977) enables source rock characterization and evaluation. The resulting S1 curve and corresponding values provides the amount of hydrocarbons present in the rock in a “free or adsorbed state”. S2 gives the hydrocarbons and hydrocarbon-like compounds generated from pyrolysis of kerogen. The pyrolysis S3 represents volatiles containing oxygen such as carbon dioxide, this zone is measured in a limited temperature interval so that only carbon dioxide from the kerogen will be represented by the S3. Tmax represents the temperature at which the maximum hydrocarbons were generated

during pyrolysis and is used for the maturation stage. The hydrogen Index (S_2 /organic carbon) and the Oxygen Index (S_3 /organic carbon) are used to characterize the type of kerogen. The hydrogen/Oxygen indices are independent of the organic matter and are strongly related to the elemental composition of kerogen, (Tissot and Welte, 1984). The hydrogen index and the H/C ratio as well as between the oxygen index and O/C ratio were found to have a good correlation. This enables the hydrogen index and the oxygen index to be plotted instead of the van Krevelen diagram and be interpreted the same way (Tissot and Welte, 1984), as shown in Figure 3.2.2 below;

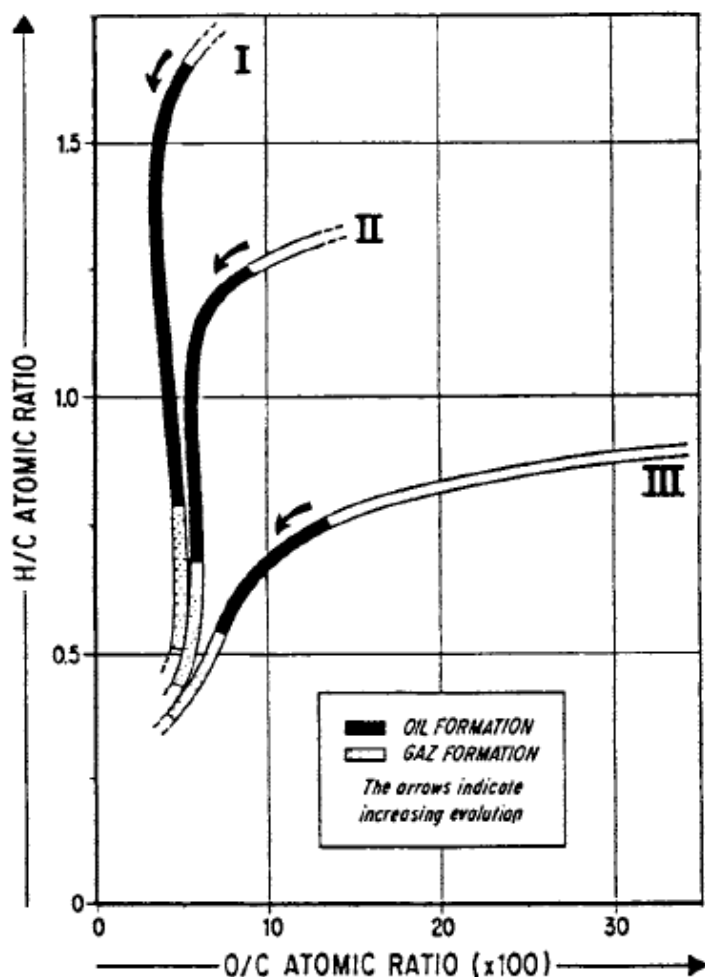


Figure 3.2.2 Adapted from Tissot and Welte, (1984). Elemental composition changes of different kerogen types with varying levels of maturity. The diagram shows the three main evolution paths.

Pyrolysis can be used to give a semi quantitative evaluation of the genetic potential of source rocks. The Rock Eval pyrolysis technique includes the initial progressive heating of a sample to 550°C in an inert atmosphere, using a preselected rate of heating. ‘The quantity S_1 represents the fraction of the original genetic potential which has been effectively transformed into hydrocarbons. The residual potential is given by the S_2 quantity which describes the genetic potential that remains and has not been used to generate hydrocarbons. The

genetic potential is then given by $S1 + S2$, given in kg hydrocarbons per ton of rock. This represents the abundance and type of organic matter (Tissot and Welte, 1975).

The plot by Espitalie et al. (1977) (Figure 5) of the oxygen index against hydrogen index allows the distinction between an immature rock with a low generation potential from a more mature rock that originally had elevated genetic potential. Transformation ratio and /or peak temperature T , are possible indicators of thermal evolution.

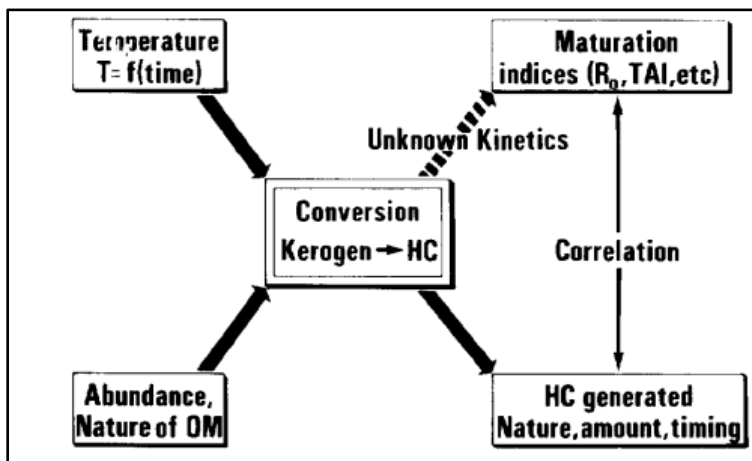


Figure 3.2.3. Adapted from Tissot et al. 1987 shows the conversion of kerogen to oil and gas in the subsurface is most sensitive to temperature effects in time.

Conversion of kerogen to oil and gas is a chemical reaction controlled by nature and the amount of the kerogen, temperature and pressure. The combined effects of these parameters account for most of the petroleum generated in sedimentary basins. Chemical reactions that alter the nature of the maturation indices are controlled by chemical kinetics on kerogen thus determining the amount of hydrocarbons that can be generated by the kerogen.

Genetic Potential and Transformation ratio

Transformation ratios gives information on the fraction of convertible kerogen converted at a given time and temperature. (Tissot and Espitalie, 1975) used calculated transformation ratios for Type III kerogen to relate it to vitrinite reflectance using empirical data.

A petroleum source bed will consist of bitumen (a soluble organic matter) and kerogen (an insoluble organic matter). An active or potential source rock must contain kerogen. Source rock analysis includes establishing the kerogen type and composition of the solvent extractable hydrocarbons and non-hydrocarbons. Optical

and/or physiochemical properties allow the determination of the evolutionary stages of kerogen (or maturation of source rocks). The amount and type of kerogen and bitumen and the stages of maturity gives the source rock quality (Tissot and Welte, 1975).

The nature of the organic matter and the temperature history in time, and of lesser importance pressure determines the temperature corresponding to the thresholds and the volumes of hydrocarbons generated, during the evolution stages of kerogen in hydrocarbon formation (Tissot and welte, (1984), as shown in Figure 3.2.3. The genetic potential and the transformation ratio were used by Tissot and welte, (1984) to evaluate the influence of the kerogen composition and of the catagenesis intensity. The genetic potential of a particular formation gives the amount of oil and gas that can be generated by the kerogen when exposed to enough temperature during a sufficient interval of time. The potential depends on the type and concentration of kerogen which depends on the formation history of the kerogen. “A quantitative evaluation of the genetic potential can be made on the basis of a standard pyrolysis technique Espitalie et al., (1977),” (Tissot and Welte, 1984). The genetic potential of a shallow immature petroleum source rock is equivalent to the total oil and shale volumes generated by an oil shale upon pyrolysis depending on if the organic richness is sufficient (Tissot and Welte, 1975).

The transformation ratio is controlled by the nature of the organic material and the geological history mainly controlled or affecting the temperature history. The transformation ratio is described as the ratio of oil and gas that the kerogen is capable of generating otherwise the bitumen ratio can be used to estimate the transformation ratio but only until before the wet gas zone is reached (Tissot and Welte, 1975).

4.0 Kinetics

4.1 Introduction

Chemical kinetics are responsible for hydrocarbon yields from kerogen in organic matter in sedimentary basins and the changes observed in maturation indices such as optical and pyrolytic indices. Geological conditions, the concentration of the available kerogen, temperature and pressure that are prevailing in a particular zone in time control changes resulting from complex alterations of the structure and composition of kerogen. The complex alterations that occur during kerogen transformation make it difficult to clearly know these changes. Temperature has been shown to be the most sensitive parameter, (Tissot et al.1987). In theory (Wood, 1988), the Arrhenius equation is an expression that determines the rate at which the concentration of convertible kerogen reduces with time (Connan, 1974). The rate of the chemical reaction has an exponential dependence on the prevailing temperatures (Connan, 1974), and the chemical reaction is influenced by the exponential factor, A and the activation energy, E kinetic parameters. The two kinetic parameters are obtained experimentally for each kerogen type (Snowdon, 1979). The exponential factor must be independent of the temperature in the range of temperatures that occur in the sedimentary basins (Wood, 1988). For the same pre-

exponential factors for all bond types, changes in activation energy as small as a few kilocalories per mole can lead to major differences in the temperature and timing of hydrocarbon generation. For varying pre-exponential factors vary among the bond types, it is more difficult to make general comments about sensitivity.) Thus, in comparing kinetic parameters for different models, one must look at both the pre-exponential factor and the activation energy. Different kinetic models can predict similar generation trends over a range of geologic conditions but only for similar activation energies and pre-exponential factors are, (Waples in Magoon and Dow, 1994).

Two of the mainly used techniques are the Lopatin method and the method based on the Arrhenius equation. “The *“Lopatin method”* relies on geological calibration using data from well-understood basins. The other group of methods is better grounded in chemical kinetics, but is calibrated using the kinetic parameters A and E derived from laboratory pyrolysis studies,” (Barker, 1996). In 1971 Lopatin (Wood, 1988) observed that there are fundamental differences between the methods. Wood, (1988) reveals that the Lopatin typically “underestimates the level of thermal exposure at low heating rates relative to thermal maturity levels estimated by Arrhenius equation.”

Wood (1988) summarized the empirical and theoretical relationships which are the basis for establishing the level of thermal exposure and the extent of petroleum generation as;

1. Waples (1980) developed the TTI scale and (Royden et al. 1980) developed the C scale base on the Lopatin (1971) assumption of a reaction rate of kerogen that almost doubles for every 10°C rise in temperature.
2. The Arrhenius equation theoretically expresses the exponential dependence of the rate of a chemical reaction on temperature (Connan, 1974). The evaluation of the equation requires values for two kinetic parameters that must be obtained experimentally for each kerogen type (Snowdon, 1979): a pre-exponential factor, A (it must be independent of the temperature in the range of the temperatures experienced by sedimentary basins), and the activation energy, E.
3. Pyrolysis experiments results have shown that kerogen degradation follows first order rate equation (Tissot, 1969). This implies that the concentration of convertible kerogen (X_0) falls exponentially with time at a rate determined by the Arrhenius equation (Connan, 1974c; but cf. Price.1983).

Tissot and Espitalie, 1975, Tissot and Welte, 1978) simplified that matter by establishing the chemical kinetics for three broad groups of kerogen types: Type I, II, and III. The groups are established based on the atomic H/C and O/C ratios of kerogen and distinctive trends toward low H/C and O/C ratios that they follow on a van Krevelen diagram during progressive stages of organic metamorphism. Kerogens of the same type may show very different chemical kinetics (Lewan, 1985). This complicates the detailed application of this method to frontier basins, (Wood, 1988).

The total volume and composition of hydrocarbons in the reservoir can be computed when the total thermal exposure during the time of burial including during migration and the oil cracking process while in the reservoir are taken into account (Waples in Magoon and Dow, 1994). Modeling thermal evolution of sedimentary rocks thus involves a combination of kinetics describing thermal maturation process, burial history and thermal history through time. Tissot and Espitalie first introduced the principles of kinetics to models in 1975. Well sample data is used as control points to constrain the model when extrapolating from present day to find representation of geologic and thermal events in time (Barker, 1996). This is a good representation of the area but to go further and build 2D and 3D models requires carbon contents and permeabilities. Kinetics is the driving mechanisms in converting kerogen to bitumen and carbon residue. It was found that the rate of change of kerogen at constant temperature is dependent on the quantity of kerogen remaining, which can be presented as;

$$dV/dt = k(V_0 - Vt)^n \quad *k \tag{21}$$

where k is a rate constant and n is the order of reaction.

Petroleum generation and maturation reactions are treated as first order reactions. K remains constant as long as the temperature remains constant. However as petroleum generation really occurs under burial conditions of non - isothermal conditions, k is better approximated by the Arrhenius equation as;

$$k = A.e^{[-E/RT]} \tag{22}$$

A is the frequency factor, where E is the activation energy. E is the energy to be surpassed to produce hydrocarbons from kerogen which depends on the bond type. R gives the gas constant and T is the absolute temperature. Lopatin found the rate of oil generation to double at every 10°C temperature increase. As the temperature increases kerogen is used up at accelerated rates.

$$V = V_0.exp. (-kt) \tag{23}$$

The equation calculates the rate of consumption of the kerogen. V_0 is the initial amount of kerogen, whereas V is the amount that remains after time t.

4.2 The first Kinetic models

The Lopatin Method

The Lopatin method proposed in 1971 is a calibrated method to determine the depth of onset of petroleum generation, and limits for oil and gas condensates. The discovery of this method heightened the use of thermal modeling to calculate thermal maturity. The effects of time and temperature were first realized when scientists

investigated coalification and effectively the maturation process. Luis and Tissot introduced the first model of petroleum generation from kerogen in 1967 which Tissot went on to describe in 1969. Lopatin established that the maturation process has an effective heating time which is the time spent at temperatures above 100°C. Hood et al. 1975 in (Barker, 1996) described the “Level of Organic Metamorphism” as the time spent within 15°C of the maximum temperature plus that maximum temperature. This gives the oil generation and destruction levels which were found by Lopatin to be equivalent to a petroleum generation reaction rate that doubles for every 10°C increase in temperature. Use of this method incorporates using studied data from known basins as calibration of thermal maturity indicator data. This allows the positioning of the start, end and peak oil generation times as well as the oil window and the upper limits of the different hydrocarbons. Since this method requires that a reference temperature be set, Lopatin chose the reference interval to be between 100°C and 110°C. Thus the rate of reaction will double when the temperature is 10°C above the reference. From this a temperature factor could be defined for each interval n so that;

$$g = r^n \quad (24)$$

r being 2.

The amount the organic sediments matures by in every 10°C temperature increase, is directly proportional to the time spent in that interval, but varies as the nth power of the temperature.

$$\Delta Maturity = (At_i)(r^{ni}) \quad (25)$$

where i represents the ith interval.

All the maturations achieved at every 10°C interval are summed to give the total maturity, termed the Time Temperature Index (TTI) by Lopatin. This can be achieved through a plot of burial depth versus age and an estimate of the geothermal gradient through time. The cumulative TTI obtained is compared to calibration data from well-studied basins, equating the cumulated TTIs to maturity indicators such as vitrinite reflectance or TAI, to give organic maturity. The r is almost always equal to 10°C. Waples calibrated r by vitrinite reflectance and equivalent TAI data. It gives the time levels of hydrocarbons occurrence. This method does not distinguish between uplift and burial except for accelerated reduction in temperature factors during uplift. Other researchers have used different values of r and ΔT trying to overcome the limitations of the Lopatin method. The best calibration is achieved when using closely related geologic settings. Two processes that move the oil window to shallower depths are initially rapid sedimentation followed by a rate that slows down in time or maturation of rocks at a constant depth and temperature. Thus the faster the sedimentation rate, the deeper the oil window. Estimation of the oil window position on uplift is slightly more complex as the link between the generation rate and the oil window is not very obvious as generation steadily decreases on uplift. The Lopatin method is useful when there is limited geological data and for simplicity. It is most reliable at

lower maturity levels although it seems to overestimate the role of time (Bustin, 1989) and underestimate the effect of temperature (Quigley and Mackenzie, 1988). The underlying assumption of a doubling reaction rate every 10°C is less valid at higher temperatures. “The Lopatin method only provides a rough guide to the depth and timing of the oil floor and the onset of gas generation. In general it does not work well for the extremes of sedimentation rate, and results can be unreliable for young basins with high geothermal gradients, or old basins with low geothermal gradients, (Barker, 1996).

Although vitrinite reflectance provides the most reliable kinetic data, Makhous and Galushkin (2005), discusses the uncertainties that result from these measurements from different sources induced by factors other than temperature and time during burial. The use of biomarkers as kinetic indicators is limited by uncertainties introduced by the complex chemical reactions that they undergo (Abbot 1990 in Waples 1991). Uncertainties in the thermal conductivity estimates for basin modeling can also be due to inaccuracies from completions or other log information assessments (Makhous and Galushkin, 2005). Furthermore, thermal modelling is subjective as it depends on the individual performing the modelling and their interpretation of geologic data also upon which basin modelling program they use. Additional discrepancies can result from heat flow equations, thermal parameters, boundary conditions and calibrations to well data. Uncertainties when dealing with fluid movements arise from applying hydraulic and paleohydrologic techniques. “Absolute maturity cannot be judged without independent knowledge of kerogen composition”, (Makhous and Galushkin, 2005).

Kinetic Model of Tissot (1969) to Tissot and Espitalie (1975) / Ealier Models

The model proposed by Tissot in (1969) and later discussed more fully by Tissot and Espitalie (1975) was the first hydrocarbon generation model to explicitly account for both time and temperature variations through first order kinetics. Modelling as defined by Tissot (1969) and Tissot and Espitalie (1975) considers 21 parameters in the model algorithm. The first six independent first order reactions describe the breakdown of kerogen. The cracking of oil to gas is described by one first order reaction. This gives 7 values of activation energies and 7 values of frequency factors. 7 more values are contributed by each kerogen component’s capability to generate oil. Within this is factored in the possibility of the oil to convert to gas. The model of Tissot and Espitalie (1975) (see schematic in Figure 7) was “calibrated on the maturation of Type III kerogen so that the Transformation Ratio (TR) $X = 0.5$ (50% TR of kerogen) corresponds to the end of liquid hydrocarbon generation ($R_o = 1.3\%$),” (Makhous and Galukshin, 2005).

The Lawrence Livermore Laboratory (LLNL) follows a similar concept but additionally considers the chance that the kerogen also directly forms gas. The LLNL additionally has multiple values of E and assumes only

one value of A. The differences in activation energies between the IFP and LLNL models are largely compensated by the differences in pre-exponential factors, resulting in similar predictions about oil generation for most geologic histories,” (Waples in Magoon and Dow, 1994). Choosing a particular kinetic model (e.g., LLNL or IFP) for correctly identifying type I, II, or III kerogen would be unlikely to affect exploration decisions, (Waples, 1992). The S₂ peak generated from thermal maturation of organic matter in potential source rocks gives the distribution of the E and A values. A single pair of E and A values can be used to estimate kinetic parameters for Type 1 kerogen to give maturity levels similar to those estimated by the geology. Preferred is obtaining a range of E and A pair values from different heating rates. This requires the fit of pyrolysis data by a range of E values. The Lopatin assumption of the reaction rate doubling every 10°C results in a much lower global value than for any single reaction. A and E values estimated from geological values, taking advantage of their linear relationship of the E to log A requires reliable thermal history. The kinetic parameters are most commonly obtained from laboratory pyrolysis. There are concerns that the high temperatures that are achieved in such short times might be following different reaction mechanisms. A wider temperature range is achieved in natural geological setting than is achieved in the laboratory.

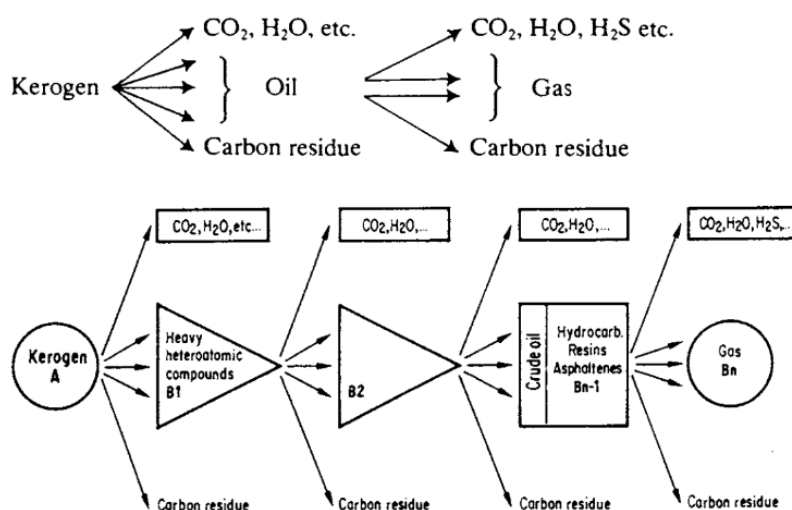


Figure 4.2.1. Kerogen degradation process used by Tissot and Espotalie (1975) in the kinetic model. The model considers gas to result from oil cracking.

The process of identifying the kerogen types is done so as to model hydrocarbon generation but this can present problems in modeling hydrocarbon generation. Waples et al. (1992) have shown that normal errors in estimating the proportions of standard kerogen types II and III in a typical mixed-type kerogen can lead to important differences in modeling results. They also showed that incorrectly identifying a high-sulfur Monterey-type kerogen (type 11-S) as a standard type II kerogen (or vice versa) could lead to significant errors. The same cautions probably apply to a variety of other nonstandard kerogens, such as high-wax or resin-rich types, (Waples in Magoon and Dow, 1994).

“The kinetics of gas generation from kerogen has received less attention than that of oil generation. Most models have either ignored gas generation or have included it almost as an afterthought, assigning it the same kinetics as oil generation. The total amount of hydrocarbons generated is then simply partitioned into oil and gas according to a predefined ratio for each kerogen type (e.g., Burnham, 1989; Burnham and Braun, 1990; Burnham and Sweeney, 1991). Use of compositional kinetic models should improve our ability to predict gas generation,” (Waples in Magoon and Dow, 1994).

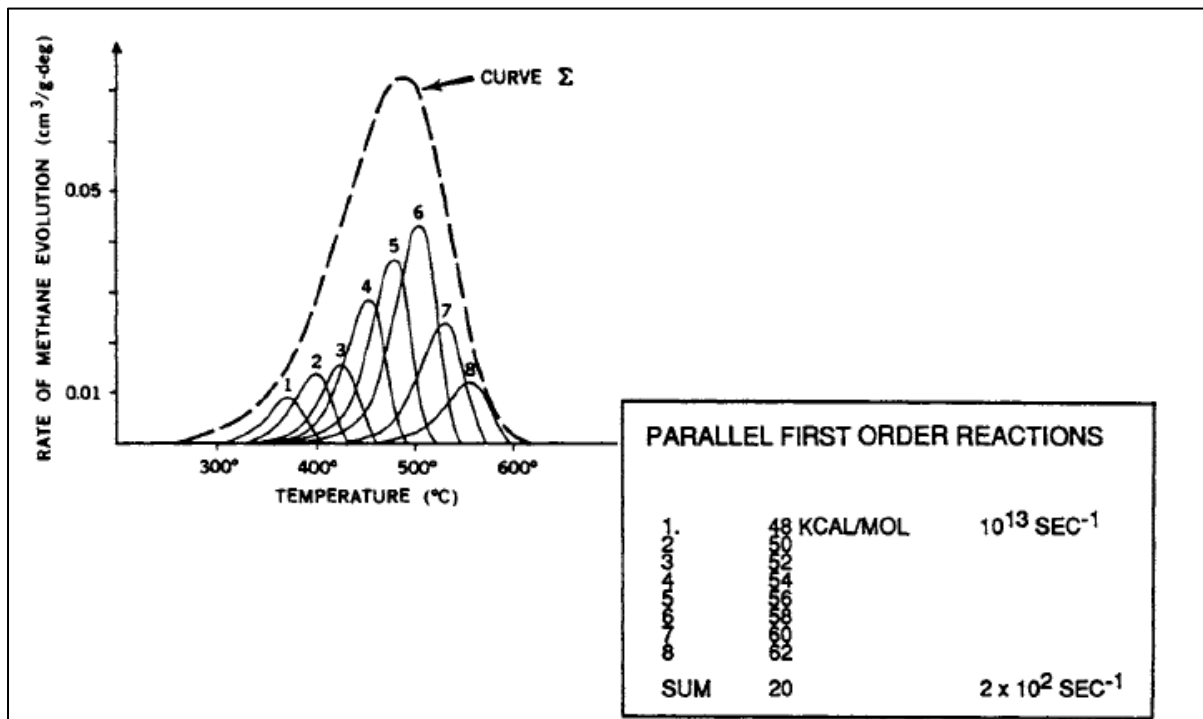


Figure 4.2.2. Bitumen production curves for 8 individual, first order reactions with varying activation energies, and the total evolved bitumen curve. Adapted from Barker (1996).

For simplicity some earlier models assumed the kinetic reactions of petroleum generation to be a single reaction and so used ‘global values’ of a single pair of A and E values. Figure 4.2.2 adapted from Barker,(1996) shows the rate of generation of products (of methane) for eight parallel first order reactions together with the cumulative curve. The result was an unchanged value of A and despite the varying ranges of activation energies of 48 kcal/mol up to 62 kcal/mol for individual reactions, the ultimate pseudo-activation energy (the "global" value) is only 20 kcal/mol.

The Arrhenius Equation

The Arrhenius equation theoretically expresses the exponential dependence of the rate of a chemical reaction on temperature (Connan, 1974). The evaluation of the equation requires values for two kinetic parameters that

must be obtained experimentally for each kerogen type (Snowdon, 1979): a pre-exponential factor, A (it must be independent of the temperature in the range of the temperatures experienced by sedimentary basins), and the activation energy, E. (Snowdon, 1979) observed that selecting appropriate values or ranges for the pre-exponential factor (A) and the activation energy (E) were a major problem encountered when directly applying the Arrhenius equation to modelling thermal maturation. Their evaluation of published A and E values for the generation of petroleum products and related by-products during the degradation of kerogen returned results of positively correlated values that generally fall within the ranges of $E = 100\text{-}300\text{kJ/mol}$ and $\log e A = 40\text{-}80/\text{m.y.}$ These are consistent with the formation of petroleum from kerogen by a series of sequential component reactions with similar mechanisms (Wood, 1988). The components formed at low temperatures have lower A and E values than the later formed components.

Kerogen is a chemically complex material that thermally decomposes to form many by-products, each controlled by different activation energies. Tissot and Welte (1984) observed that significant amounts of kerogen have to be converted to liquid hydrocarbons prior to the commencement of expulsion and primary migration processes of hydrocarbons. From this they concluded that the mean value of the frequency distribution of activation energies is adequate to use to model thermal maturity of a certain kerogen. Wood, (1988) had theorized that the low E values of $50\text{-}60\text{kJ/mol}$ found by (Connan, 1974) for the 11 basins worldwide represent values for the earlier formed components and not the complete crude oil generation. His suggested theory, he found is supported by the findings of the newer hydrous pyrolysis technology. Using a single set of kinetic parameters induces bias by sticking to the mean value as it ignores the effects resulting from the early and late forming components from a specific kerogen (Wood, 1988). The result is a narrower petroleum window than when applying a series of parallel reactions. Early formed products of kerogen are devoid of petroleum and do not have sufficient volumes to migrate. Using the Arrhenius equation, a single set of kinetic parameters is able to accurately model the peak stage of generation which excludes the earlier products of kerogen decomposition. The late products are typically decomposed to gas and so only have a small percentage of the products that would have formed at peak conditions (Wood, 1988). First-order Arrhenius equations with a single activation energy are chemically unrealistic and show the failure of using an Arrhenius-reaction approach with a single activation energy to adequately describe the maturation process (Barker, 1989).

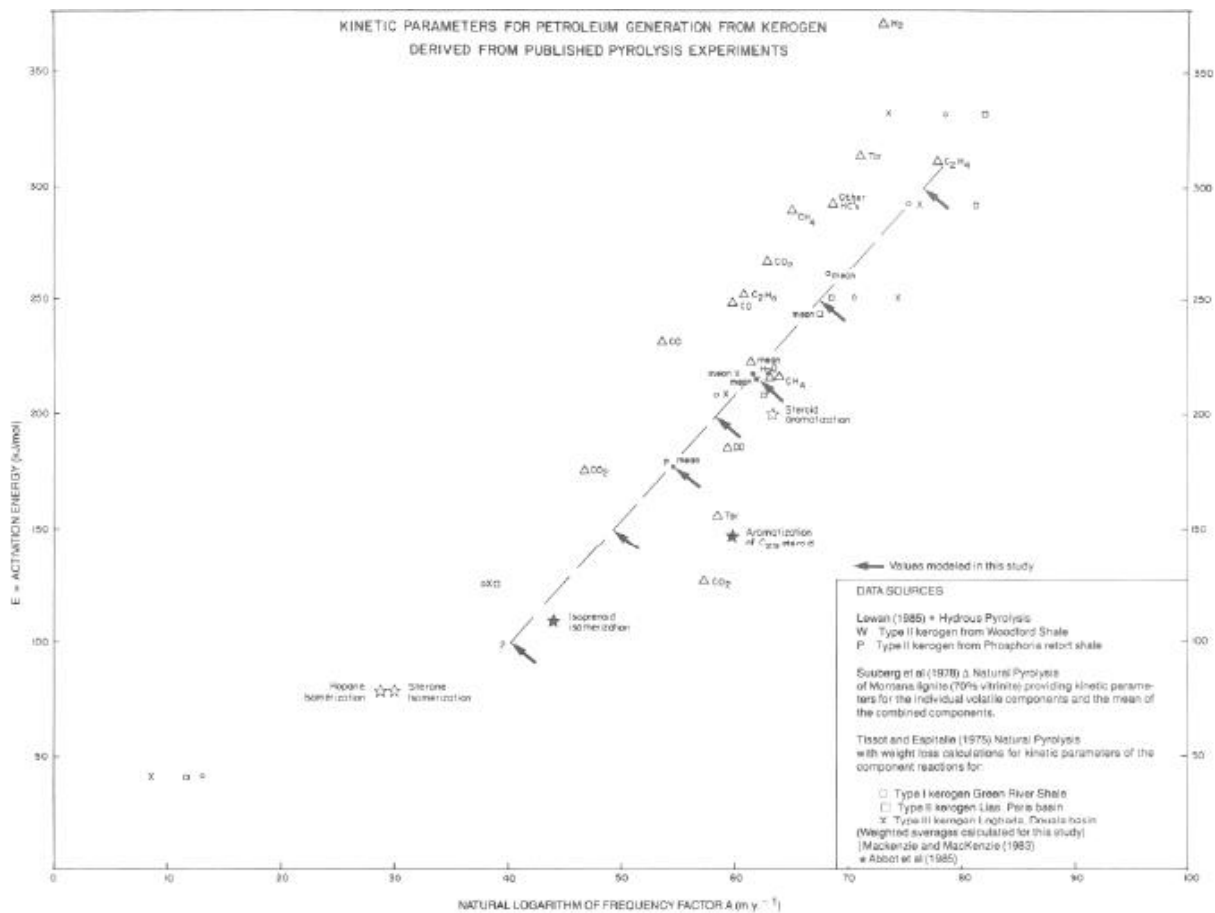


Figure 4.2.3 above adapted from (Wood, 1988) had been produced by plotting the “kinetic parameters calculated from sediment extracts (McKenzie & McKenzie, 1983) and those obtained experimentally (Abbot et al.1985) for specific steroid aromatization and hopane and sterane isomerisation reactions. The steroid aromatization reaction has kinetics closest to the mean kinetics for kerogen degradation indicated by other studies.”The result shows that biochemical maturity indicators have kinetics that follow the same trend as the kerogen degradation reactions.

The mean A and E values for Types I and II kerogen calculated by Tissot and Espitalie (1975) for the components reactions were found to be lower than values of Type II and III kerogens from other studies (Wood, 1988). Pressure is considered to be of relatively lower importance for Type I and Type II kerogens whereas the higher oxygen content of Type III kerogens such as vitrinite seems to need data at high pressures in order to derive rate constants that are correct and effective, (Burnham and Sweeney, 1989). Tissot and Espitalie, (1975) found a “close relationship between vitrinite reflectance and the transformation ratio calculated for their Type III kerogen using a combination of component reactions.” Tissot and Espitalie, (1975) define X_o a total amount of hydrocarbons that can be formed by a certain kerogen depending on if it is heated to a high enough temperature in enough time;

$$x_o = \sum x_o \tag{26}$$

This is equivalent to the genetic potential of the kerogen. The resulting value is controlled by the original composition of the kerogen. The transformation ratio r , is a measure of the stage of evolution giving the ratio or fraction of the kerogen (Tissot and Espitalie, 1975). This gives the relation of X_o and the transformation ratio as;

$$r = \frac{\sum x_{i0} - \sum x_{io}}{\sum x_{io}} = \frac{x_o - \sum x_i}{x_o} \quad (27)$$

“The transformation ratio is zero at shallow depths and progressively increases to 1, reached when all liable organic material has been expelled leaving a carbonaceous residue.

“Lerche, et al, 1984 showed that the change in vitrinite reflectance with depth is due to the thermochemical decrease in number density of molecules, which can be approximated by a first order reaction process,” in Wood, (1988) but because different types of vitrinite reflectance change their reflectance at different rates during the same time-temperature history (Lewan, 1985), different vitrinite reflectance data from different basins will probably not be accurately modelled by applying the Arrhenius equation.

Vitrinite values corresponding to the critical temperature of 10-30C below which there will not be maturation of vitrinite as suggested by Lerche, et al, 1984 are 0.35-0.4%. Based on this (Wood, 1988) deduced that accumulated TTI values calculated based on the Arrhenius equation with the proper kinetic parameters should closely correlate with vitrinite reflectance. Accordingly the total cumulative TTI value of 0 will correspond to a vitrinite reflectance value of approximately 0.35. Burnham and Sweeney, (1989) observed that the effective mean activation energy for vitrinite maturation close to the oil window approached 50kcal/mol for oil generation, a result they found agreed with that of Larter (1989). After evaluating oil generation with vitrinite and having compared with previous results using biomarkers, Burnham and Sweeney, (1989) concluded that the Arrhenius Equation with an activation energy distribution was a superior approach.

4.3 More recent thermal maturation models

Introduction

Several workers have developed models to simulate the vitrinite maturation process in basins. “Thermal maturity models were established on similar basic concepts but will yield different results when estimating thermal exposure in certain burial histories. There is not much published comparison studies of the application of thermal maturity models to different sedimentary basins,” (Wood, 1988).

(Tissot et al.1987) categorized the various available models as follows;

- 1) Models developed by (Price, 1983; Barker and Pawlewicz, 1986) where vitrinite maturation only depends on temperature).
- 2) Models by (Hood et al. 1975; Bostick et al.1978; Barker, 1989) in which time is a controlling factor.
- 3) Models by (Middleton, 1982; Anita, 1986; Wood, 1988; also Barker, 1989) in which vitrinite maturation is an Arrhenius first order chemical reaction having a single activation energy.
- 4) Models by (Lerche et al., 1984; Armagnac et al., 1989, he includes Waples, 1980 and Ritter, 1984) in which vitrinite maturation is an Arrhenius first order chemical reaction having a single activation energy but the activation energy is a function of temperature.
- 5) Models by (Larter, 1988) in which vitrinite maturation with parallel Arrhenius first order chemical reactions are described with a Gaussian distribution of Activation energies.

Models in the first category simulate the dependence of vitrinite reflectance on temperature and the second group models time dependence, while the third to 5th group models show a dependency of models on the Arrhenius. Models in the first to 4th groups are empirical but the first two groups have to depend on frequently poorly constrained maximum temperature estimates when applied to geological settings (Tissot et al.1987). Those in the third and fourth group suffer the limitations of applying a single reaction which is not enough to accurately model complex reactions over wide ranging temperatures and heating rates (Braun and Burnham, 1987 in Sweeney and Burnham, 1990).

Comparing kinetic models; Some Examples

In this section a brief description of the newer available kinetic models is given but ultimately this section compares other models (the older model TTI and the latest available model the Basin%Ro) to the now widely accepted to be better Easy%Ro model. The Pepper and Corvi (1995) model is included as an alternative.

Evolution from the Vitrimat system (Burnham and Sweeney [1989]) to the Easy%Ro (Sweeney and Burnham [1990])

Advancement to kinetic models of vitrinite maturation allowed more accurate calculation of Ro than the TTI method. According to these models the, process can be described by n independent first order Arrhenius reactions, equation (22), (Makhous and Galushkin, 2005).

In the vitrimat system of Burnham and Sweeney [1989] 35 parallel reactions controlling the expulsion of water, carbon dioxide, methane and more heavy hydrocarbons are considered. Sweeney and Burnham [1990]

then developed a more accurate system (Easy% R_o) than the Vitrimat system to describe vitrinite transformation by 20 parallel reactions with a single frequency factor A, (Makhous and Galushkin, 2005).

The Easy% R_o developed by Sweeney and Burnham, (1990) is widely used (Nielson, 2015) to model the maturation of vitrinite with increasing time and temperature. This is a simplified Arrhenius reaction version of the Vitrimat model by Sweeney and Burnham, (1987), that incorporates a distribution of reaction energies representative of the involved chemical reactions. The Vitrimat was proposed to overcome the shortcomings of the previous models such as the use of activation energies that are also functions of temperature as in the Armagnac et al.(1989) model, or the Larter (1988) chemical kinetic approach which limits the correlation of vitrinite reflectance and the eventual chemical changes to the range of the oil window with a range of vitrinite reflectance values between 0.5 and 1.3%. With the use of a distribution of activation energies Larter, (1988) was able to establish that vitrinite reflectance is a stronger dependence on temperature than time. The Easy% R_o utilises an Arrhenius first-order parallel reaction approach that has a distribution of activation energies. The reaction energies are representative of the involved chemical reactions which allows for application of heating rates of 1C/week in the laboratory to 1C/10m.y. in slow subsiding geologic basins. Although, “Burnham and Sweeney, (1989) found that for reasonable Arrhenius models, the relationships between oil generation and vitrinite reflectance is independent of heating time.” TTI correlation applies only when % R_o values are greater than 0.4. Sweeney and Burnham, (1990) calibrated the Easy% R_o based on the chemical properties of coal vitrinite. It allows the formulation of a vitrinite vs time profile for a certain stratigraphic level, provided the time-temperature history for the level has been estimated or is known. The Easy% R_o can also be used to compute profiles of the percent of vitrinite reflectance with depth on multiple stratigraphic levels, which will be compared with well data and used to optimize thermal history models. Easy% R_o applied to vitrinite reflectance values of 0.3 to 4.5% will model the thermal history incorporating non-deposition, uplift and cooling and heating rates that vary with time, and provide the results in % R_o –depth data (Sweeney and Burnham, 1990).

Integrated in the Vitrimat model are the chemical kinetic equations over time and temperature to account for the (elimination) expulsion of water, heavy hydrocarbons, carbon dioxide and methane from vitrinite. The calculated compositions can then be used to determine H/C and O/C atomic ratios and carbon content. Vitrinite maturation being due to reactions that have a wide range in reactivity was stated as the reason for the observed correlation of the logarithm of % R_o (in the Vitrimat and earlier experiments), with the maximum temperature exposure (Sweeney and Burnham, 1990). “For a distribution of parallel reactions with equal stoichiometric factors, the extent of reaction is a linear function of temperature for a given heating time or rate. Thus % R_o is exponentially related to the overall extent of the reaction,” (Sweeney and Burnham, 1990). With some adjustments of the stoichiometric factors of Easy% R_o a similar trend of the approximate non-linear variation of % R_o with maximum temperature experienced in Vitrimat was reproduced in the Easy% R_o .

to have the same results of the %Ro. Easy%Ro includes a calibration to the correlation that uses the H/C and O/C atomic ratios of residual vitrinite to match with geological observations. The end result was an Easy%Ro with activation energies in the range of 34 to 72kcal/mole that are an approximate match to those used to describe oil and gas generation albeit their range is wider. The Vitrimat and the Easy%Ro compute over a range of vitrinite reflectance values between 0.3 to 4.5% and for heating rates of 1C/week in the laboratory, 1C/day in igneous intrusions, 10C/100yr in geothermal systems, to 1C/10m.y. in slow subsiding geologic basins. Easy%Ro returns equivalent results to the Vitrimat but with the advantage that Easy%Ro is computationally faster and offers easier application in a spreadsheet or a personal computer. Limiting the accuracy of the model is the limited available vitrinite data throughout the sedimentary basin and the fact that the time-temperature histories of geological basins are approximations, (Sweeney and Burnham, 1990).

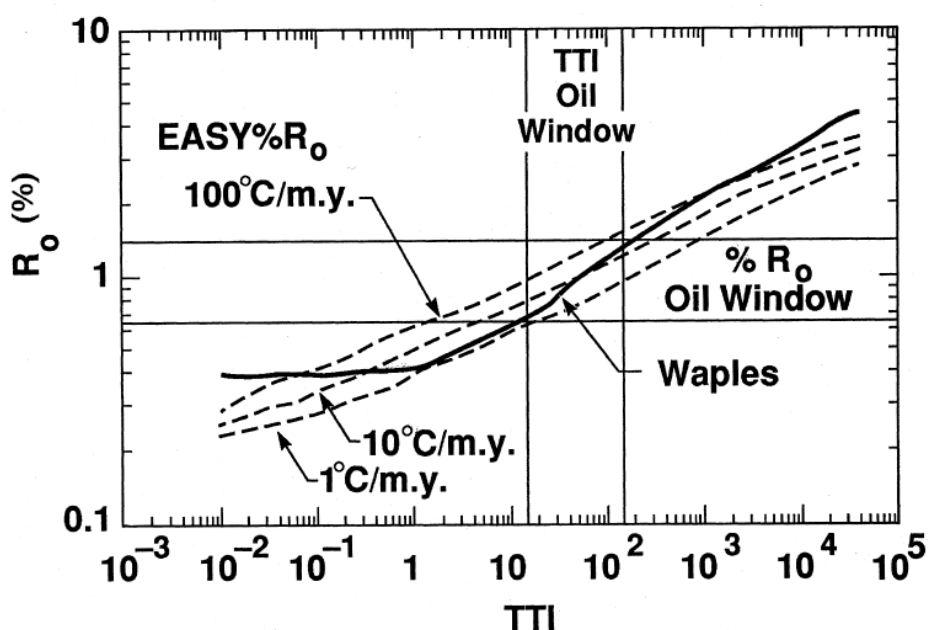


Figure 4.3.1. Values of %Ro at different heating rates estimated by Easy %Ro as a function of Time Temperature Index (TTI) (dashed lines. Sweeney and Burnham (1990) compared their results to Waples (1980) correlation (solid line).

Limitations of Easy%Ro

The major limitations of Easy%Ro is that it does not adequately model laboratory data for heating times of less than a few days and it can only calibrate vitrinite reflectance data in the range 0.3-4.5%, Sweeney and Burnham, (1990). Thompson (used an inversion scheme with capabilities for assessing the uncertainty range of a parameter in a forward model to investigate amongst others the resolution limits of the Easy%Ro method in calculating vitrinite reflectance. After comparing measured Ro values to those calculated by the Easy%Ro, Howaz and Thomsen found they could explain the resulting anomalous geothermal gradients and thermal

regimes in their models geologically. They also confirmed the Easy%Ro model inability to calibrate beyond the limits stated by Sweeney and Burnham, (1990). Nielson, (2015) reports that Easy%Ro model overestimates vitrinite reflectance in the interval 0.5–1.7% R_o by up to 0.35%. “Delimiting of oil generating intervals by prediction of vitrinite reflectance may lead to significant underestimation of the generative potential, which may call for a revision of some petroleum systems. The overestimation by Easy%Ro may have fuelled the idea of pressure retardation of vitrinite reflectance evolution under sedimentary basin conditions, where pressures in fact are too low for this to be important”, (Nielson, 2015).

The Basin%Ro model (Nielson et al., 2015)

(Burnham and Sweeney, 1989) established that the existence of a compensation effect between the pre-exponential factor A and the activation Energy E. The result is that a unique set of kinetic parameters can only be found for considerations of a large range of heating, (Nielson et al., 2015). “For sedimentary basins the temperature problem can be reduced by selecting calibration wells, which have maximum temperatures at the present day. Then the present-day temperature, which in principle can be observed, is most relevant (e.g. Issler, 1984),” (Nielson et al. 2015). The basin %Ro developed by Nielson et al., (2015) takes into consideration the uncertainty associated with vitrinite reflectance calibration data for rebuilding of the thermal evolution of the calibration data. Basin %Ro accounts for this uncertainty by parameterizing deviations from the reference thermal history based on relative variations of heat flow and absolute variations in surface temperature, Nielson et al., (2015).

The process involves inverting the entire data set for the kinetic parameters of the reflectance model under consideration of uncertainty in the temperature histories of the calibration samples. The calibration method considers all data but ensures that inconsistent data has no influence on the results, Nielson et al., (2015). The procedure can be applied to many data sets simultaneously. This is expected to diminish the influence of the temperature uncertainty and data inconsistencies to ultimately solely relate the underlying relationship between the temperature and the vitrinite reflectance histories.

“The model follows closely the general behaviour described by Suggate (1998) in terms of an upper segment with a linear gradient from 0.2–0.25% R_o at the surface to 0.6–0.7% R_o; a middle segment in which reflectance increases rapidly to *ca.* 1.0%R_o; and a lower segment in which the gradient is again linear, but reflectance increases more rapidly than in the upper segment,” Nielson et al., (2015).

A calibration procedure on wells that were not part of the well calibration data set by Nielson et al., 2015 yielded results that showed that basin %R_o performs excellently in wells which exhibit very high overpressures. These findings emphasized the conclusion by Nielson et al., (2015) that overpressure is not a parameter in vitrinite reflectance evolution for the pressure conditions encountered at usual drilling depths in sedimentary basins.

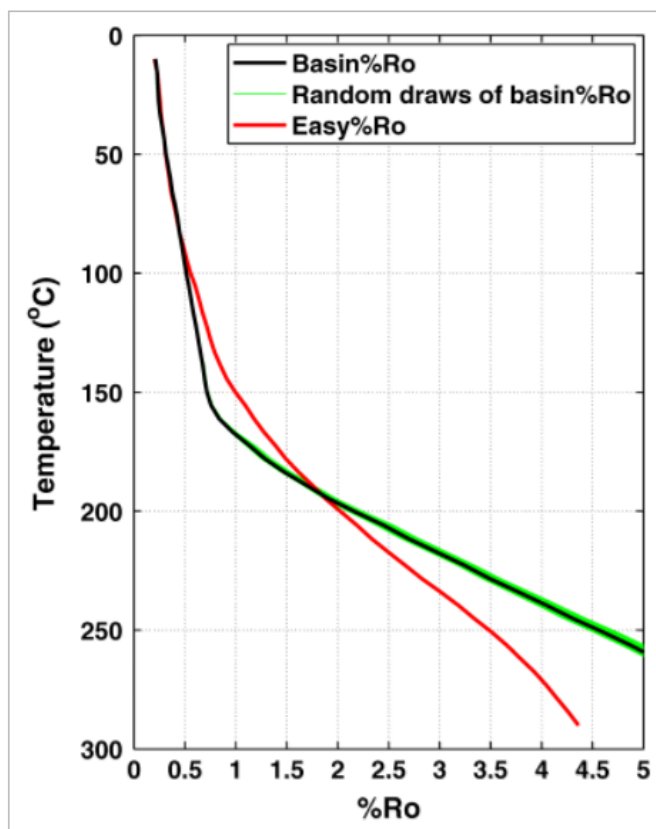


Figure 4.3.2. Adapted from Nielson et al.,2015. Comparing the behaviour of vitrinite reflectance with temperature variation for the two models; Basin%Ro and Easy%Ro.

Comparison of Basin%Ro to Easy%Ro by Nielson et al. (2015)

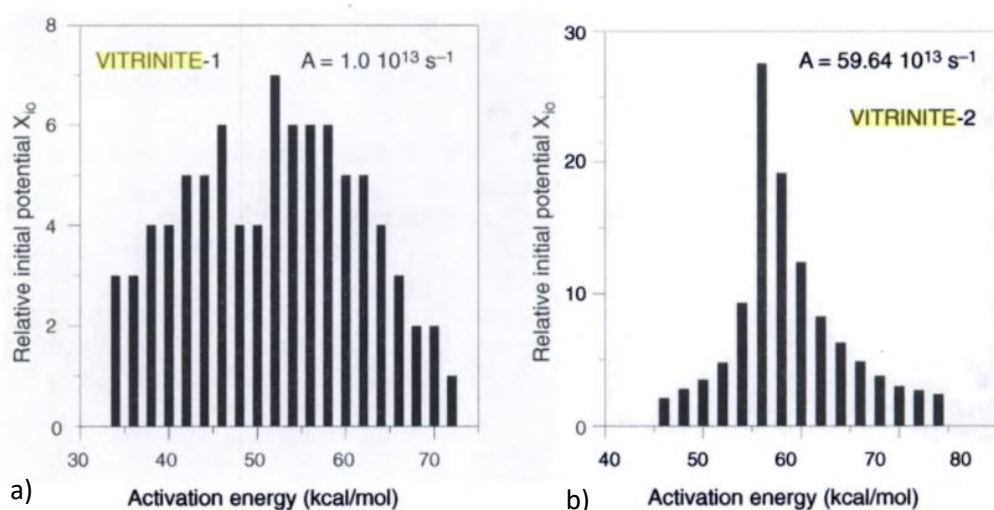
Nielson et al. (2015) found that the Easy%Ro model performed better than their Basin%Ro model when dealing with pyrolysis data which they attributed to their having given a greater weight to the pyrolysis data in the calibration of the Easy%Ro model. They observed that the long-duration pyrolysis experiments by Saxby et al. (1986) had a better agreement with the vitrinite reflectance models, basically the basin data. They attributed this to either the long-duration laboratory experiments being better at simulating geochemical processes pertaining to vitrinite reflectance evolution under sedimentary conditions or that the long-duration experiment is less influenced by the transient nature of vitrinite reflectance evolution, which is important to rapid heating rate experiments.

Comparison of basin%Ro and easy%Ro at heating from 10°C at a rate of 2.8°C/Ma revealed the models to be virtually identical until c. 0.45%Ro (c. 80°C). The easy%Ro-model yields significantly higher reflectance predictions in the reflectance interval which is commonly believed to be important to the detection of oil generation (c. 0.55–0.8%Ro), and to the cracking of oil to gas (c. 0.8–1.0%Ro). Morrow & Issler (1993) observed this tendency in the easy%Ro-model. Based on careful thermal modelling they found that the Easy%Ro-model slightly overestimates vitrinite reflectance in low to medium mature strata of up to 0.9% Ro.

Their analysis led them to suggest that Easy%Ro overestimates vitrinite reflectance values by up to 0.35%Ro in the interval from c. 0.45%Ro to c. 1.7%Ro. The differences in reflectance predictions transform to significant temperature differences. To achieve reflectance predictions in interval 0.6–0.7% Ro, the basin %Ro-model requires *ca.* 15–23°C higher temperatures than the Easy%Ro-model (the numbers depend on heating rate). Everything else being equal this temperature difference is large enough to significantly change estimates of heat flow, uplift and erosion, and the depth and extend of the oil generation window. The quality of industrial borehole temperatures and the fact that they are biased towards too low temperatures are the probable cause that the Easy%Ro model essentially has remained untested, save for Morrow & Issler (1993). Nielson et al., (2015) determined that two test could only be thoroughly evaluated and compared provided there was an unusual combination of accurate equilibrium formation temperature measurements, reliable vitrinite reflectance measurements, and reliable stratigraphic and lithological information.

Comparison of the Sweeney and Burnham (1990) and Tissot et al. (1987)'s models

Workers such as Tissot (1987) and Sweeney and Burnham, 1990 have since been basing on Lopatins first model to developed more refined vitrinite maturation models such as the Easy%Ro presented above. (Makhous and Galukshin, 2005) compared Transformation rations against Ro plots for the Sweeney and Burnham (1990) and Tissot et al. (1987)'s model which resulted in the plots below (named the vitrinite 1 and Vitrinite 2 respectively), which were created from a range of activation energies at a constant A value for certain initial potential for reactions of vitrinite maturation X_{i0} . These values are different in both models. The range of Ei values used in the Sweeney and Burnham (1990) model range between 34 and 72 while those for the Tissot et al. (1987) model range between 46 to 74 with a higher A value. Resulting are the two most popular kinetic spectra for maturation of vitrinite (Makhous and Galukshin, 2005) shown below;



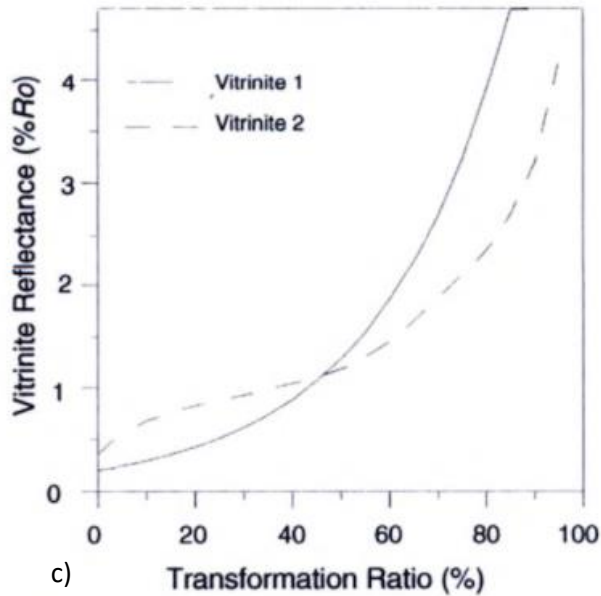


Figure 4.3.3. Kinetic spectra of vitrinite thermal transformation (Figure 19 (a) and (b) and the correlation of transformation ratio with %Ro lower right for two models (Figure (c) for two models: Vitrinite -1 of Sweeney and Burnham (1990) and Vitrinite -2 (Kerogen IV) of Tissot et al. (1987).

The plots allow formulation of expressions from which the transformation ratio and the vitrinite reflectance values can be computed. The expression by Tissot and Espitalie, (1975) shown below, allows for the evaluation of the transformation ratio for vitrinite reflectance for the Sweeney and Burnham (1990) model;

$$Tr_1(t) = \sum_1^n \{1 - \exp[-\int_{10}^1 K_i(t') \cdot dt']\} \quad (28)$$

The expression below enables the determination of the values of vitrinite reflectance in the Sweeney and Burnham (1990) model;

$$Ro\% = \exp[-1.6 + 3.7 Tr_1(t)] \quad (29)$$

Makhous and Galukshin, (2005) report a good correlation between transformation ratios $Tr_1(t)$, $Tr_2(t)$ and % Ro in the various basins which they considered.

“The kinetic model of vitrinite maturation [Sweeney and Burnham, 1990] is usually considered as the primary method for maturity estimation in basin modeling,” (Makhous and Galukshin, 2005).

The evaluation of the transformation ratio for vitrinite reflectance for the Vitrinite 2 Tissot et al. (1987) model;

$$Tr_2(t) = Tr_1(t) / \sum_1^n X_{i0} = Tr_1(t) / 113 \quad (30)$$

“Different vitrinite reflectance equations employ different kinetic parameters and also different calibration sets. The resulting depth trends vary according to the heating rate, and deviation is most pronounced at low heating rates. This affects the optimization of the temperature history. The new models are more satisfactory in this respect, particularly the model of Burnham and Sweeney (1989), which showed an almost perfect fit with observed data when extended from laboratory scale to basin scale conditions. The successful use of vitrinite reflectance as a check parameter for paleotemperature reconstruction in basin modeling is dependent on precise calibration and selection of the correct model,” (Makhous and Galukshin, 2005).

The Pepper and Corvi, (1995) kinetic model

This model provides a complete description of petroleum formation providing descriptions of generation, oil-gas cracking and expulsion generated as oil is itself potentially subject to thermal degradation in the source rock, (Pepper and Corvi, 1995). The model has separate parameters for the oil- and gas-generative fractions which enable calculations of the evolving concentration and composition of the products. The model of Pepper and Corvi, (1995) assumes normal distribution for the activation energy distributions for each fraction. The model requires ten (5 x 2) kinetic parameter sets (A, E_{mean} , σ_E). Known chemical properties enable the reconciliation of differences in kinetic parameters. Mean activation energies governing oil generation increase systematically in the order A-F, which result in a corresponding increase in generation temperature.

“Five kerogen kinetic organofacies, each characterized by a specific organic matter input and early diagenetic overprint, can broadly be related to sedimentary facies/age associations, even using seismic sequence stratigraphy alone: A, aquatic, marine, siliceous or carbonate/evaporite, any age; B, aquatic, marine, siliciclastic, any age; C, aquatic, non-marine, lacustrine, Phanerozoic; D/E, terrigenous, non-marine, ever-wet, coastal, Mesozoic and younger; and F, terrigenous, non-marine, coastal, late Palaeozoic and younger,” (Pepper and Corvi, 1995). The reference heating rate for the model is 2°C/Ma. At this heating rate the oil generation window of 10-90% oil generative kerogen degraded rises from ca. 95-135°C to 145-175°C. The gas generation ‘window’ ranges from ca. 105-155°C to 175-220°C. Pepper and Corvi, (1995) established per experience that the 2 °C/Ma is close to a global average for many basins currently in the post-rift stage of thermo-tectonic evolution. “Thermal stress results from a combination of temperature and time: an order of magnitude increase (decrease) in heating rate elevates (depresses) reaction temperatures by ca. 15°C; heating rates in subsiding sedimentary basins can vary by two orders of magnitude, (Pepper and Corvi, 1995).

The Arrhenius equation (22); dictates that the reaction rate (k) will never be zero provided the temperature remains anywhere above the absolute zero (-273°C), the exponent ($-ERT$) always has some small value. Pepper and Corvi, (1995) thus deduced that the kerogen conversion process never completes until infinite temperature is reached. The result is that all kerogen degradation profiles are asymptotic with respect to temperature. In the absence of an industry-wide consensus on a definition of the oil- and gas-generation ‘window’, Pepper and Corvi, (1995) defined their arbitrary definitions as: oil generation window at least 10% (= oil generation threshold) and up to 90% of oil generative kerogen degraded to oil; and gas generation window at least 10% (= gas generation threshold), but no more than 90% of gas generative kerogen degraded to gas.

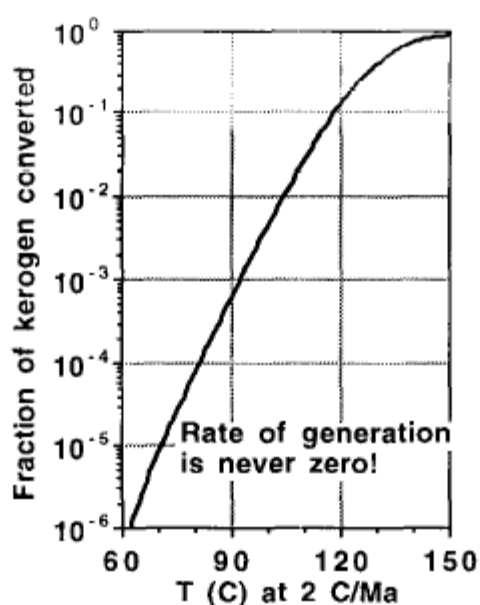


Figure 4.3.4. Rate of generation of oil is never zero and so generation temperatures includes reference to some arbitrary value of generation level. Pepper & Corvi, (1995) chose 10-90% limits

Apart from the limitation that these single bulk Gaussian models are not equipped to account for any small proportion of gas-generative kerogen present (which forms the extended high temperature tails on the organofacies B and C curves in our model), there is some sense of best fit provided by our global organofacies examples. Overall, extrapolation of the LLNL parameters to geological heating rates seems to systematically underestimate reaction mid-point temperatures by around 10°C .

5.0 Modeling in PetroMod

5.1 Introduction

PetroMod version 2017 is a Schlumber software that traces the hydrocarbons of a petroleum system or petroleum systems from source to trap. The software package has 1D, 2D and 3D that are integrated. “IES software is supported on Windows XP®, Linux®, and UNIX® operating systems on PC, Silicon Graphics Incorporated® (SGI), and Sun® computer platforms that have the same user interface and data formats,” (Higley et al, 2006). Some of the software capabilities are defined below;

1Dmodel

Building a 1D model requires a prior knowledge of the stratigraphy of the region which is input as formation names, thicknesses and ages. The lithologies and deposition and erosion ages in millions of years before present (Ma) must be assigned to the intervals and the sections defined as overburden, source rock, seal and reservoir rock in order for the PetroMod software to appropriately assign properties and make calculations. The model will define the petroleum system thus the petroleum system elements and boundaries can be assigned at later stages in the burial history models. PetroMod utilizes the input data listed above and in Table 5.1.1 to create burial history plots that show the combined relative effects of these parameters on formation of hydrocarbon at point locations in the region being modelled taking into account the effects from tectonic events, igneous intrusions and salt movements. Input data also includes strata depth or elevation relative to sea level in meters or feet. The model avails the user the option to use own values or default values of paleo-water depth, heat flow, and surface temperatures over time. Table 5.1.1 lists some of the 1D model capabilities and required data.

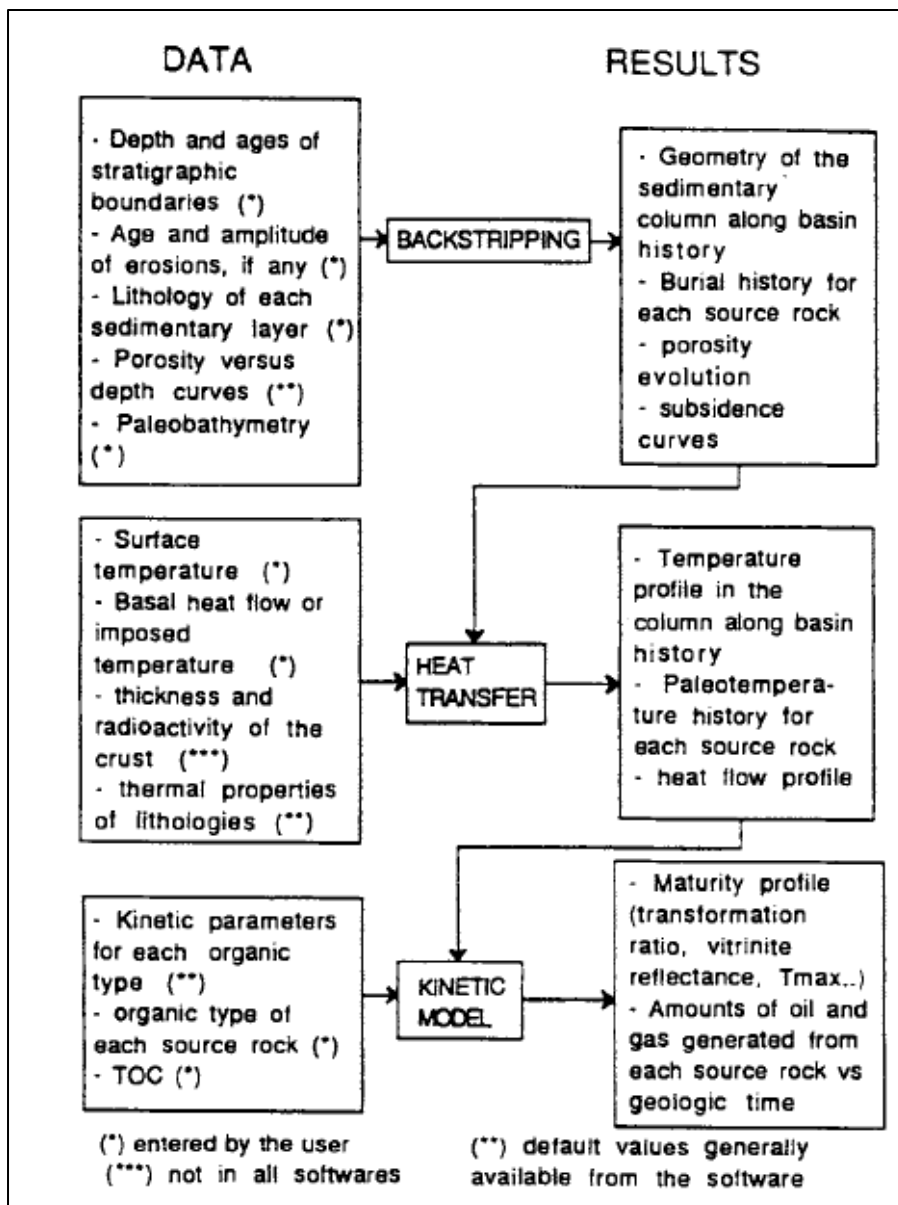


Figure 5.1.1 A generalized scheme showing typical inputs of a 1D model for modelling petroleum generation (Ungerer, 1993).

Table 5.1.1. Capabilities and required data for creating a 1D model

1D model capabilities	Required Data
Constructing burial histories	formation contacts from wells, outcrops, seismic sections, publications, or 1-D extracts from 3-D models.
Porosity/permeability compaction histories	Lithologies default in PetroMod or lithologies created using petrophysical properties in PetroMod
It is possible to calculate PVT and provide a range of petroleum generation kinetic algorithms	Allows additions of user-defined activation energies and transformation ratios for kinetic algorithms. The software models primary and secondary generation of hydrocarbons of

	source rocks.
Thermal effects calculations for processes such as tectonic processes, igneous intrusions and salt movement through time	
Surface temperature can be user defined or calculated using the software	Surface temperature and heat flow values as well as PWD affect thermal maturation of petroleum
Results include depth against Ro, time versus transformation, petroleum system events charts	Including risked temperature and Ro through time and relative to burial depth.

For better visualisation of results through comparison; corrected borehole/drillstem test (DST) temperature and Ro are used for external calibration of the models. The information used for 1-D burial history modeling will also be used in the assessment and building of 1-D models. 1D can display the burial and temperature history of the basin, estimate the timing of oil and gas generation, create an isopach of ancient to present-day erosion, and calibrate a 3-D model. PetroMod also allows the use of analogs to model compaction history. The full 1-D modeling package, the 2D and 3D provide a range of petroleum generation kinetic algorithms that add user-defined activation energies and transformation ratios for kinetic algorithms. An incomplete PetroMod 1D version is available for download which does not allow the use of the ‘editors’ offered in the full version, (Higley et al, 2006). 1D modelling typically combines the reconstruction of burial history, and transfer and hydrocarbon generation as shown in Figure 20. The major limitation of 1D model is that it represents only a point source and the associated calculations of temperature, pressure, and fluid flow are also one dimensional (Higley et al, 2006). The time, personal and equipment requirements for 1D modelling are given in Table 5.1.2.

2D model

The 2D modelling simulates two dimensional flow path modelling using two dimensional maps and cross-sections to rebuild the basin geological history. Facies and lithologies assignments enables the tracing of the oil and (or) gas formation processes from source rocks, its migration, and accumulations. 2D modelling ultimately calculates and defines the resulting different fluids volumes due to the varying pressures. The simulator uses the properties of the source rocks and the heating and temperature histories to model the formation of hydrocarbons such as heavy oil, dry gas, wet gas. The 2D capabilities include defining faults as open or closed, anticipating salt movements and the ability to ‘retrace’ the salt movements and effects of igneous intrusions. The Darcy and hybrid Darcy simulators incorporated in the IES PetroFlow 2D enable modeling of flowpath and 3phase migration. 2D modelling in PetroMod allows integration with various formats of other softwares enabling direct reading of seismic sections and paleo-sections (Higley et al, 2006). Cross sections can be exported from PetroMod to other structural modelling softwares. Boundary conditions

have to be set for paleo water depth, sediment water interface and heat flow (SLB PetroMod version 2017 manual).

A 2D model in PetroMod creates a present day model by using all the available map and line data to mimic and represent a geological section which includes layers of varying facies subdivided by horizons and any occurring faults. Between each layer of a stratigraphic sequence in a basin is occurs a horizon. The horizons can be interpreted from seismic reflection surfaces in 2D model. Well data is used as calibration points to inter and extrapolate the horizons on a 2D surface map. The space must be divided into sections to allow the volume to be assigned properties by first performing horizon stacking. Geological facies that can repeat in several parts of any layer are created by grouping parts of each layer according to the similar sedimentation environments. PetroMod then follows stratigraphic principles and well data to create a facies map according to the stratigraphic tables that are edited by the user. Seismic maps, dips and well data allow the user to add fault planes to the strata (Higley et al, 2006).

A stratigraphic table allows the present day layers and horizons to be assigned ages according to when they were deposited and eroded in the geological sequence including any hiatuses if applicable. The erosion ages represent the eroded thickness. Provided there was no erosion the horizons represent particles deposited during the same age. The appropriate water-depths are included in the erosion maps in order to simulate the basin uplift events. Ideally the horizons of stratigraphic sections with facies variations are limited to a number between 10 and 50. Simulation of migrating patterns of facies through time is difficult but better carried out through a Wheeler diagram, (Hatchel and Kauerauf, 2009). The major limitation of 2D modelling is that it simulates data that is represented as two-dimensional surfaces. This has an advantage when dealing with areas in which oil and gas are structurally trapped. Areas that contain stratigraphically trapped or continuous hydrocarbon accumulations may just show passage of hydrocarbons through these zones. Better modelling results of a petroleum system are produced when 1D is integrated with 2D. The time, personal and equipment requirements for 2D modelling are shown in Figure 5.1.2.

3D model

3-D modelling rebuilds the history of petroleum systems and analyses vertical and lateral variations in lithology, heat flow, hydrodynamics, PVT behaviour, etc at reservoir to basin scales for both conventional and unconventional exploration. Under-pressured or over-pressured zones affect the rock maturation and therefore petroleum generation potential differently. PetroMod calculates and assesses the combined effects of these processes including those from capillary pressures and trapped gas, compaction and sealing effects in time on lithologies. The large scale basin analysis allows assessments of hydrocarbon migration into virgin or underexplored zones. 3D modelling allows the subdivision of basin areas into smaller areas delineated with well and seismic data to avoid complex computations that demand a lot of time. The subsets can be performed

at finer grid spacing than typically accepted in most models. The subset can then be used as a full model for that region or as an analog for other sections of the basin. In 3D modelling the user is able to distinguish and exclude assessment of petroleum generation from immature and over-mature source rocks. The 3D model traces the liquid and gas of both hydrocarbon and non HC volumes in-place through time from their generation, through migration to accumulation and also calculates the lost volumes. In 3D modeling it is possible to view flash calculation charts and numbers for hydrocarbon volumes at surface conditions. 3D also models occurrences and effects of salt movement, open and closed faults, paleo-geometry, permafrost and igneous intrusions through time. Changes arising from compaction, temperature, faulting, heating history, and other variables are included in the multicomponent PVT analysis to calculate the volume, composition, density, and HC and water viscosities in the phases they occur in. Calculations can be performed and displayed for occurrences in individual petroleum systems through time. The 3D modelling outcome is PVT history, lithologic as well as fault and formation capillary pressures that yield distinct compositions of certain hydrocarbon groups and non-hydrocarbons including C3-C5, C15 and aromatics, C15 and saturated hydrocarbons, and water. Risk analysis is possible in PetroMod by the PetroRisk risking module in the 1-D, 2-D, and 3-D. A series of Monte Carlo (Waples, 1992; Hatchel and Kauerauf, 2009) and Latin Hypercube simulations in 3D allow assignment and calculations of uncertainties in geologic/geochemical data for all stages of the petroleum system from petroleum charge to migration. “3-D modeling can incorporate Darcy (vertical), flow-path (lateral), or hybrid Darcy (vertical and lateral) fluid flow to model the consequences of mechanical and chemical compaction as well as fluid expansion on pressure,” (Hatchel and Kauerauf, 2009). Each of the 1D, 2D and 3D models tabulates and archives the parameters that have been assigned during the modelling. The modelling carried out in 3D space can then be displayed in 1D, 2D and 3D space and time.

1D, 2D and 3D

Burial history models rebuild the geologic history at one or more points in a region to mimic as closely as possible the petroleum systems. IES PetroMod 1-D, 2-D, and 3-D models are able to use the same variables as used in each of the 1D, 2D or 3D models for petroleum systems modeling. They utilize information from wells, outcrops, seismic sections/maps and 1D extracts from 3D models to pinpoint and infer lithological contacts. 1D, 2D and 3D models all need to model validation to compare model results to real data. Validation information is from maps, cross sections Ro data or other thermal maturity data, including temperature and pressure. Parameters that can be validated include temperature, rates of erosion, heat flow. The major trouble with validation data are the uncertainties. Advantage in PetroMod includes seamless integration between the 1D, 2D and 3D model parameters. 1-D extractions from both 2D and 3D models can be used as calibration data in the 1D. All models include modeling through time of PVT, salt movement, hydrodynamic flow, igneous intrusions, temperature, transformation ratios, and other factors important to hydrocarbon generation and migration. Generated hydrocarbons are then graphically displayed or tabulated and can be shown as they occur at depth or converted to surface conditions. PetroMod also outputs the relative contributions of petroleum source rocks

for each accumulation. These accumulations can be compared to known reservoirs to calibrate location, volumes of and relative percentages of hydrocarbons, and contributing source rocks; this also has the advantage of calibrating the model parameters for modelled accumulations in unexplored areas (Higley et al, 2006).

Table 5.1.2. Time, Equipment and Personal requirements

	1D	2D	3D
Time	Burial history modeling is relatively rapid. It learning the software requires only several hours. Data compilation for models takes the most effort and time.	2D modelling requires lots of effort and time to process required input and calibration data including maps and (or) cross sections, seismic sections and to create facies and horizons. This information is also required for model assessment. The process of model editing and assessment can range from a day to weeks.	Data and results of previous research on the province and areas to be modelled must be compiled and assessed. The primary petroleum system elements of reservoir, source, seal, overburden, or underburden for all stratigraphic intervals in the model must be assigned. This does not need to be at the initial stage. Construction of a 3-D basin model can take a year or more to complete and evaluate for use in geologic and resource assessments.
Personal capabilities	Can be used by a geoscientist or anyone using a 1-D template that is populated by a geoscientist. Coordination of methods used is paramount if there are several people working on	Some projects require the aid of GIS support staff overseen by a geologist. An experienced user can take a relatively short time.	Requires considerable data, personnel, training.

	the 1D modelling to avoid different results.		
Equipment/ processing and data requirements	Generating 1D models requires relatively small amounts of disk space and computer time. It can be run on any of the computer platforms.	Generating 1D models requires relatively small amounts of disk space and computer time. It can be run on any of the computer platforms.	Requires lots of computer processing capabilities. The models also require many gigabytes of storage space. Storage space, memory, and processing ability also determine the choice of resolution that can be processed and displayed. Modelling at a province scale is better carried out using a Linux cluster of linked PCs which results in shorter computing and display time because of the multiple processors.
		Edited map can be created using EarthVision® or ARC® software, export the grid in zmap format, and create and run a 2-D map model using PetroMod®. 2D grid files allows isopach and (or) structure grid files to be accessed and used by others.	Considerable data are required for a full 3-D model, and data quality and distribution are critical.
			PetroRisk® software that analyses risk needs long processing times.
			Updating the software after the release of newer upgraded versions can significantly alter the results

4D model

4D modelling allows the subsurface to be modeled through time (Martinelli, 2010).

The table below summarizes the capabilities of 4D modeling as described by (Martinelli, 2010).

- “4D petroleum systems organize data, allowing deficiencies or inconsistencies to be identified (examine data, appraise the reliability of geological concepts, models, or geochemical input, and extract needed information).
- Facilitate visualization of geologic processes and communication with stakeholders (developing predictive exploration and reservoir models, integrating sequence stratigraphy and assessment units, predicting the extent and timing of petroleum generation in source rocks, structural deformation that disturbs basin architecture, migration pathways, and locations of potential traps and accumulations).
- Add value by converting static data into dynamic processed data and interpretations”.

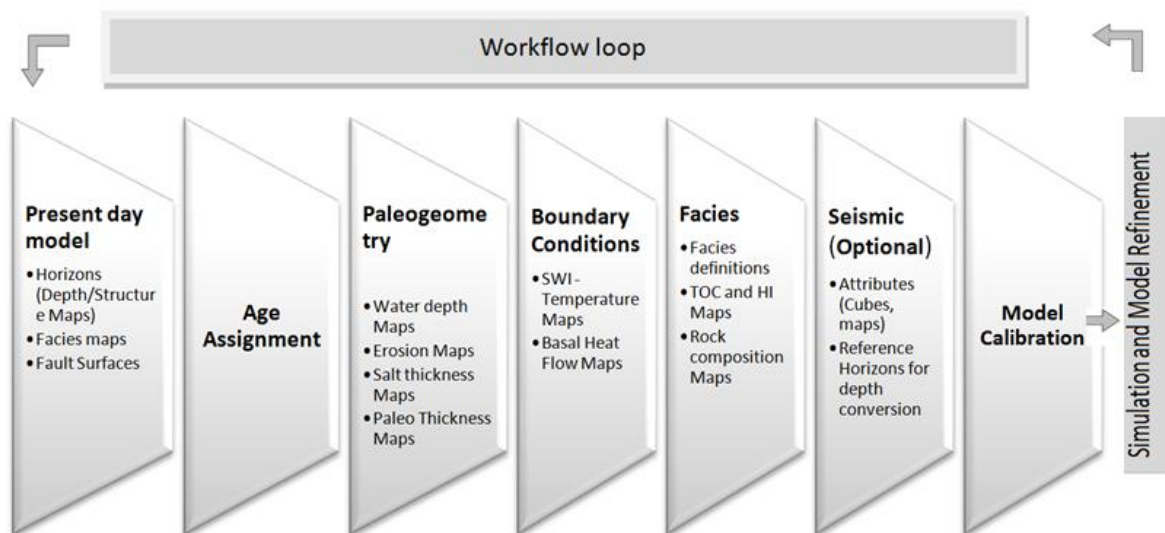


Figure 5.1.2. A schematic model workflow with basic elements of model input edited from Hantschel Kauerauf, (2009) including the model calibration to Simulation and refinement (Martinelli, 2010).

Creating the Present Day Model

Input into the software is the model geometry that extend anywhere between tens to thousands of kilometers and to a depth of 10 km into the subsurface. The present day model consists of depth horizons, facies maps and fault planes of events that occurred over millions of years. Layers containing geological information of a stratigraphic sequence are separated by horizons. The lithologies in each layer give the layer special characteristics that define it. Horizons are usually defined from seismic sections, coupled with inter and

extrapolations to zones outside the seismic section. Horizon stack construction is an energy intensive part of creating a model. The horizon map stacks allows assignment of volumetric properties to the space of the model. This allows the creation of geological facies of geological sections having similar sedimentary environments. Geological facies can be found repeating several times in the same layer or can repeat in several different layers. A single facies map in each layer usually describes the distribution of facies depending on well data and sedimentological principles. The facies information defines rock properties such as compaction parameters, permeability, thermal conductivities and heat capacities. High resolution seismic facies maps enables very detailed facies maps to be built whereas in simple cases a single unique facies type can be used to describe a layer. Seismic and well data as well as dips allow the construction of fault planes. Creating horizons, layers and facies requires a lot of effort.

Age Assignment

The age assignment also referred to as the stratigraphic table allows allocation of the horizons and layers with the geologic age of deposition, erosion and hiatus. Horizons in layer sequences without erosion represent all sedimentary particles that were deposited during the same period. Additional maps have to be added to represent amounts of erosion that must be combined with the appropriate water- depth in order to describe the related uplift of the basin. Model horizons in the range of 10 – 50 are preferred in stratigraphic diagrams that have a great range of facies variations. A Wheeler diagram is used instead of a single simplified age table for migrating patterns of facies through time.

Paleo-Geometry Data

Building the paleo-model depends on knowledge and principles from historical and regional geology, sedimentology and tectonics. The burial and uplift mechanisms of the basin are described by water depth maps. These maps are derived from crustal stretching models that consider isostasy and incorporate assumptions made about variations in the global sea level. “Water depth maps can also be derived from known distributions of sediment facies and vice versa,” (Hantschel and Kauerauf, 2009). Constructing depth maps is generally much simpler than building erosion maps. A simple approach of constructing a simple case where a layer is partially eroded during a single erosion event is to build the lost erosion amount separately for every layer. This is coupled with an assumption of a uniform erosion during the erosion event. The calculation of the erosion thickness involves decompacting the present day thickness and thereafter removing from the assumed approximately uniform depositional map.

Rebuilding salt layers

Rebuilding salt layers typically depends on geometrical principles. Paleo- thickness maps are necessary for the main phases of salt doming. Simple cases implement linear interpolation of the present day thickness map to a uniform depositional map. The resulting paleo-geometries are checked and corrected to ensure that the rebuilt

base salt maps remain realistic. Another manner in which the salt layers can be reconstructed basing on calculated lithostatic pressures or total stresses occurring at the salt boundaries. This is linked to the salt movement along the gradient giving the smallest amount of mechanical resistivity. “The reconstructed salt thickness maps can be implemented in the input model by two methods: paleo-thicknesses for autochthonic salt layers and penetration maps for allochthonous salt bodies. Autochthonous salt maps through geologic times can be simply realized by adjusting the layer thickness in each gridpoint,” (Hantschel and Kauerauf, 2009). The occurrence and timing of the salt windows is often very important for petroleum migration and pressure development as subsalt fluids and pressures are released afterwards. The penetration of shallower sediments by salt and the formation of single allochthonous salt bodies is usually implemented with the replacement of the original sediment facies by the salt facies. Both methods have to be combined with adjustments of the other sediment thicknesses to maintain the mass balance. These correction maps can be added to the input data as paleothickness maps during the corresponding events. The interplay of paleo-water depth, erosion, salt thickness, and other paleo-thickness maps finally determines the paleo-geometries and often requires some experience of the basin modeler to build geological reasonable scenarios.

Boundary conditions

The settings for the boundary conditions strongly influences the quality of the simulation and thus must be defined for the geological setting being modelled in order to analyse the heat, pore pressure, and fluid flow. Typically the required boundary condition data for the heat flow analysis are temperature maps on the sediment surface or the sediment–water interface and basal heat flow maps for the respective events. The sediment – water interface Temperatures (SWIT) can be user defined or automatically extracted by the software to provide the standard temperature at sea level over geological time based on the present day geographic location and latitude (based on Wygrala, 1989). Incorporated in PetroMod are basic paleo-climate databases with surface temperature maps and basal heat flow. Basal heat flow maps are created using crustal models calibrated with thermal calibration parameters and igneous intrusion temperature maps. Real data can be used to calibrate the present day heat flow but paleo heat flow must be calculated. PetroMod 1D has the McKenzie Crustal Model based on the crustal stretching model by Jarvis & McKenzie (1980) as the default model to define stretching factors and the parameters for rifting/thermal subsidence. The user has the option to define the matrix heatflow production value to influence the radiogenic heat production of the crust and mantle lithologies. Groundwater potential is the upper boundary condition for pore pressure analysis that is calculated from groundwater maps. The groundwater potential is necessary for onshore basins or erosion events.

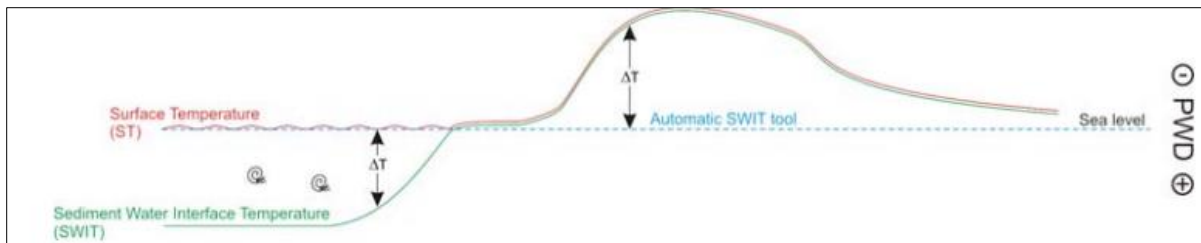


Figure 5.1.3. shows the relationship between the surface temperature, SWIT and the values defined by the Automatic SWIT tool. The difference between the temperature at sea level and the SWIT is shown as (ΔT).

Facies properties

PetroMod has a library of rock property tables that are assigned to appropriate lithological units. The main rock properties are thermal conductivities, heat capacities, radiogenic heat production, permeabilities, compressibilities, and capillary entry pressures. This allows the model to assign appropriate temperature and porosity values to different lithologies which will then be used to assign values for temperature indicators such as vitrinite reflectance and compaction. Lithologies with common properties are referred to as facies. Facies information that defines the petrophysical properties, reservoir or characteristics of source rocks is stored in a facies map. Two sub-group facies types; the lithology and the organic facies (or organofacies) describe the facies. The organic facies includes all kinetic parameters for the generation and cracking of petroleum and the parameters that determine the amount and quality of organic matter. “The kinetic parameters are mainly Arrhenius-type activation energy and frequency data for primary and secondary cracking of hydrocarbon components,” (Hantschel and Kauerauf, 2009). Distribution maps typically define the total organic content (TOC) and the hydrogen index (HI). The fluid properties such as critical temperatures, pressures, specific volumes, densities and viscosities are either given directly for the different fluid phases or calculated from compositional information,(Hantschel and Kauerauf, 2009).

Petroleum system elements

Source rock definition and Petroleum system elements Assignments is carried out in the main input. The Petroleum system elements are the overburden, underburden rock, source, seal, reservoir rock, and trap formation. The deposition history input into the main input are displayed in a petroleum system elements chart or plot and the user can alter it as required defining the generation/migration/accumulation, preservation and the critical moment of the petroleum system in an edit area as shown in Figure 5.1.4.

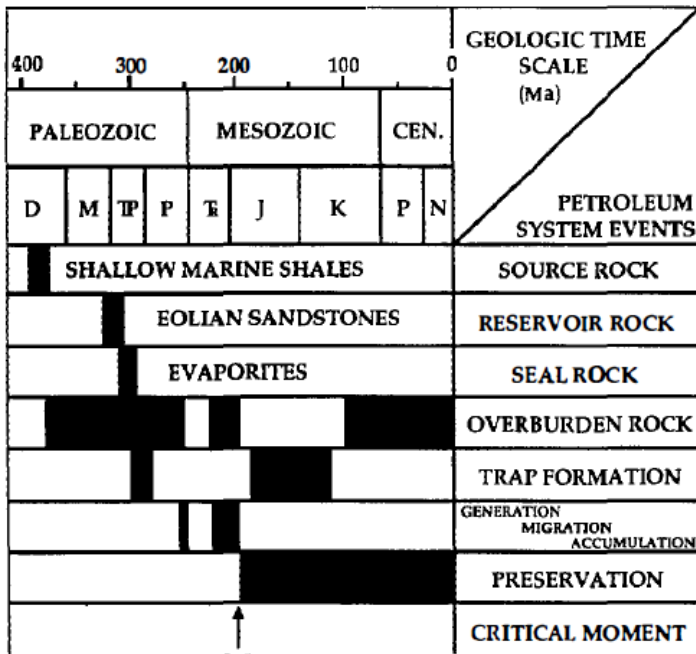


Figure 5.1.4: The events chart for the Barreirinhas –Itaituba(!) petroleum system Adapted from the works of Mello et al., in Magoon and Dow, (1994) summarising the temporal relations of the essential elements and processes .

Additional submodel inputs in PetroMod

PetroMod allows additional inputs of cementation, crustal layer, thermal calibration parameters, salt movement, erosion, intrusions, fault properties, fluid phase properties, secondary cracking and more to enable better simulation of the real field situation. Cementation describes porosity reductions due to lithification. PetroMod gives the users the option to create their own crustal layer model to calculate heat flow rather than using the McKenzie model that is default in the boundary conditions table. Fracturing effects can be assigned to specific zones via a fracturing submodel that uses parameters in the Lithology Editor and the either using the default 80% pore pressure limit or user defined values. Intrusions occurrences of specific ages can also be modeled to a specific layer. A thrust model and paleo models are standard in PetroMod 1D to define layers that thrust onto paleo models.

Discretization of a model

The description of macroscopic scale heat and fluid flow systems are typically solved based on a continuum approach. The discretized models solely produce practical solutions. A mesher generates grids with the cells as the smallest volumetric units of the geological model. The basin or region of interest is assumed to be covered continuously with cells. Every physical or geological quantity such as temperature, pressure,

saturation, concentration, permeability, thermal conductivity, etc. is well defined in the cell as a single, effective or average value. Furthermore, the value can vary continuously from cell to cell at least within parts of the structure. Each cell is used as a finite element or finite volume within the mathematical solvers. The approach requires that the size of the cell must be small compared to the system being modeled (basin scale) while large compared to the pore scale and grain size. The lower range of sizes are typically between 10^{-9} - 10^{-8} m at molecular scale with pore scale at 10^{-6} – 10^{-3} and bulk continuum at 10^{-3} to 10^{-2} m. The larger sizes range between 100 to 102m for cells of the grid and the basin scale ranges between 103 to 105m.

Modern simulation programs might have different grid scales and even different basin scales for the modeling of different geological processes. Such multi-grids are typically created with sampled and refined representations of a master grid. Optimal methods can then be applied for each geological process. For example, heat flow is often modeled on the full basin scale with grid cells seldom smaller than 100m, whereas petroleum systems modeling is sometimes restricted to smaller areas of source rock expulsion and active migration pathways with corresponding grid cells, which can become very small. However, sophisticated up- and downscaling functions (e.g. for fractal saturation patterns) may be required. Many quantities can be defined as gridded maps at certain events. Alternatively, geological time dependent trend functions are often specified at individual well locations. Maps are then generated for each event by spatial interpolation over the whole model area. In both cases maps are the central objects for the creation of a basin model.

Size of a model

The objective of basin modelling is mainly the assessment of exploration risk after estimations of generated and accumulated petroleum volumes in varying geological basins. The basin to reservoir scale models are used from a total length of hundreds of kilometers down to only a few kilometres. Resource assessments extend over even larger geographical zones such as entire countries, resulting in estimated total volumes of oil and gas resources over several layers. Included in the resource assessments are source rock maturity studies that include calculations of volumes lost to migration with simplified reservoir distributions (Hantschel and Kauerauf, 2009). General requirements are;

- a minimum model resolution to approximate the geological structures of interest and;
- simulation run time should be less than half a day.

Resolution;

The average number of cells for a complete simulation is 1–2 million cells which corresponds to 200–300 gridpoints in the horizontal directions. Heat, pressure, and Darcy flow computing times depend almost exponentially on the number of cells. Doubling the number of grid-points in one direction often increases the

computing effort by one order of magnitude. As a result big improvements in computer performance and numerical methods often have only a small effect on the grid resolution.

Computing time;

Important controlling parameters, including the number of hydrocarbon containing cells, average and peak fluid flow rates or the number of migration time steps for good convergence are not known prior to the special conditions of each simulation. As a result estimating computing time is very difficult. Parallelized simulations on computer clusters have significantly improved the performance of computers.

Modelling migration

Gridding

Migration is modeled in order to make predictions on the pathways followed by hydrocarbons from source to traps including movements between traps until the hydrocarbons are accumulated. Migration is treated as if it occurs instantaneously on geological timescales. The simulators allow the option between a completely regular gridding and a gridding that follows the geological structures being modeled. Regular gridding has easier algorithms, faster implementation and higher performance in execution but might pose difficulties when attempting to model smaller features or structures. Non regular grids will not show the meniscus below the petroleum water contact as it follows the structure. This problem extends to even regularly gridded models as the contact resulting from models simulating aquifer flow and lateral pressure gradients is non-horizontal. Regularly gridded models neglect the deviation in direction of dipped reservoirs in long distance migration modeling and of the seal dipping when modelling the top surface of an accumulation (Hantschel and Kauerauf, 2009).

Invasion percolation

Invasion percolation describes the process of one fluid displacing another (formation water and oil) in a porous medium influenced by capillary forces (Wilkinson and Willemsen, 1983). Heterogeneity is highly significant in invasion percolation as it determines the direction the migration will follow. In the case of small capillary pressures neglecting steepness, migrating petroleum follows the grid direction to the highest neighbour site. Percolation methods also model fluid flow through faults by considering them as sites with no volume. Faults are two dimensional on a basin scale but fluid flow through faults seen on a microscopic picture is modeled by percolation methods for three dimensional faults. When using seismic data for invasion percolation modelling, seismic velocities are converted to porosities and permeabilities and eventually into

capillary entry pressures (including the porosities and clay content contributing to the entry pressures). Backstripping of the seismic data is employed to approximate paleo-times so as to avoid mis-representation by using the available present day seismic data. This has the risk of decreasing capillary pressure because of decompaction. Rebuilding flow units in the invasion percolation method requires knowledge of the rock types. These shortcomings are handled by using a well-defined model. Care has to be taken to recognize or deal with noise when using seismic data. Invasion percolation technique carries out overall migration modeling (Hantschel and Kauerauf, 2009).

Flow path modelling

Flowpath modelling simulates fluid migration in carriers until a trap is reached. A seal acts as a guide for hydrocarbon entering a carrier as the fluids head straight upwards to a seal and then follow the steepest direction upwards underneath the seal. Purely geometric analyses are used to construct flowpaths and the result is an indication of only the direction of flow. However, it almost completely neglects the timing and lateral migration in low permeability zones. Flowpath and hybrid models have the disadvantage of complex geometries. Although the full 3D flowpath concept requires huge amounts of effort, processing is very fast (Hantschel and Kauerauf, 2009).

Comparison of the three flow models

Darcy equations describe anisotropy but not invasion percolation. The invasion percolation emphasizes higher resolution and has shorter migration distances. Flowpath and invasion percolation dedicate all the time control to hydrocarbon generation and expulsion. The invasion percolation method is not physically very different from flowpath migration modelling, but it has the advantage that it can model hydrocarbons percolating through a whole basin model of complicated geometries with significantly varying migration properties. It is able to include the effects of relatively small scale structures such as lamination, cross-bedding, and pervasively faulted strata to a high degree of accuracy. Table 5.1.2 (a) lists the requirements that are important to the three flow model types and (b) list the capabilities of the flow model type.

Table 5.1.2 Comparison of the three flow models

3D Modeling requirements :	Darcy	Flowpath	Percolation
Dynamics	++	-	-
Scaling	-	+	+
Processing speed	--	+	+-

Data and availability	+	+	+
-----------------------	---	---	---

Petroleum System Components :

Source and Expulsion	+	-	-
Migration – low permeability units	+	--	+
Migration – high permeability carriers	-	++	+
Reservoir bodies	--	++	+

Risking in PetroMod Petrorisk

Risk evaluation on the results from 1D, 2D and 3D modeling is carried out to define boundaries and distributions of variables including source rock thickness and its richness as well as reservoir and trap geometry. Methods such as Monte Carlo and Latin Hypertude and multiple process runs allow statistical evaluations and for the results to be correlated enabling assessment of uncertainties of the data on the results of the modelling (Higley et al, 2006). Table 5.1.3 lists some PetroRisk capabilities;

Table 5.1.3 Results that can be obtained from Petrorisk

PetroRisk results	Comments
Timing and extent of the thermal maturation for each source rock interval.	3D results include map images, cross sections, or as point sources through 1-D extractions
Migration flowpaths and vectors in 2-D to 3-D space	Shows generation in time, directions of flow, and accumulations of oil and gas.
Percent contributions and volumes of generated hydrocarbons through time for each source rock unit.	Can show results in scales of single accumulations to the entire model.
kerogen transformation (%) in source rocks to oil and (or) gas.	Produces graphics and tables of transformation results
Coal rank through time can be evaluated using Sweeney and Burnham (1990) Easy%Ro, adsorption mass, and other modeled calculations.	Results will be invaluable in assessment of coal and coalbed methane resources.
PVT calculations for all intervals, including capillary, lithologic, and hydrodynamic pressure	Aids in making predictions .on hydrocarbons formation Volume factor (FVF) and possibly fluid composition, gas-oil ratios, condensate occurrences, and pressure history. Hydrocarbon composition and

	volumes are calculated by PetroMod
Compaction history using default values assigned by PetroMod or user-defined porosity/permeability/depth through time can be used for the lithologies.	Analogs can be applied for this and numerous other parameters in the modeling.
Catchments are mainly used for migration pathways, spillpoints, and accumulations across these surfaces in a model	
Timing of hydrocarbon generation relative to trap formation.	Also includes the consequences of events such as faulting, basin uplift and tilting, salt percolations and intrusions on petroleum migration

The F_well Petroleum System Case Study

An attempt is made to carry out thermal modelling of a hypothetical F_well (.) petroleum system. The modelling is mainly based on geological information from a well log and geochemical data from the well samples. Eighteen samples had been measured to subsurface depth of approximately 4300m.

Sensetivity regarding the data used does not allow for the sharing of the data from this well or its location. As such the well is placed somewhere in the Meditarrenean and regional geology is inferred from a very broad perspective of the geology of this zone and the available measured data.

6.0 Results and Discussions

6.1 Analysis of vitrinite reflectance and pyrolysis data

Prior to modelling in Petromod 1D, the pyrolysis results and vitrinite reflectance data were analyzed to determine the kerogen types and estimate the potential of the layers.

Pyrolysis of immature source rock catalyzes the reactions that initially release the oil, oil generating, gas generating and inert components of the organic matter. Rock-Eval pyrolysis data input into the Geochemistry Editor in PetroMod to produce maturation indicator plots but the same plots were produced using excel and in matlab to superimpose our data on van Krevelen type diagrams etc.

Analysing Rock Eval Pyrolysis Data

Rock-Eval pyrolysis data provides the indication of when sufficient oil has been generated to allow oil to be expelled from the source rock. The Rock Eval pyrolysis technique includes the initial progressive heating of a sample to 550°C in an inert atmosphere, using a preselected rate of heating. The Rock-Eval instrument measures the amount of hydrocarbons evolved from a sample as the sample temperature is raised. The quantity S1 represents the fraction of the original genetic potential which has been effectively transformed into hydrocarbons. The residual potential is given by the S2 quantity which describes the genetic potential that remains and has not been used to generate hydrocarbons. The genetic potential is then given by S1 + S2, given in kg hydrocarbons per ton of rock. This represents the abundance and type of organic matter (Tissot and Welte, 1975).

Analysing the petroleum Quality using TOC (%), S1 and S2.

TOC % values are generally below 1, with an average of 1.21. Layer 4 and Layer 5 samples show a very wide range consisting of both the lowest values and the highest values (Figure 6.1.1). F_well TOC (%) data generally have poor HC source potential. However some Layer 1 and Layer 4 samples indicate fair source potential and half of Layer 5 samples indicate very good source potential.

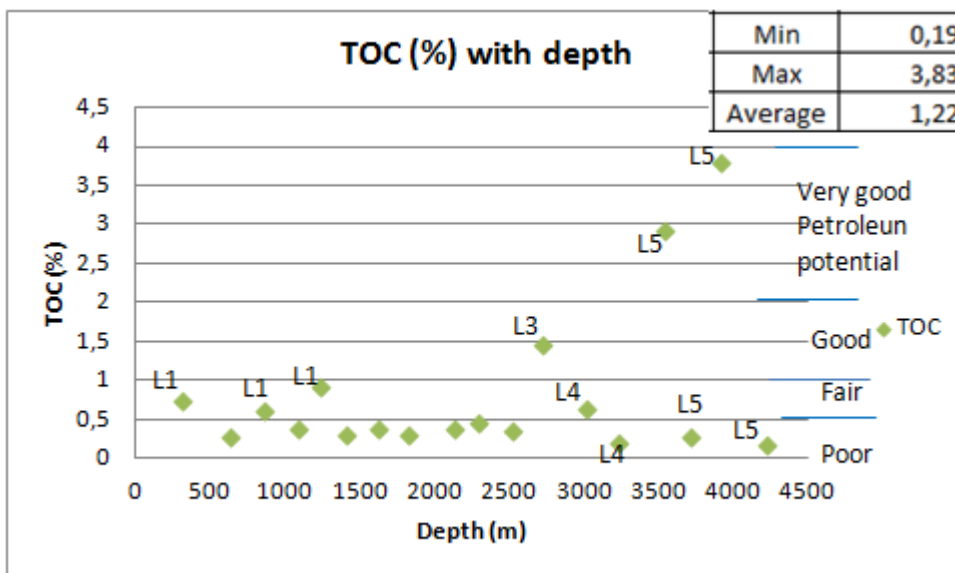


Figure 6.1.1 TOC (%) A significant number of samples with the majority belong to Layer 1 samples and one sample from Layer 4 plot as poor source potential. The remainder of the Layer 1 samples and one Layer 4 sample have fair source potential. Half of the Layer 5 samples plot as poor source rocks while the other half show very good source potential.

S1 and S2 (Figure 6.1.2 and Figure 6.1.3 below) provide description of kerogen type and the character of expelled products to give approximate values based on thermally immature source rock. S1 representing the hydrocarbons present in the source rock prior to cracking. When analyzing S1 results, the samples fall within the poor petroleum potential zone categorized as samples with 0 – 0.5 mg HC/ g dry rock while 2 of the 5 Layer 5 samples plot in the 0.5 – 1 mg HC/ g dry rock distilled by pyrolysis. Only 2 samples both from Layer 5 of 18 samples in F_well fall in the very good hydrocarbon potential having 10 – 20 mg HC/ g dry rock cracked from kerogen by pyrolysis (S2), the rest of the samples fall within the 0 – 2.5 mg HC/ g dry rock according to the tables from Magoon and Dow, (1994).

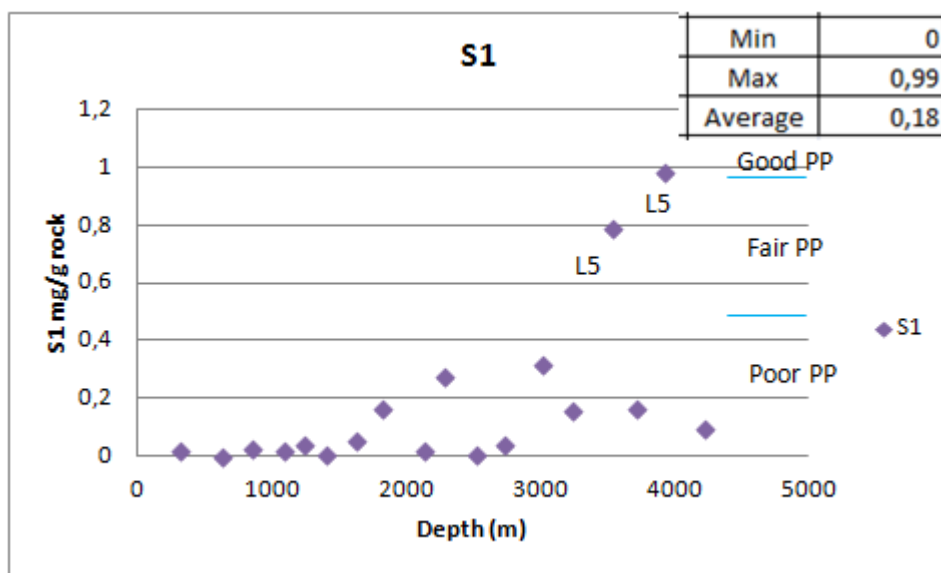


Figure 6.1.2 Petroleum potential distribution of F_well samples. Hydrocarbon potential represented by hydrocarbons that formed from temperature cracking of the immature source rock. Only Layer 5 samples show considerable potential.

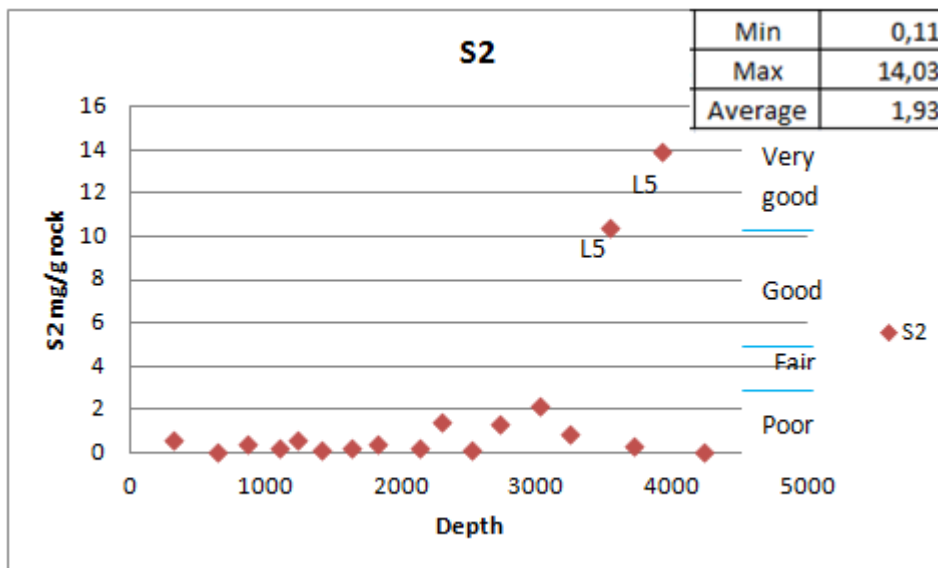


Figure 6.1.3 Hydrocarbons resulting from thermal cracking of kerogens

Describing Kerogen Type by the Hydrogen Index

Hydrogen Index (HI) values are evaluated to determine kerogen type. Figure 6.1.4 shows that there are no type I kerogen and Type II /III kerogen samples in this batch (>600 mg HC / g TOC). The majority of the samples which are mainly from Layer 1 , (with the remaining samples of Layer 2, 3 and 4) classify as a type III kerogen. Half of Layer 2, 3, 4 and 5 samples indicate the organic matter in these rocks to be kerogen type II.

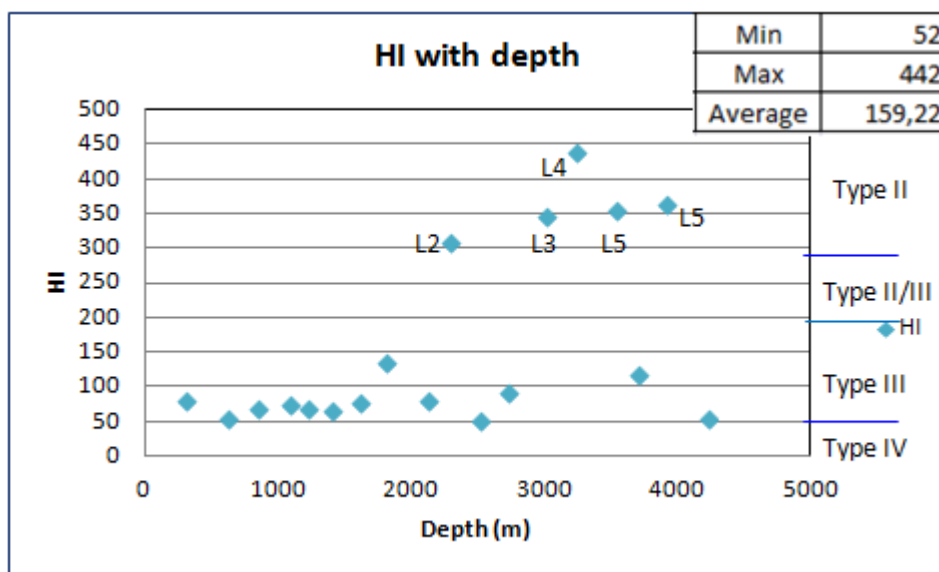


Figure 6.1.4. Hydrogen Index to determine kerogen type mg HC/g TOC for F_well samples, according to the classification tables in Magoon and Dow, (1994).

Evaluating Thermal Maturation by Rock Eval pyrolysis data

Thermal maturation of the F_well rocks were evaluated based on Ro data, Tmax and Productivity Index.

Cross-plots of Rock Eval pyrolysis Tmax versus (measured) vitrinite reflectance (%Ro) in Figure 6.1.5 below indicates that the majority of Layer 1 samples are immature while some Layer 3 and Layer 4 samples indicate early maturity. Samples indicating peak maturity all belong to Layer 5.

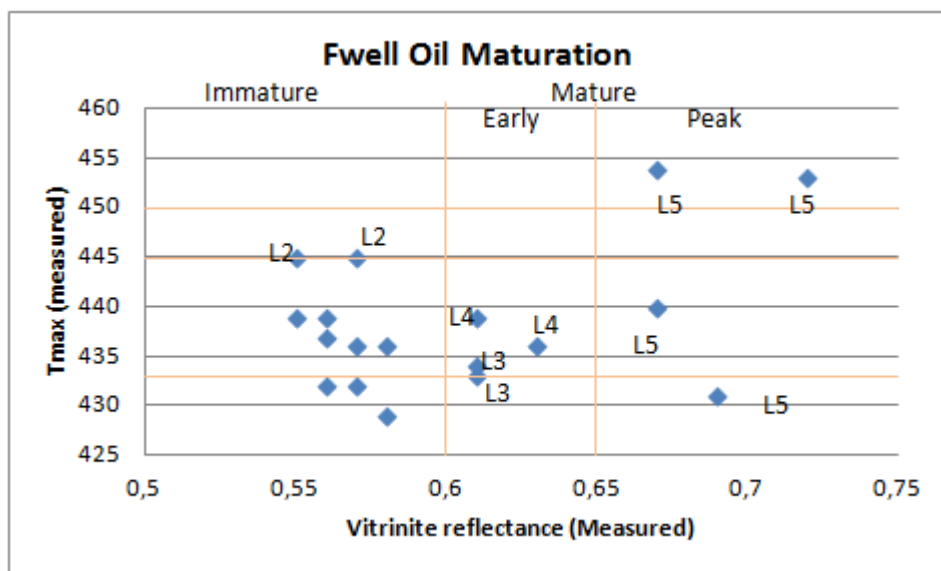


Figure 6.1.5 Cross-plots of Rock Eval pyrolysis Tmax versus vitrinite reflectance (%Ro) (measured), showing the maturation of the F_well samples.

Analysing maturity of the source rocks by vitrinite reflectance

The droplet diagram (Figure 6.1.6) allows for the approximation of the hydrocarbons that can be expected from the vitrinite reflectance data of F_well (.) petroleum system. Measured non suppressed vitrinite reflectance values range from 0.56 to 0.72% Ro. The vitrinite reflectance values calculated from Tmax range from 0.56 to 1.01% Ro. The vitrinite reflectance was calculated from the relation of $(0,018 * Tmax - 7,16)$. Both vitrinite reflectance data ranges indicate that the source rocks being simulated have oil forming capabilities. Furthermore, the Ro% values calculated from Tmax values show that the source rock is also gas forming.

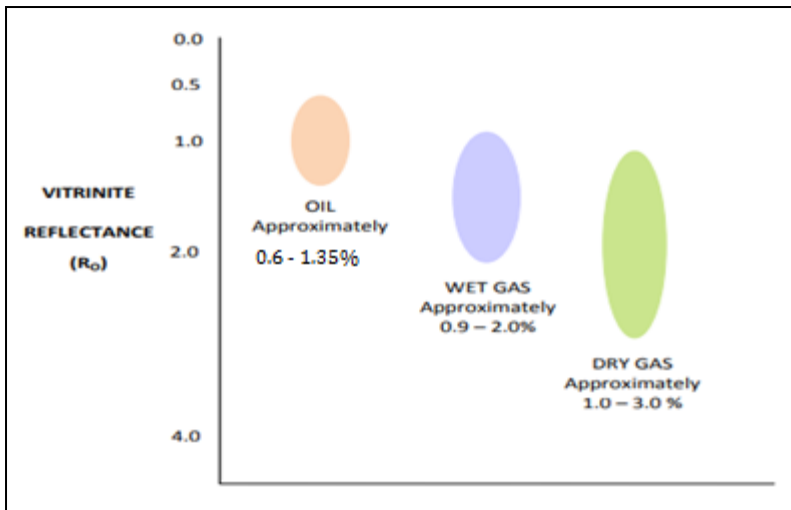


Figure 6.1.6 Edited from the British Geological Survey based on droplet diagram first presented by W.Dow in the Journal of Geochemical Exploration 1977

Table 6.1.1 Vitrinite reflectance as a maturity Indicator; comparison values are taken from the British Geological Survey.

Maturity level	Definition	%Ro	Layers within the range	Comments
Under mature	Insufficient exposure to heat for HC generation	-	-	
Oil window	Onset of oil generation	0.5 - 0.6	L1, L2, L3	L4, L5 at 0.63 – 0.72
	Termination of oil generation	0.85 - 1.1	-	Only Ro% some values calculated by Tmax
Gas Window	Onset of gas generation	1.0 - 1.3	-	
	Termination of gas generation	~ 3.0		
Over mature	Spent rocks; HC generation potential depleted	-	-	

From the Table 6.1.1 it can be deduced that the source rocks in Layer 1, 2 and Layer 3 have vitrinite levels at the onset of oil generation while L4 and L5 are in the oil generation zone.

Evaluating Tmax

The Tmax values from F_well pyrolysis data (Figure 6.1.7) were measured using Rock-Eval 2. The Tmax values measured by this method have been reported to overestimate results by (20 to 30°C), (personal communication by supervisor). The F_well Tmax values range from 429 – 454 °C, with an average value of 438 °C. L2, L4 and L5 have Tmax values in the range of peak maturity of 445-450 °C. Figure 31 shows some L1 and L2, including half the samples from L4 samples to fall within the immature zone stages. Most of the L1 and L3 samples and both L4 samples fall within the early maturity stage. Layer 5 samples also show to be in early maturity zone. Only layer L5 have Tmax values in the late stage maturity of oil.

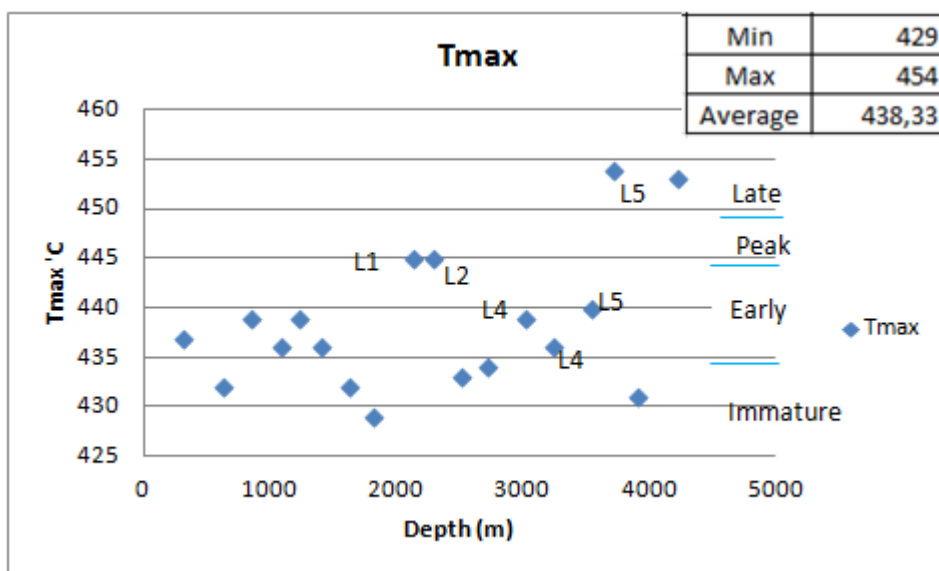


Figure 6.1.7. Tmax distributions in F_well. Maturation intervals are as per maturation tables from Magoon and Dow (1994).

As per the productivity Index graph (Figure 6.1.8) most of Layer 1 samples have low level conversion falling within the $PI < 0.1$ interval, together with half of the Layer 5 samples. The layer 4 samples and the other half of the Layer 5 samples indicate high level conversion. Magoon and Dow (1994) class the Layer 4 samples as Early maturity samples while the two Layer 5 samples each indicate peak to late maturity. The production Index (PI) values for the F_well are in the range 0 – 0.5, with an average of 0.12. When analysing the petroleum potential of F_well samples, only layer 5 have considerable potential showing as fair to bridging between fair and good.

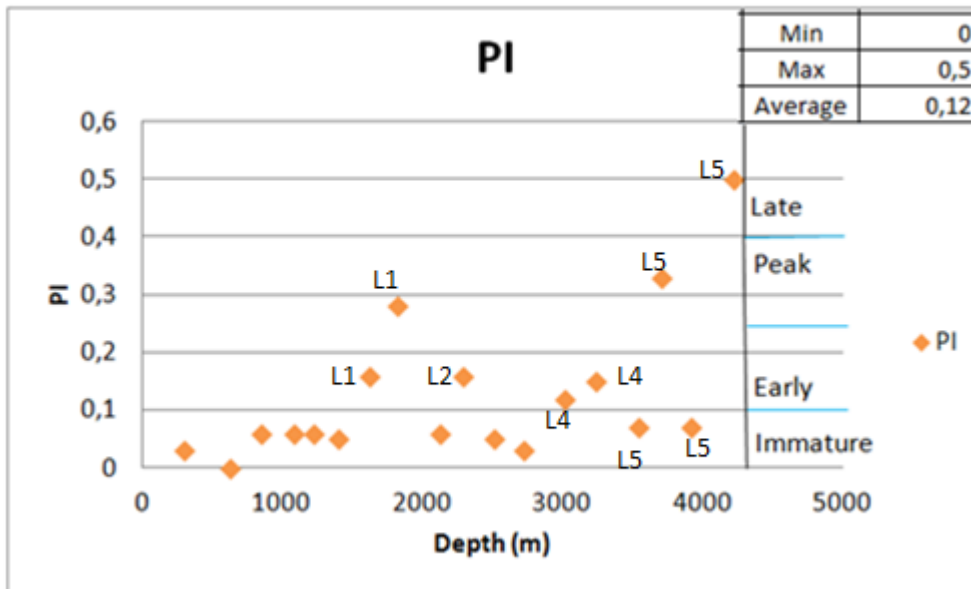


Figure 6.1.8 PI < 0.1 indicates low level conversion and PI > 0.1 indicates high level conversion. The Layer 1 sampling that plots at 0.28 PI is probably an outlier as it is the only high value within the depths below 3500m.

Evaluation of Quality and quantity of organic matter from combined plots

TOC% and other Rock–Eval pyrolysis data such as S1 and S2 can be used to assess source rock potential in sediments Tissot and Welte (1984). The total organic carbon content values for the F_well samples are between 0.19 and 3.83 wt% indicating poor to fair source rocks. The relation of S1 versus TOC (%) (Figure 6.1.9) indicates that the all the studied rock samples were characterized by (autochthonous) hydrocarbons, which indicates that the oil produced from the F_well migrated from another source rock.

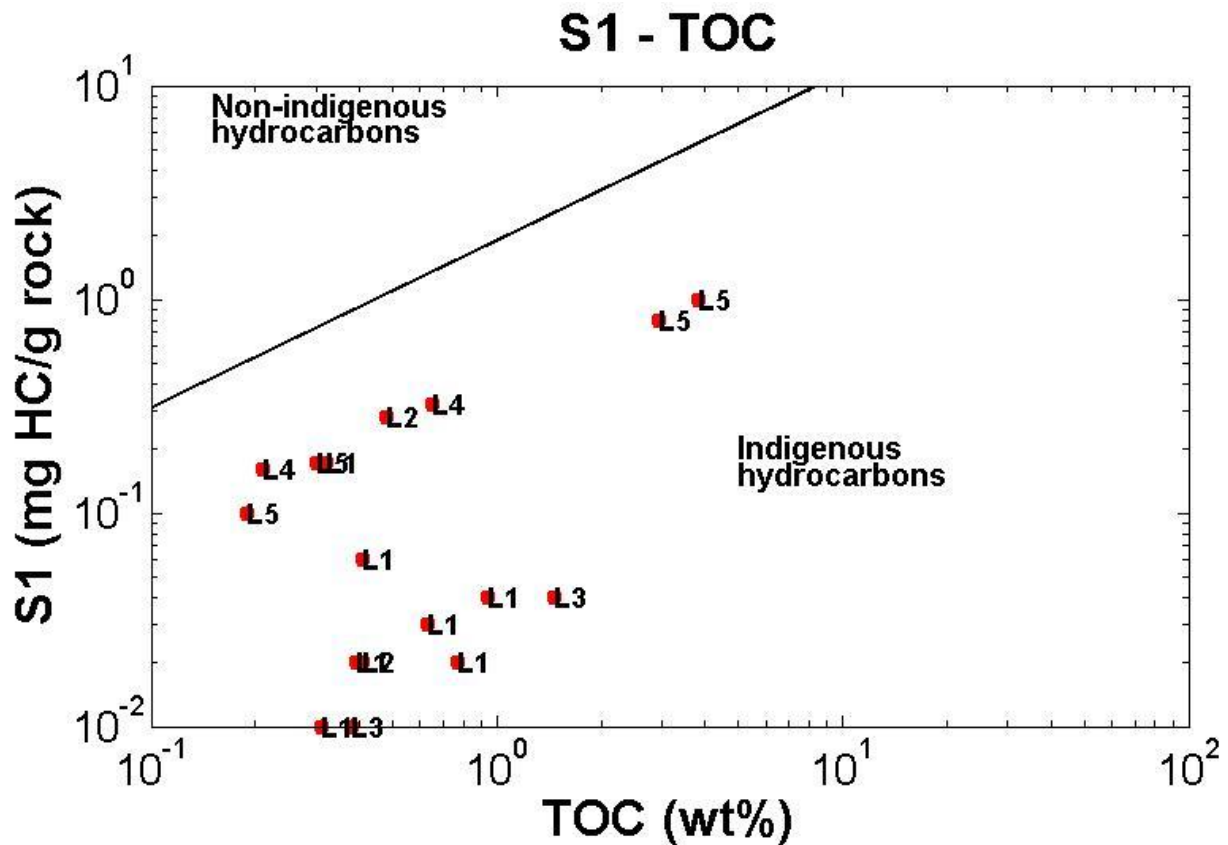


Figure 6.1.9. Free hydrocarbons/ absorbed organic matter (bitumen) (S1) plotted with the total organic carbon. The plot distinguishes the indigenous hydrocarbons (autochthonous) and non-indigenous hydrocarbons (allochthonous).

Generating potentials

S1 + S2 gives the generating potential (GP) for the F-well. Hunt (1996) categorized source rocks with a GP <2 to have poor generating potential, those between 2 to 5 have a fair GP, those falling within 5 to 10 to have a good GP and >10 to have very good generation potential. The F_well samples shows Layer 1 and 2 rocks to be source rocks with a poor to fair generating potential (Figure 6.1.10a). Some of layer 3 has poor generating potential and some good generating potential. Layer 4 samples show to have a poor and fair generating potential but layer 5 samples are good generating potential source rocks. On the other hand, the plot of TOC (wt%) versus HI mg/g (Figure 6.1.10b) shows that the F_well samples from layer 1, 2 and 3 are mainly fair gas and/or oil source rocks. Layer 2 and Layer 4 are indicated to be good oil source rock. One Layer 4 sample is considered to have been contaminated or stained. Conversely layer 5 samples plot as very poor to fair source rocks in the (Figure 6.1.10b).

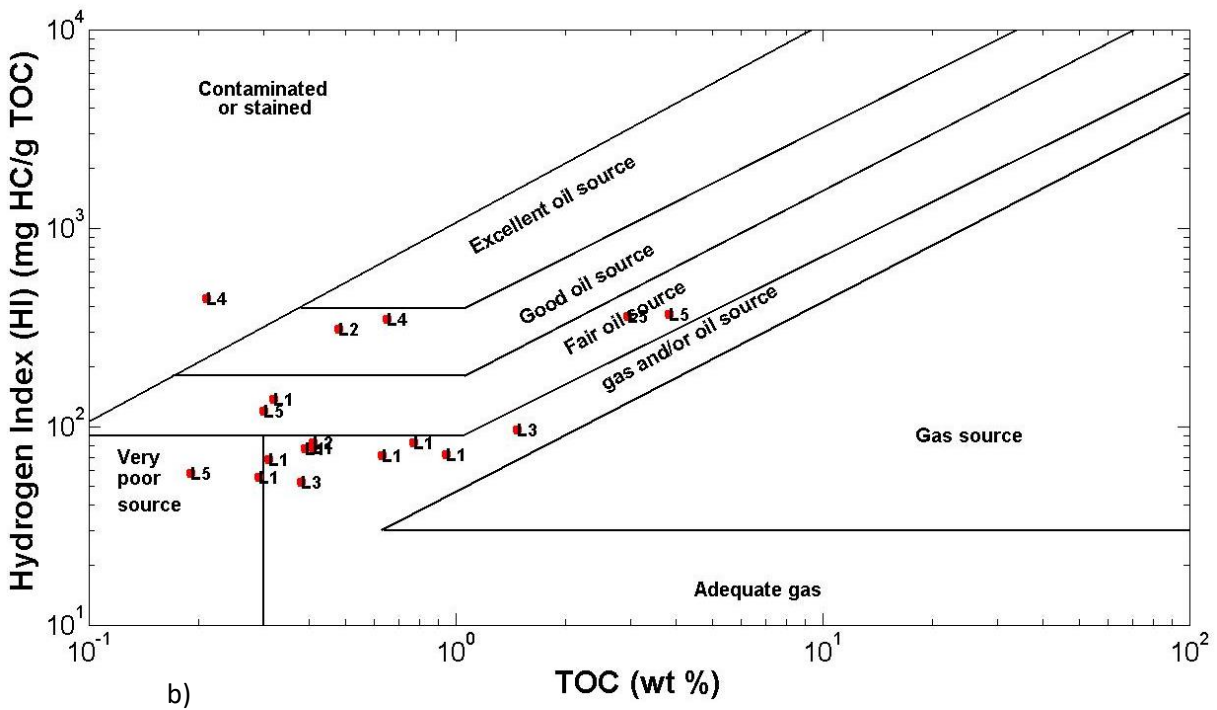
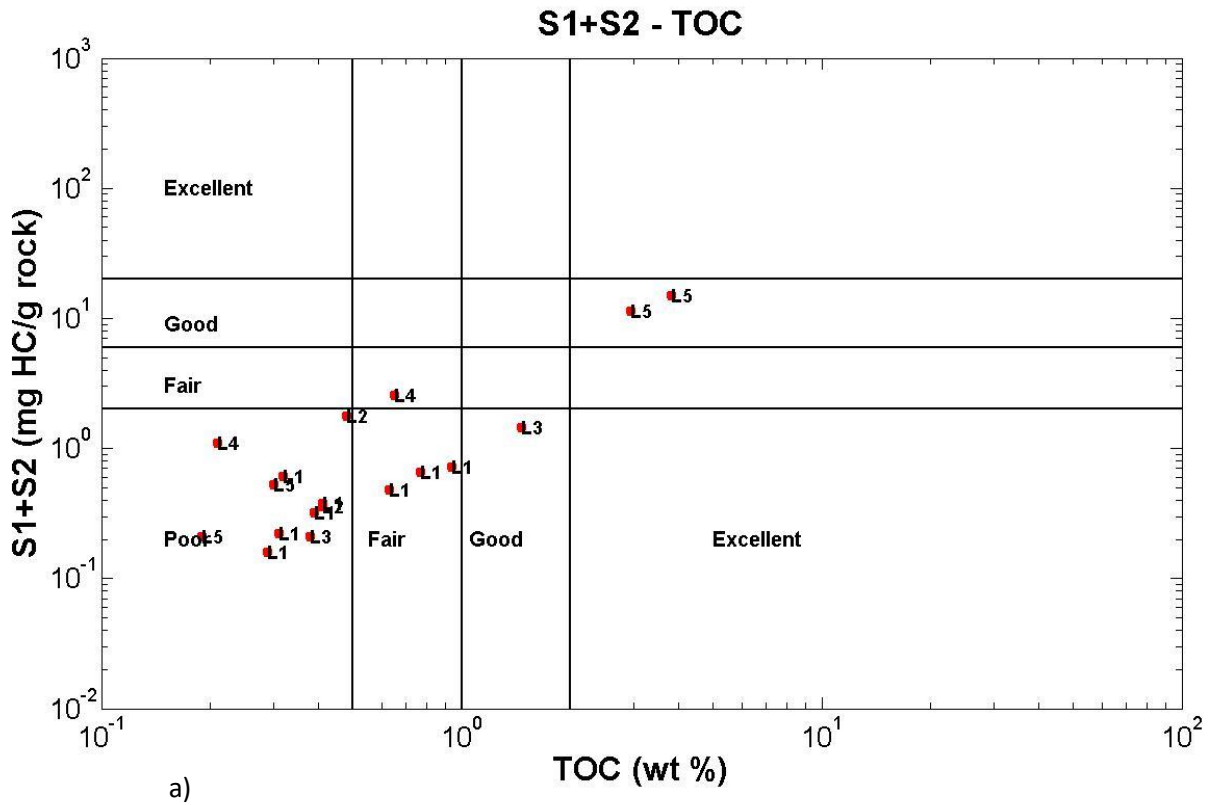
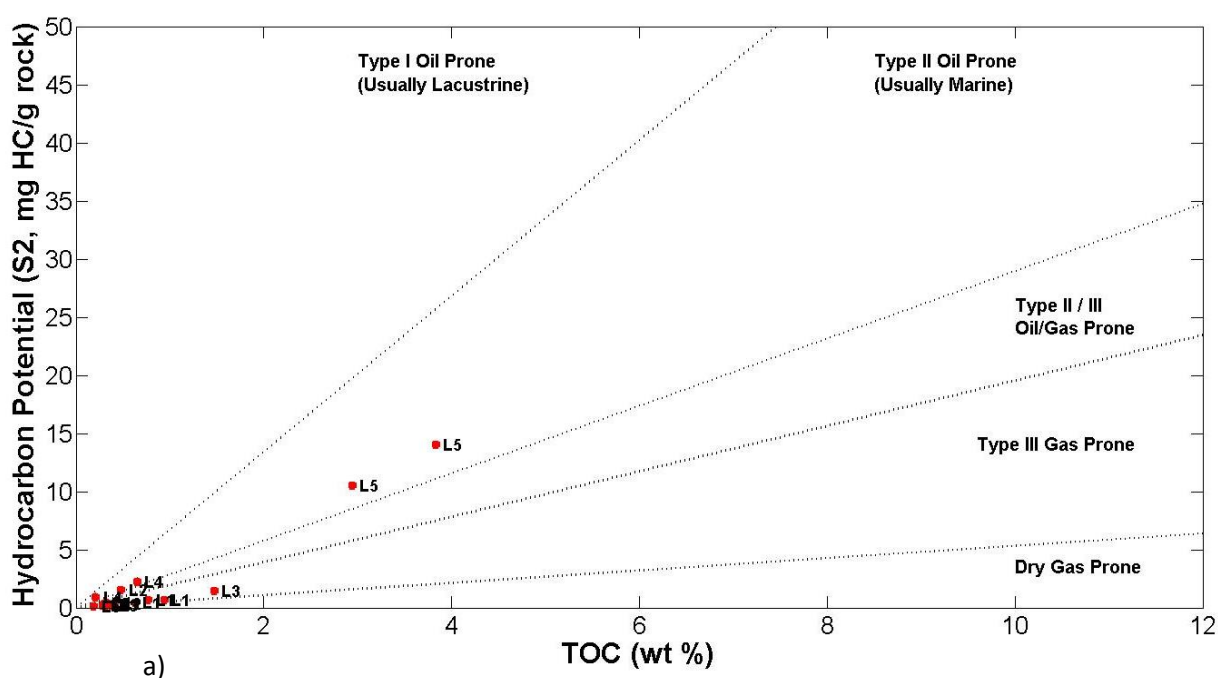


Figure 6.1.10.a and b. Generating potentialities of F_{well}

Genetic type of organic matter

Knowing the initial genetic type of organic matter of a certain source rock allows for the prediction of oil and gas potential. The kerogen type diagram by Langford and Blanc-Valleron (1990); (Bordenove et al, 1993) is used here to show how TOC plots against S2 (Figure 6.1.11a). This diagram shows that the F_well source rocks in layer 4 and in layer 5 are characterized by kerogen of type II (oil prone). Layer 3 samples plot as type III Gas prone. Based on pyrolysis data kerogen classification diagrams were constructed using the HI versus OI plot as carried out by Van Krevelen (1961), which is used to determine the kerogen type (Figure 6.1.11b). The good correlation correlation between the hydrogen index and the H/C ratio as well as between the oxygen index and O/C ratio enables the hydrogen index and the oxygen index to be plotted instead of the van Krevelen diagram and be interpreted the same way, (Tissot and Welte, 1984). The results show the F_well samples from mainly layers 1, 2 and 3 to be found in both type II and type III zones. The layer 2, 4 and layer 5 samples plotted in kerogen type II zone.



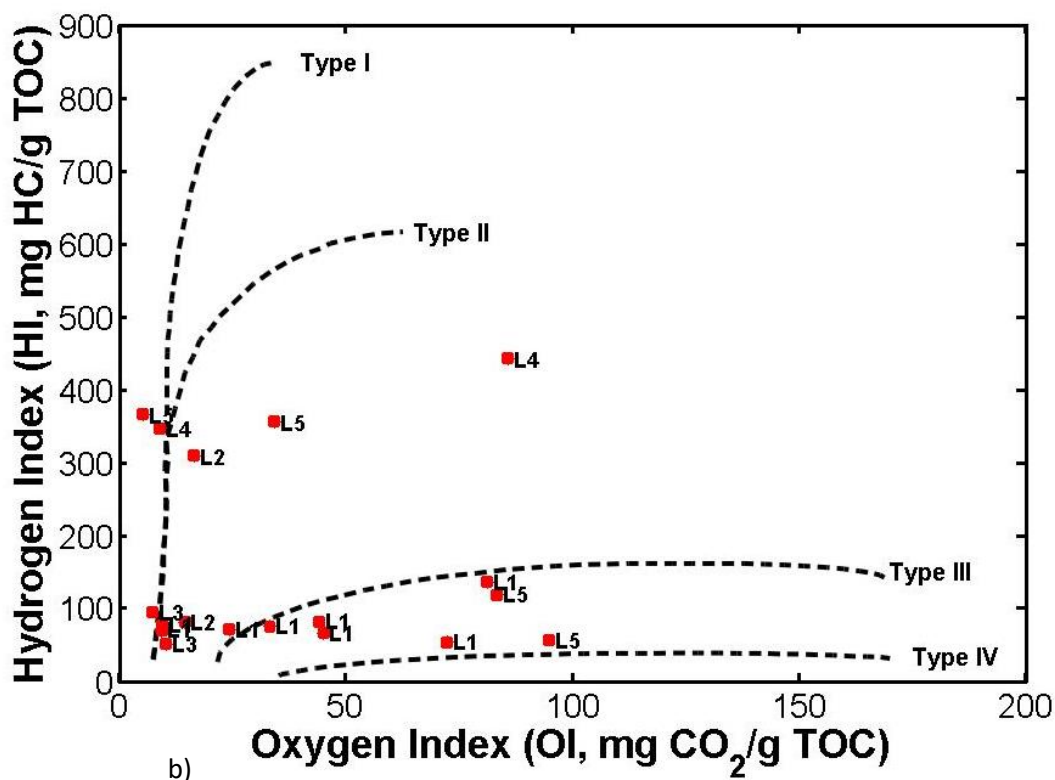


Figure 6.1.11 (a) and (b) Genetic type of organic matter of F_well

Thermal maturation

Sediment burial mechanisms as well as temperature variations influence the thermal conversion of organic matter (Tissot and Welte, 1984). The concentration and distribution of hydrocarbons in a particular source rock are determined from the kerogen type and level of thermal alteration (Longford and Blanc-Valleron, 1990). Rock–Eval temperature pyrolysis “Tmax” and production index “PI” are used to analyse and determine level of thermal maturity of source rocks (Espitalie et al. 1985). Peters (1986) and Espitalie et al. (1985) define the oil generation from source rocks to begin at Tmax = 435–465 °C, and production index “PI” between 0.2 and 0.4, the organic matters are in immature stage when “Tmax” has a value less than 435 °C, and “PI” less than 0.2 and the gas generation from source rocks begin at “Tmax” 470 °C, and production index “PI” more than 0.4.

The HI versus Tmax plot as was previously used by workers including (Espitalie et al. 1985) was used in this case study to determine the kerogen type and maturity level (Figure 6.1.12a). The results show that the F_well samples are mainly type II kerogens. A few samples; L1 and L5 fall within the immature zone but the majority of the samples fall within the type II mature kerogen zone. The layer 4 and layer 5 samples plot in the mature zone grading to marginally mature zone with kerogen of type II–III and type II. The plot of Tmax

versus PI diagram (Peters 1986; Waples, 1985), (Figure 6.1.12b) indicates two layer 1 and one layer 5 samples to be immature, while all others plot in the mature oil window with layer 4 and layer 5 samples showing the more significant productivity index.

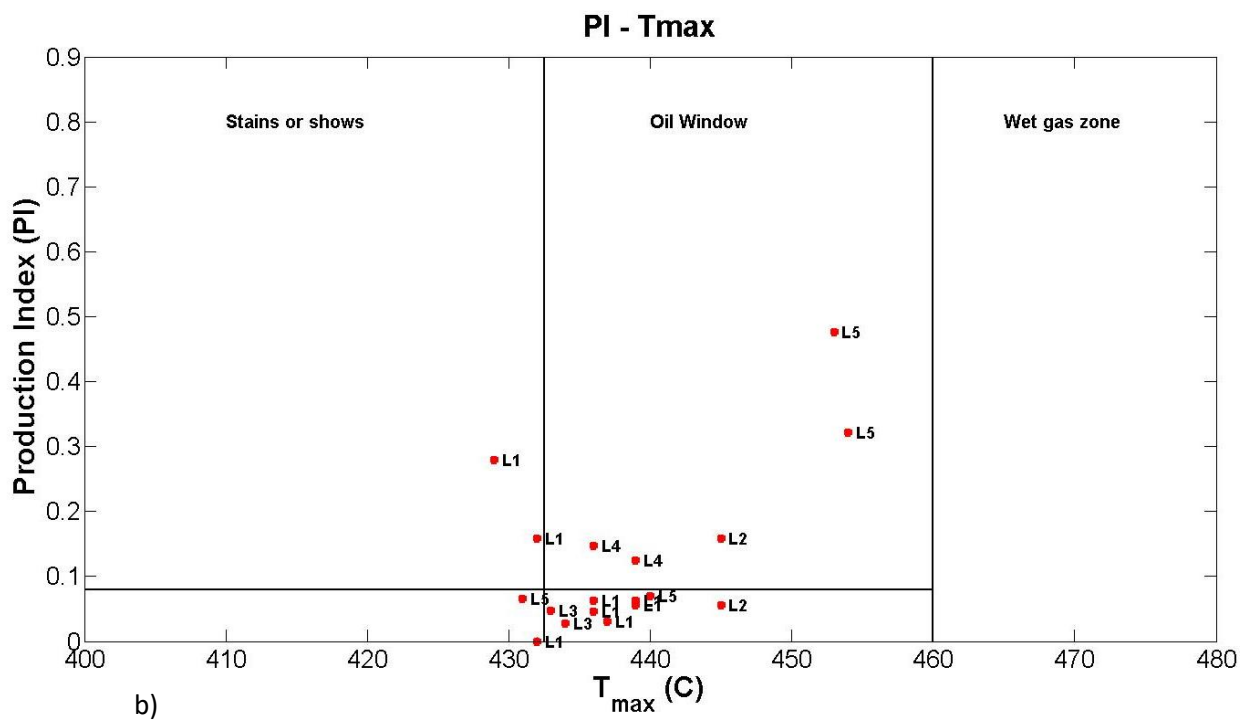
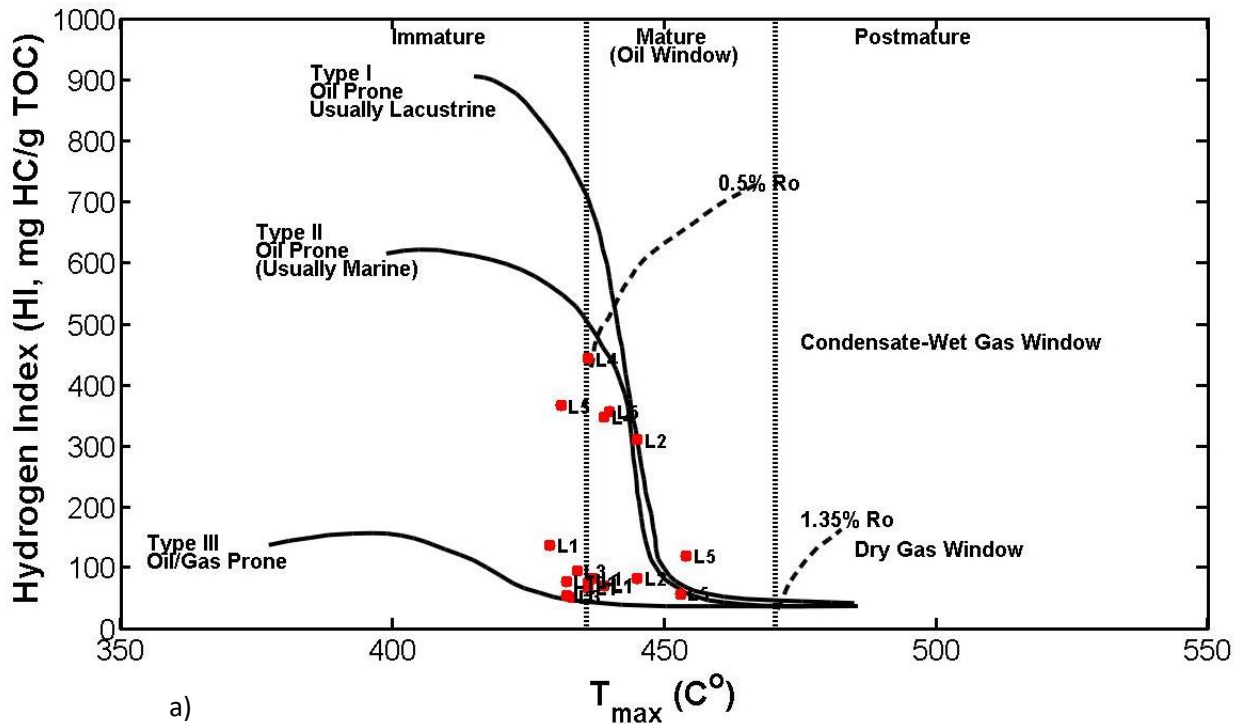


Figure 6.1.12 Thermal maturation of F_well rocks.(a) Tmax versus Hydrogen Index and (b) Tmax versus productivity Index.

Summary

Source rock origin and quality

The studied F_well rock samples were characterized as (autochthonous) hydrocarbons, which indicate that the oil resulting oil migrated from another source rock. L1, L2 and L3 are mainly gas and / or oil producing rocks with L1 and L2 indicating poor to fair generating potential while L3 has both poor and good GP. L2 and L4 are good oil source rocks but L4 is indicated as having poor to fair generating potential. L5 is indicated as very poor to fair source rock that has a good generating potential.

Both the Rock Eval pyrolysis results when the pyrolysis parameters were plotted against depth (assessment 1) and, when the data were superimposed in graphs to compare with known ranges confirm that Layer 1 and Layer 2 immature samples are poor source rocks. The plots also confirm that the Layer 3 rocks are good source rocks. Layer 4 samples are indicated to have fair source potential but the TOC/HI plot (assessment 2) shows there might be some contamination. The assessment 1 plots indicate that half of Layer 5 samples are poor source rocks, while the other half indicates very good source potential. However the S1 +S2 plot indicates all Layer 5 samples to have very poor source potential.

Determining Organic matter type

HI versus depth plot from Assessment method 1 indicates that Layer 1 and some zones in layers 2, 3, 4 and some parts of Layer 5 have Type III kerogen. The rest of the Layers 2, 3, 4 and Layer 5 samples classify as Type II kerogen. The plots from Assessment method 2 show that most of the samples have very low TOC (%) and S2, thus they plot very low in the diagram (Figure 6.1.11 a) (mainly Layer 1 and some from Layer 2 samples as well as half of the Layer 5 samples. However some of these samples clearly plot as dry gas prone samples. Half the samples from Layers 2, 4 and the other half of Layer 5 samples plot as type II/III (oil/gas prone). The HI/OI plot (Figure 6.1.11 b) show all Layer 1 samples and half of Layer 5 samples as Type III kerogen. Layer 2, Layer 3 and Layer 4 and half of Layer 5 are indicated to be composed of Type II kerogen.

Correlation to geology

When the above findings are correlated to the geology from the well log, it is possible that Layer 1 samples can be poor source rocks as Layer 1 is composed of sandstone and siltstone with marl. Layer 2 is composed of Limestone, (which can sometimes be a good source rock). Layer 3 which is indicated by both methods to be a good source rock is actually a conglomerate with some quartz. This seems an error as conglomerate is not normally considered to be good source potential rocks. Contamination or human error can be expected here. Layer 4 is composed of limestone and so might be expected to have some source potential. The Layer 5 unit is composed of mainly dolomite interbedded with some shale and chert. Following this analysis Layers 1, 2 and

3 will not be considered as source rock material. Layer 4 and Layer 5 (while showing conflicting results), have potential as source rock material.

Thermal maturity assessment

Layer 1, 2 and some of Layer 3 samples plot as immature in the (assessment method 1) Tmax vs depth plots. One Layer 3 and both Layer 4 samples indicate early maturity. All Layer 5 plots indicate peak maturity. The Tmax versus HI plot in Assessment 2 method show half of Layer 5 samples to be immature but most of Layer samples plot midway between immature and mature. Layer 4 and Layer 5 samples plot in the mature oil window zone. Most of the Layer 1 samples, half of the Layer 2 samples and all Layer 3 samples indicated low level thermal conversion. Both layer 4 samples have high conversion level with $PI > 0.1$ but the Layer 5 samples have much higher productivity index (corroborating the assessment 1 findings).

Determining onset of Oil generation

Table 6.1.1 shows that Layer 1,2 and 3 samples are at the onset of oil generation zone, while the Layer 4 and Layer 5 samples are within the oil window.

Determining onset of Expulsion

The value of S1/TOC should increase until oil expulsion begins. “After oil expulsion begins, the value of S1/TOC remains approximately constant over a limited depth interval and then decreases with increasing depth and thermal maturity. F_{well} data doesn’t seem to follow this trend. For the Norton basin analysis (in Magoon and Dow (1994) the S1/TOC had to reach the values of 0.1 – 0.2 for oil expulsion to start, if used here that zone is as shown in (Figure 6.1.13). If that reasoning is followed, F_{wel} lithologic units below 1620m are not capable of oil expulsion at any level of thermal maturity level. The majority of the L1 samples fall within this category.

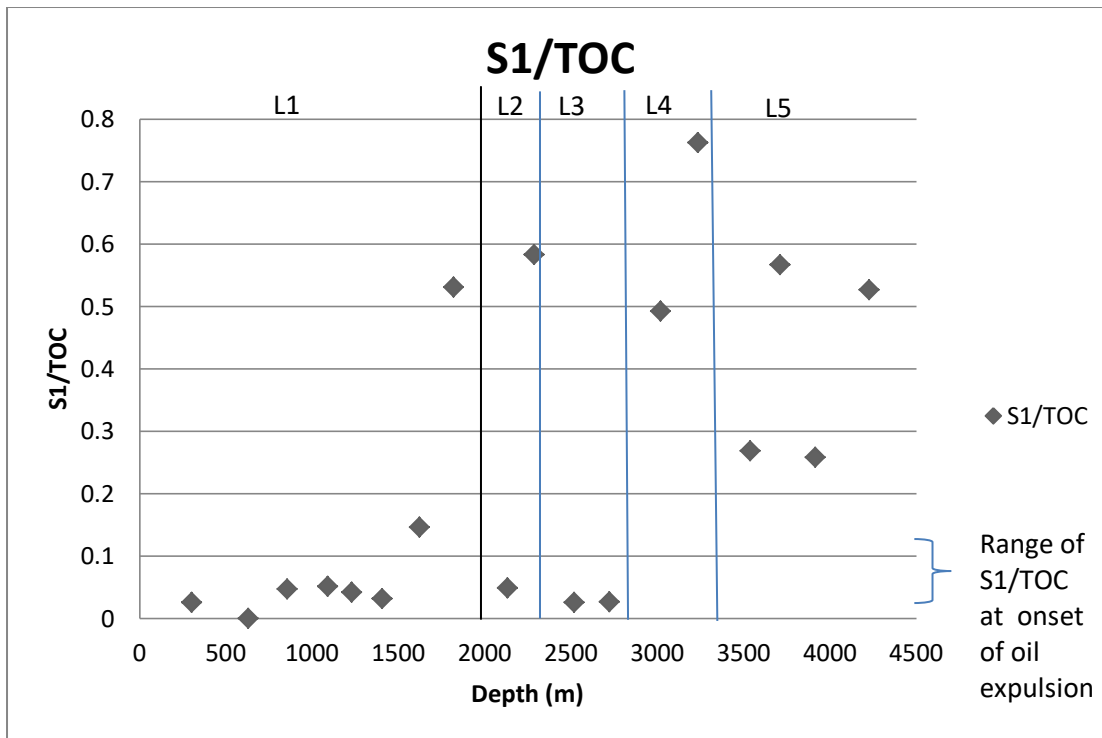


Figure 6.1.13 Determining onset of oil generation for F_well.

Figure Oil content/TOC as shown by the S1/TOC for the F_well. To determine the range of samples at the point of onset of oil expulsion if a value of 0.1 to 0.2 used for the Norton basin in Magoon and Dow (1994). This plot confirms the categorization in Table 6.1.1 that Layer 1, Layer 2 and L3 samples are at the onset of oil generation.

6.2 Modeling F_well (.) Petroleum system in PetroMod 1-D

Based on the indications provided by analyses of geochemical data in section 6.1, and the geology log an attempt to model the F_well petroleum system was carried out.

Model validation-Ro data

The modeling of source rock maturation focusing on evolution of the thermal history was performed with the IES PetroMod 1D software. Well sample data is used as control points to constrain the model when extrapolating from present day to find representation of geologic and thermal events in time (Barker, 1996). The only available validation data was the measured vitrinite reflectance data and the vitrinite reflectance data calculated from the Tmax from F_well pyrolysis results. Rock Eval pyrolysis results and vitrinite reflectance measurements had previously been carried out on only 18 samples in the F_well. Some projects have vast amount of available model validation data from several wells over a wide area enabling the data to be

screened for outliers or impossible data sets and still remain with a representative number of samples to work with. The same cannot be said for this case study. Ro values of Layer 1 from the measured vitrinite reflectance show a vertical trend while the Tmax-derived Ro data in the same layer increase linearly to the base of Layer 1. Majority of these values except for one were not considered for the model validation exercises. It is clear from the pyrolysis data analysis exercise (section 2.3) that layer does is not a source rock and so its significance is only as overburden material and or reservoir. The model simulation requirements for the two types of vitrinite reflectance data were the same, but the Tmax-derived Ro data model approximated the real data more closely.

Geological constraints

The location of F_well in the Mediterranean zone cannot be elaborated on as it is (unpublished data). Geological constraints are crucial when attempting to simulate the burial history of any zone. Attempts are made to infer geological constraints in this case study to closely as possible approximate a possible geological scenario. Some prominent thrusting of mainly a thick limestone layer occurs in the regional geology of the area where F_well was drilled. By geological reasoning a thrust zone will obviously have some faulting and fracturing occurring in the surrounding layers. The F_well geological log indicates an unconformity underlying limestones which is inferred to the main hiatus occurring regionally in the zone where F_well is located. There is no indication of folding in that zone in the regional geology publications or the well log. Also there is no indication of the bedding or layer inclinations. This information would be helpful in ascertaining the presence of a trap or possible migration directions in that region. The presence of salt layers has been indicated in several publications covering the regional geology of the zone. Some workers have estimated a large erosional thickness for a certain section in this region and this information was inferred to estimate possible erosional losses in the area of our F_well. Source rocks in this zone are simulated to be occurring in Layer 4 and Layer 5. This is because the lithologies of these two layers fit descriptions of source rock lithologies. Also the analysis of the vitrinite reflectance data and pyrolysis data above indicate these two layers to have some source rock potential.

PetroMod calculates the thermal conductivity values for the lithologies using the Sekiguchi model. Conductivity value ranges for the layers estimated at certain temperature intervals are given in Table 6.2.1.

Table 6.2.1 Lithotype conductivities

Age	Lithotype	Layer	Depth (m)	Temperature (C)	Heat flow mW/m ²	Conductivity W/m/K
0	Marly SS with Siltstone	L1	0	~17 - 28	60	2.41

34	Marly SS with Siltstone	L1	1950	~28 - 30	50	2.41
56	Limestone (Waulsortian mound)	L2	2200	~30 - 33	40	2.95-2.93
90	Conglomerat e	L3	2730	~33 - 55	40	2.67 - 2.61
111	Limestone (Waulsortian mound)	L4	3280	~55 - 70	40	2.85 - 2.72
160	Dolomite and Shale	L5	4287	~70 - 90	25	2.57 – 2.52
201	Dolomite and Shale	L5	4287	~90 - 100	15	2.57 – 2.52

Some of the conductivity values are average estimations between the nearest values as the simulator gives conductivity values at every 10 °C.

Model Inputs

Main Input table

Lithological units, erosional events and unconformities can be input into the Main input table in PetroMod with the ages of deposition of the units as well as the ages when the other events took place. PetroMod 1D gives the option to create a model from scratch or extract 1D models from 2D and 3D. The F_well 1D model was created directly by typing in the stratigraphy data into the main input table. The events are entered in a hierarchal manner in the sequence which they occurred to mimic the stratigraphy of the zone being modeled in the model space. The 2017.1 version PetroMod allows the user to only enter the year of deposition of a lithological unit and the depth of that layer, and the software calculates the thickness. The lithological units have specific petrophysical properties that allow PetroMod to calculate the e.g the heat flow trends, temperatures and thermal conductivities of the model. PetroMod will already calculate the parameters it needs for the model from just the lithologies, ages and depth input. The model changes as more editions are made to the model input including boundary conditions and kinetic data. The rock unit ages are shown relative to depth as would be in a drill-well log (Figure 6.2.1), but maturity modeling requires that it be converted to a burial history plot for maturation modeling (the burial history plot overlain with temperature; Figure 6.2.5).

The difficulty accounted is deciding on the time as well as the amount of deposition and erosion that occurred during unconformities.

As the F_well layers have variations, some composed of two or more lithologies, the ‘mixing’ option in PetroMod was used to create layers that are more similar to the logged F_well geology or at least brings the vitrinite reflectance model closer to the real data. The Lithology Editor in PetroMod enables the editing of lithologies. The default PetroMod lithology properties were used to mix several lithologies together in ratio that must add up to a 100%, to represent a lithological unit for a layer. The ratios of the units making up one lithology had to be changed several times to bring the model vitrinite reflectance closer to that of the calibration data. The lithologies created for F_well data are shown in Appendix A. Data usually used to constrain the model include facies, petroleum system elements, sedimentation rate, vitrinite reflectance, temperatures etc. The F-well model was calibrated with the only available measured well data; the measured vitrinite reflectance and the vitrinite calculated from the Tmax from Rock-Eval pyrolysis data. Model calibration at this stage allows for a controlled stratigraphic model. The calibration data is entered in Well Editor tables. Figure 6.2.1 shows the main inputs for F_well lithologies including the main unconformities and erosional events. The PetroMod software also requires that the kinetic model that will be used to calculate the kinetics for the model be defined in the Main input table.

Age [Ma]	Name top/well pick	Depth [m]	Thickness [m]	Event type	Name layer/event	Paleodeposition/erosion [m]	Lithology	PSE	Kinetic	TOC [%]	HI [mgHC/gTOC]
30.00	L1 Erosion	0	0	↑ Erosion	Erosion in present	-500					
34.00	Oligocene	0	1950	↓ Deposition	L1	500	L1 litho	Overburden Rock			
56.00	Eocene	1950	250	↓ Deposition	L2		Limestone (Waulsortian mound)	Seal Rock			
90.00	Upper Cretaceous	2200	530	↓ Deposition	L3		L2 Litho	Reservoir Rock			
111.00	End of Lower Cret	2730	550	↓ Deposition	L4		Limestone (Waulsortian mound)	Source Rock	Pepper&Corvi(1995)_TII(B)	2.94	356.00
155.00	Erosion of L5	3280	0	↑ Erosion	Erosion of L5	-200					
160.00	Upper Jurassic	3280	1007	↓ Deposition	L5	200	L3 Litho	Source Rock	Pepper&Corvi(1995)_TII(B)	2.94	356.00
201.00	Start of Lower Jurassic	4287	0	- Hiatus	Hiatus before L5						
210.00	Hiatus before L5	4287									

Figure 6.2.1 F-well Main Inputs

The units entered in the main input table are then defined as petroleum system elements as over- and underburden rock, source rock, reservoir rock or seal rock to represent the functions of the units in the basin. The petroleum system chart then depicts the events and process that are entered into the Main input table. The user is allowed to edit this events chart to best represent the petroleum system elements with the events of trap formation, generation/ migration/ accumulation and preservation as well as their timing. The petroleum system history chart shows how the essential elements relate spatially with processes and the preservation

time. The critical moment is chosen by the modeller as the point in time that best represents the generation to migration to accumulation in a trap of most hydrocarbons in a petroleum system (Magoon and Dow, 1994). Figure 6.2.2 shows the F_well petroleum chart.

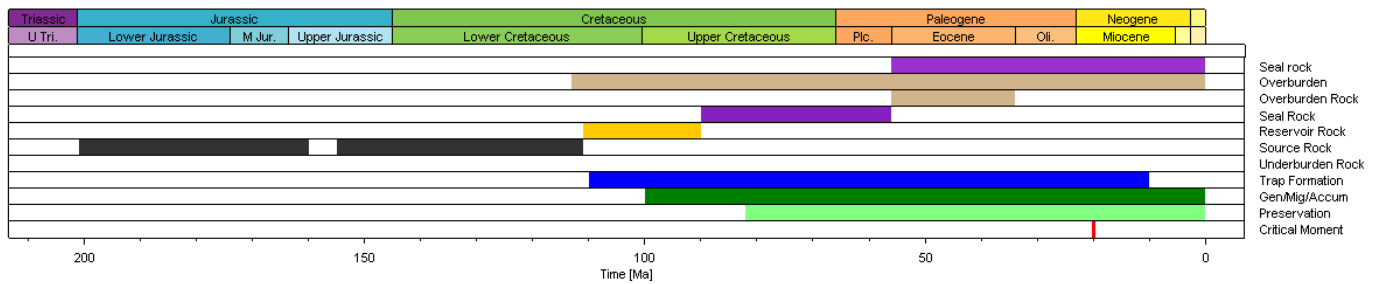


Figure 6.2.2 F_well Petroleum System Elements Chart

Also entered into the Main input table are the kinetics. PetroMod has several options of models available to choose from for modeling the chemical reaction mechanism followed the maturation process of the F_well rocks. Different models assume different conditions for the chemical reactions that result in the different rates of reaction and activation energies. The different kinetic model follow different laws to calculate the activation energies A and E parameters that models the petroleum generation process. The Burnham and Sweeney (1990) is set as the default model in the PetroMod version 2017.1.

After thorough analysis of the pyrolysis data from the tables and figures in the pyrolysis data analysis (Section 6.1), Layer 4 and Layer 5 were designated to be the source rocks of the F_well petroleum system. The highest Total organic carbon (%) value and Hydrogen Index (mg HC/g TOC) in the zone were entered into the Main input table to represent organic matter richness for the layers (Figure 6.2.2).

Boundary conditions

The boundary conditions necessary for burial history modeling are the paleo water depth (PWD) (m), the surface water Interface Temperature (SWIT) (°C) and heat flow (HF) (mW/m²). It is sufficient to set the paleo water depth at 0m (personal communication), and to use the auto SWIT (surface water interface temperatures). After inputting Latitude of 39° and selecting (Southern Europe) for the Mediterranean zone, the simulator provides global mean temperature at sea level (based on Wygrala, 1989). The simulator also generated the surface temperatures shown in Appendix B. The heat flow values and ages are entered manually and the simulator uses the default McKenzie model (elaborated in section 2.3) to calculate the heat trend. As the F_well has no measured heat flow and temperature values, and there is no information on the heat trend in that zone, the heat flow model used by Muthar et al., (2013) to model heat flows in the Ganga Basin of India

was used as guidance to model the heat flow trends of the F_well model, (Figure 6.2.3). The heat flow model generated by software following the Jarvis and McKenzie (1980) model is in Appendix B.

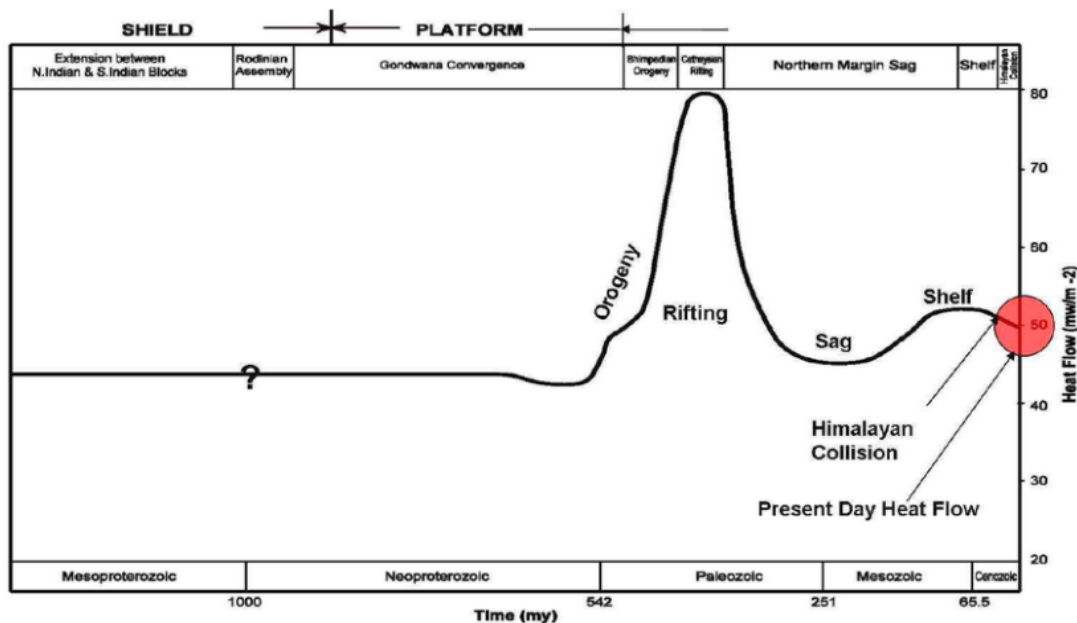


Figure 6.2.3. The rifting event shown in this model does not affect the F_well model of which the layers were deposited starting at the start of the Lower Jurassic. However, the younger events shown here seem to approximate the F_well vitrinite reflectance (Ro %) data.

Guided by the heat flow model shown above and the aforementioned inputs the vitrinite reflectance model of F_well was approximated using the heat flow values shown in Table 6.2.2.

Table 6.2.2 The values approximating the prevailing heat flow trend over time.

Age	Lithotype	Layer	Depth (m)	Heat flow mW/m ²
0	Marly SS with Siltstone	L1	0	60
34	Marly SS with Siltstone	L1	1950	50
56	Limestone (Waulsortian mound)	L2	2200	40
90	Conglomerat	L3	2730	40

	e			
111	Limestone (Waulsortian mound)	L4	3280	40
160	Dolomite and Shale	L5	4287	25
201	Dolomite and Shale	L5	4287	15

The heat flow range between 15 mW/m² at the start of the Jurassic to 60mW/m² in the present day, results in closer approximations of vitrinite values to the calibration data. Lower heat values in the ranges 30-50mW/m² and 50-70mW/m² would be expected in intra-cratonic and foreland basins respectively (Magoon and Dow, 1994). There is a slight temperature increase resulting from this heat spread into the bottom layers. Approximating the temperature ranges in the F_well petroleum system requires a good combination of heat flows in time and lithology conductivities. It was observed that the combination of the heat flows in Table 6.2.2 and conductivities specific to unique lithologies resulted in significant temperature spreads in Layer 5, getting lower in Layer 4 with much lower temperatures at shallower depths. The resulting vitrinite reflectance model and the burial history plot overlain with temperature variations in the system are shown at the end of the result section

Choice of kinetics Model

Petromod has several models available to choose from to model the kinetics pertaining to the thermal maturation process for various reactions. The reactions modeled include bulk, compositional, compositional and phase separation, biogenic and kerogen oil and gas. The kerogen oil and gas is applied in this case study. As there are 34 kerogen-oil and gas kinetic models available to choose from, three in Table 6.2.3 were chosen to show the variations in results depending on the chosen model.

The hydrocarbon calculations will be different depending on the chosen model as shown in Table 18. The table shows that there are great differences between the different kinetic models. The Tissot and Waples (1992) TII_Crack produces significantly lower barrels of hydrocarbons compared to the Pepper and Corvi (1995) TIIB model that produces the largest volumes and the Burnham (1989) TII_Crack model. The kinetics models the HC zones and generation potentials differently but the evolution of the vitrinite reflectance in time is modeled by the same equations of the Easy %Ro by Burnham and Sweeney (1990) and so produces it produces the same results for all the models. The Easy %Ro is a default model in the PetroMod 2017.1

version. The hydrocarbons zones and hydrocarbon generation potential are overlays available in the simulator to graphically show the changes in hydrocarbon processes using Pepper & Corvi (1995) TII (B) model.

Table 6.2.3 shows the resulting differences that can be incurred when from a particular choice of models. These are representative of the gas volumes in billion cubic feet. The models compared for the F_well (.) petroleum system are Pepper and Corvit (1995), the Tissot and Waples (1992) and Burnham (1989) for modeling. All models show the accumulated volumes in the reservoir to be 0 billion cubic feet.

Kinetics Model	Remaining potential	Generation balance	Accumulated in source	Expulsion balance	Migration balance
Pepper & Corvi (1995)	192.26	22.06	21.78	0.27	-0.27
Tissot & Waples (1992)	0.80	0.65	0.04	0.62	-0.60
Burnham (1989)	96.60	136.45	5.58	130.86	-130.86

The Tissot and Waples (1992) method is a development of the original Lopatin (1971) method of the Time Temperature Index (TTI) popularized by Waples (1980). This method assumed that the reaction rate would be doubling for every 10 °C rise in temperature. (Tissot and Welte, 1984) found this estimation to give wrong results when extended over the whole range of temperatures in a sedimentary basin. Waples et al, (1992) advised the use of new kinetic models such as the EASY % Ro rather than the TTI. Littke et al., (1994) modeled their vitrinite reflectance data using both the TTI and the Easy % Ro method. The result was that the TTI method required significantly less heat (20mW/m² less) but with less sediments lost to erosion in order to estimate the same Ro% values.

The Easy %Ro by Burnham and Sweeney (1990) is set as a default %Ro calculator and is not available in the drop down list of kinetic models in the Main input table. The Pepper & Corvi (1995) TII (B) model was chosen to model the kinetics in the F_well (.) petroleum study. The kinetic model is a global kinetic model that designates parameters depending on the gross depositional environment and stratigraphic age. This kinetic model designation is useful in localities of low geochemical knowledge (Pepper and Corvi, (1995)) and so it is relevant to this case study. The model incorporates descriptions of generation, oil-gas cracking and expulsion thus providing a complete description of petroleum formation. The Pepper and Corvi, (1995) TII (B) model also gives has the advantage of being equipped to account for any small proportion of gas-generative kerogen present (Pepper and Corvi, (1995)).

Erosion Events and unconformities

The F_well geological log indicates an unconformity at the base of the lithologies penetrated at the start of the Lower Jurassic, where drilling ceased. The regional geology publications of the part of the Mediterranean also mention a prominent unconformity that underlies an important extensive limestone layer in that zone. The unconformity was included in the F_well model to realize its effects on the temperature regime. “Vitrinite reflectance profiles typically show abrupt increase in reflectivity at unconformities”, (Barker, 1996). Observation of the temperature overlay on the burial history plot as well as the vitrinite reflectance model curve indicates that the ‘start of the Upper Jurassic’ hiatus is important to the thermal evolution to the stratigraphy around the F_well. Conversely the resulting %Ro curve slightly reduces towards the real data points when this hiatus is included. It was observed that including the 155Ma erosion event in Layer 5 also results in reducing Ro% data curve to better fit the real data. Thus the model behaves better with a hiatus and an Upper Jurassic erosion event. The measured vitrinite reflectance model is better approximated with the inclusion of the 30Ma erosion event in Layer 1 where 500m was lost, while the Tmax derived model behaves slightly better without this event. These events result in temperature effects that affect the hydrocarbons generation, accumulation and expulsion (see Table 6.2.4).

Table 6.2.4 The resulting effects of erosion events presence or absence on changes to thermal maturity results.

Erosion event scenario	Gas from the source rock layers; L4 and L5 (Million barrels)			
	Remaining potential	Generation balance	Accumulated in source	Expulsion balance
With all events	192.26	22.06	21.78	0.27
No 210Ma hiatus	192.26	22.06	21.78	0.27
No 155Ma erosion	192.52	22.09	21.82	0.27
No 30Ma erosion event	193.39	20.93	20.67	0.26

The scenario without the 500m of Layer 1 lost to erosion shows more remaining potential in the F_well source rocks; L4 and L5, although there is higher generation balance in the other two scenarios. An explanation for the differences in Table 6.2.4 can be that the non-eroded scenarios have more thickness thus more material with potentially more organic matter to convert to hydrocarbons. The hiatus event does not affect the hydrocarbon volumes.

Salt Effects

Salt piercing was introduced into the model to mimic some salt tectonics that have been mentioned to occur in the regional geology of the Mediterranean area (Barker, 1996; Riding, 1999). Evaporitic rocks influence the mechanisms of sourcing petroleum, controlling migration pathways, creating traps and sealing reservoirs as well as affect sedimentation and sediment accumulation (Lerche and Peterson, 1995 in Barker, 1996).

Salt layers were included in the model as they also reduce the temperature effects and so it lowers the model vitrinite reflectance values towards the measured vitrinite reflectance values. PetroMod 1D has a tools section that allows such intrusions to be input into the model. The software requires that the layer in which the salt piercing occurs be defined as well as the timing of the salt intrusion event.

Table 6.2.5 Salt piercing for the F_well Petroleum system simulated to have occurred the Miocene.

Layer	Time (Ma)	Lithology
Layer 1	10.00	Salt
Layer 2	20.00	Salt

The model was better approximated when the two salt piercing events were defined, one in Layer 2 at 20Ma and the later one at 10Ma in Layer1 (Table 6.2.5). The %Ro model reduces to better fit the vitrinite reflectance data.

Model results

The above scenarios were the best approximates to fitting both the measured and calculated and Tmax derived vitrinite reflectance validation data. Figure 6.2.4 (a) and (b) shows the resulting Ro % versus depth fitting for the two cases.

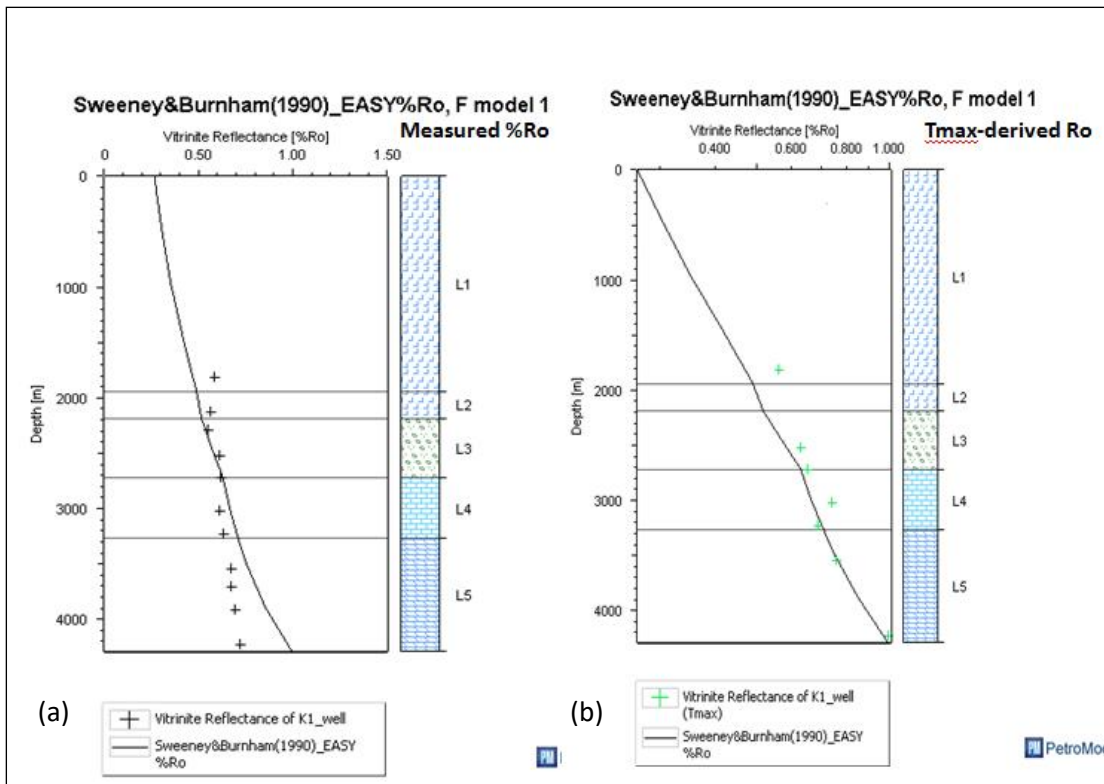


Figure 6.2.4 (a) and (b) showing the resulting %Ro models when validation data was the measured vitrinite reflectance and the Tmax - derived vitrinite reflectance data, respectively.

The ‘measured’ %Ro data curve estimates higher Ro values which is obviously an overestimation of F_well petroleum system maturation. Lithologies were edited as much as possible to result in lower, better fitting thermal conductivities to the validation data. The heat flow trends estimations to approximate the temperatures that contributed to the thermal maturation of the F_well (.) petroleum system were altered to be as low as possible. These parameters could not be changed any further to better fit the measured Ro data model in (a). Conversely, the lower part of the model curve in Figure 6.2.4(a) perfectly fits the three base data points in (b). The measured %Ro model will thus not be given further consideration. Henceforth, only the Tmax - derived Ro results will be shown.

Alternative scenario for the Tmax %Ro derived data; the thrust model

The scenario of the thrusting model was done on the Tmax-derived Ro model to see if the real data could better be approximated. Thrusting shifts vitrinite reflectance data from deeper layers to shallower depths as the more organic zones are pushed towards the surface (Barker, 1996). Such a scenario might fit the Tmax-derived data occurring in Layers 4, 3 and 1 better (see Figure 6.2.4).

One reason for the need to include a thrust model was try and mimic the possible geological history that could be represented by the higher Tmax-derived Ro data points. The other reason is that it was significant to model thrusting for this case stratigraphy to attempt to induce a trapping mechanism in the F_well (.) petroleum system. The hope was to possibly impede hydrocarbon migration somewhere laterally along the reservoir, while inducing some fracturing that might ease or encourage migration from source rock to trap so there could possibly be some accumulated hydrocarbons in the reservoir. This attempt was made even though the chance of an encouraging result was minimal as indicated by the hydrocarbon generating potential calculation in Section 6.1.

There is insufficient knowledge on the regional geology of the area to infer with better confidence any known traps in the area. The source rocks are in layer 5 and Layer 4. Layer 5 is bounded by a hiatus. Some erosional unconformities have been known to form part of traps (Biddle and Wielchowsky in Magoon and Dow, 1994). For this case we suppose that the start of Upper Jurassic hiatus impedes migration of hydrocarbons formed in the source rocks. Then the only available options are upwards towards the Layer 3 reservoir or laterally unless there are faults draining the hydrocarbons elsewhere. The conglomerate in Layer 3 was found to consist of some quartz. Overlying this layer is a limestone layer and so one could infer possible cementation within some of these layers. If this was to be the case in Layer 2 limestones, then a seal resulting from cementation could be a possibility for a potential trap mechanism. However, the geology log has no mention of such. Furthermore, as carbonate rocks are sometimes subjected to dissolution resulting in large voids, then this Layer 2 could not be a good seal anyhow. There is also no mention of dissolution in the geology log. A thrusting scenario is considered as a more plausible alternative to ensure an efficient trap possibility. Although, there is still a chance that the rocks blocking the lateral extent and the possible lateral migration of hydrocarbons out of the reservoir have high permeability resulting in no trapping mechanism.

Sweeney&Burnham(1990)_EASY%Ro, thrust_model better

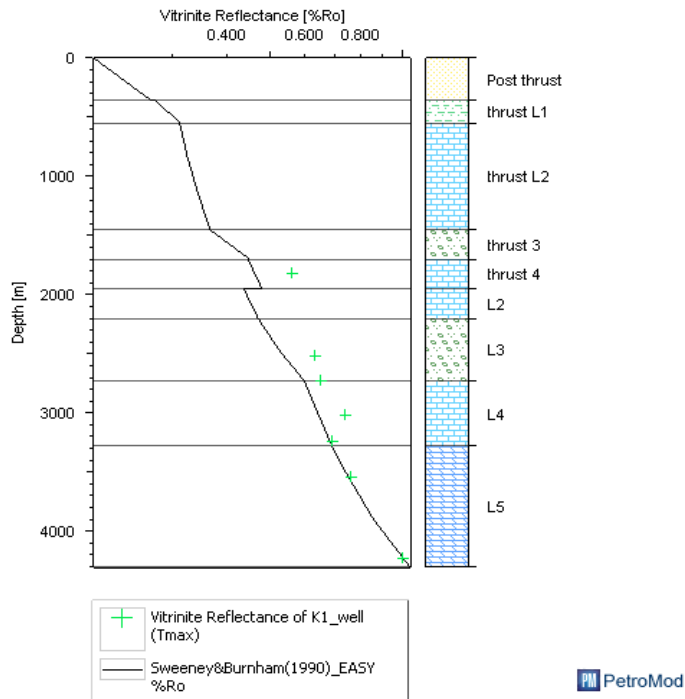


Figure 6.2.5 %Ro model resulting from thrust simulation.

Comparing no-thrust scenario to the thrust scenario

The no-thrust model fits Layer 3 data better, while the three points in Layer 5 and at the base of Layer 4 fit the same way in both cases. One could think to thrust some of Layer 5 material onto a part of Layer 4 to better fit the thrust model data but that would disagree with the logged geology as would be the result of introducing igneous intrusions. The burial history plot showing the temperature variations in time for the two scenarios are shown in Figure 6.2.6. The thrusting mechanism shifts the layers more towards to earlier in the Miocene.

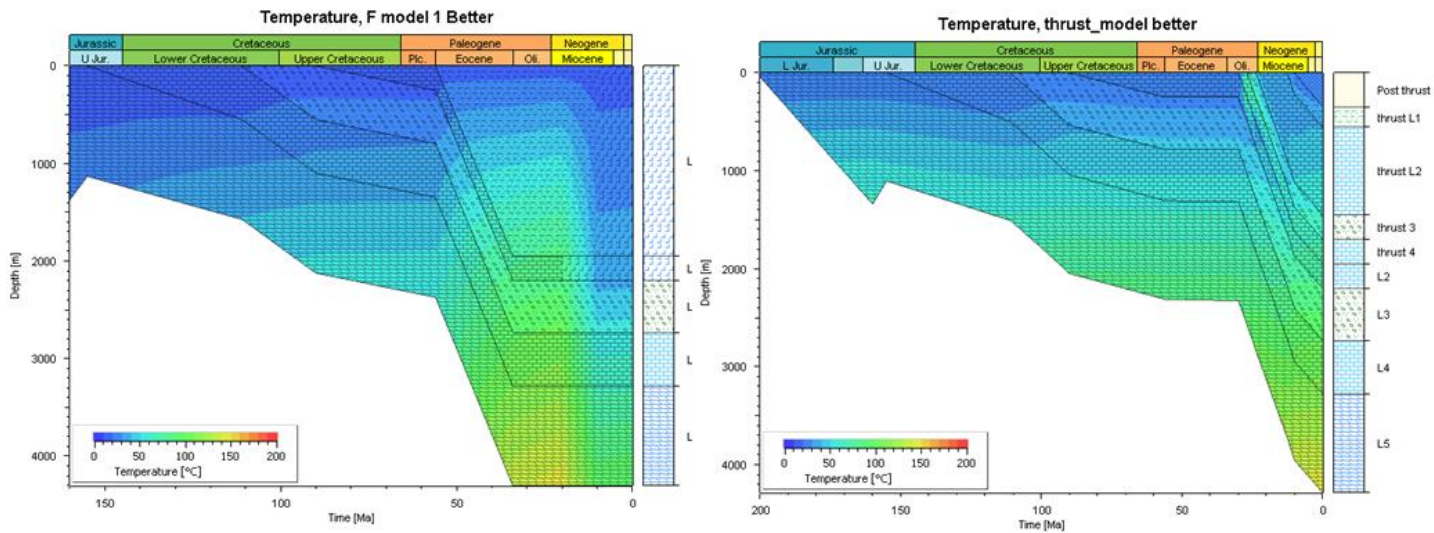


Figure 6.2.6 Temperature in time of the no thrust and thrust model overlain on a burial history plot.

The transformation results from the two scenarios

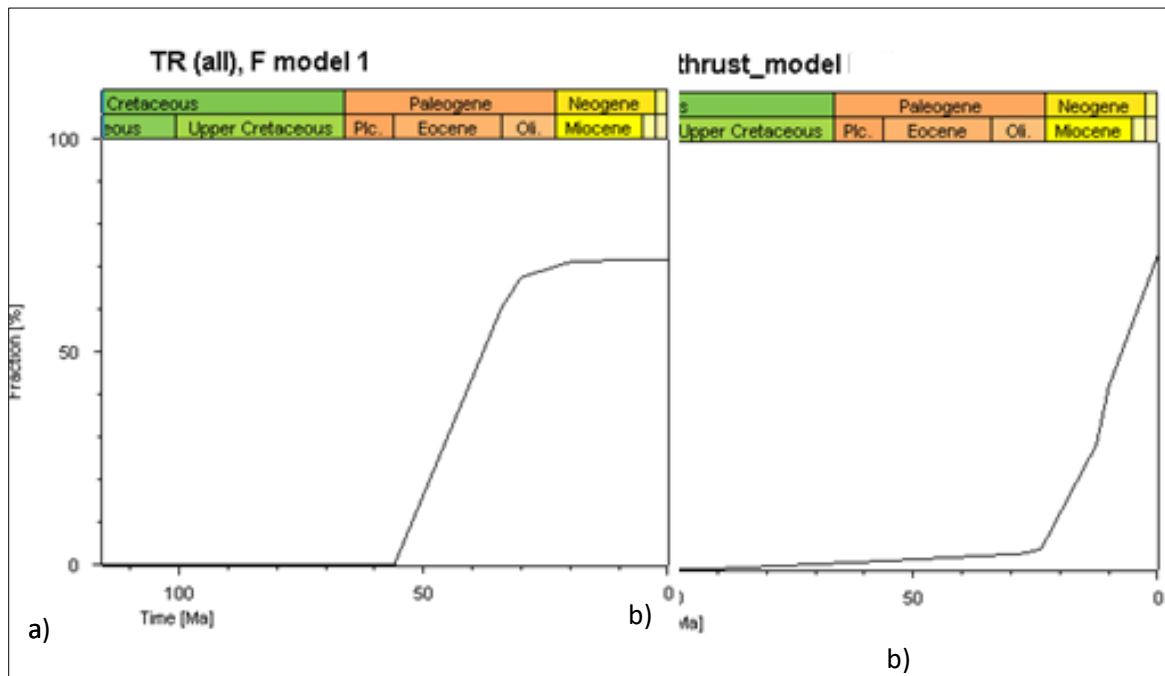


Figure 6.2.7 Transformation fraction in Layer 5 for the two scenarios; a) no thrust scenario and b) thrust scenario

Transformation ratio indicates the fraction of convertible kerogen at a given time and temperature (Tissot and welte, 1984). Pressure will have a lesser controlling effect but will influence the temperature for thresholds and the hydrocarbon volumes history. Figure 6.2.7 shows that the transformation of Layer 5 source rocks

commenced later but at a higher rate than that of the thrust model Layer 5. Thrusting shifts the higher temperatures closer to present day which results in higher transformation at present day.

The resulting hydrocarbon volumes from the two scenarios are shown in Table 6.2.6 and represented graphically in Figure 6.2.8 for the no-thrust model and 6.2.9 for the thrust model.

Table 6.2.6 (a) Lists the oil balances for the two scenarios, the no-thrust and thrust model cumulative to present day (million barrels of oil)

	Remaining potential	Generation balance	Accumulated in source	Expulsion balance	Migration balance
No thrust Tmax derived Ro model	80.16	134.09	85.23	48.86	-48.86
Thrusted Tmax derived Ro model	138.94	99.01	69.25	29.76	-29.76

Table 6.2.6 (b) Lists the gas balances for the two scenarios, no thrust and thrust model Cumulative to present day (billion cubic feet of gas)

	Remaining potential	Generation balance	Accumulated in source	Expulsion balance	Migration balance
No thrust Tmax derived Ro model	191.81	21.30	21.30	0	-0
Thrusted Tmax derived Ro model	264.06	24.73	23.34	1.39	-0.25

The hydrocarbon volumes are significantly higher in the thrust model. However, this scenario still results in no hydrocarbons accumulated in the reservoir. Ultimately this indication from the model of no hydrocarbons in both scenario results are corroborated by the earlier workers findings of no shows and no hydrocarbons found in the drilled well. It makes sense that there would be more hydrocarbons generated and accumulated after thrusting the already hydrocarbon generating Layer 4 at shallower, less productive zones. The graphics showing the HC zones for these cases are shown in Appendix C.

The no-thrust oil volumes (million barrels)

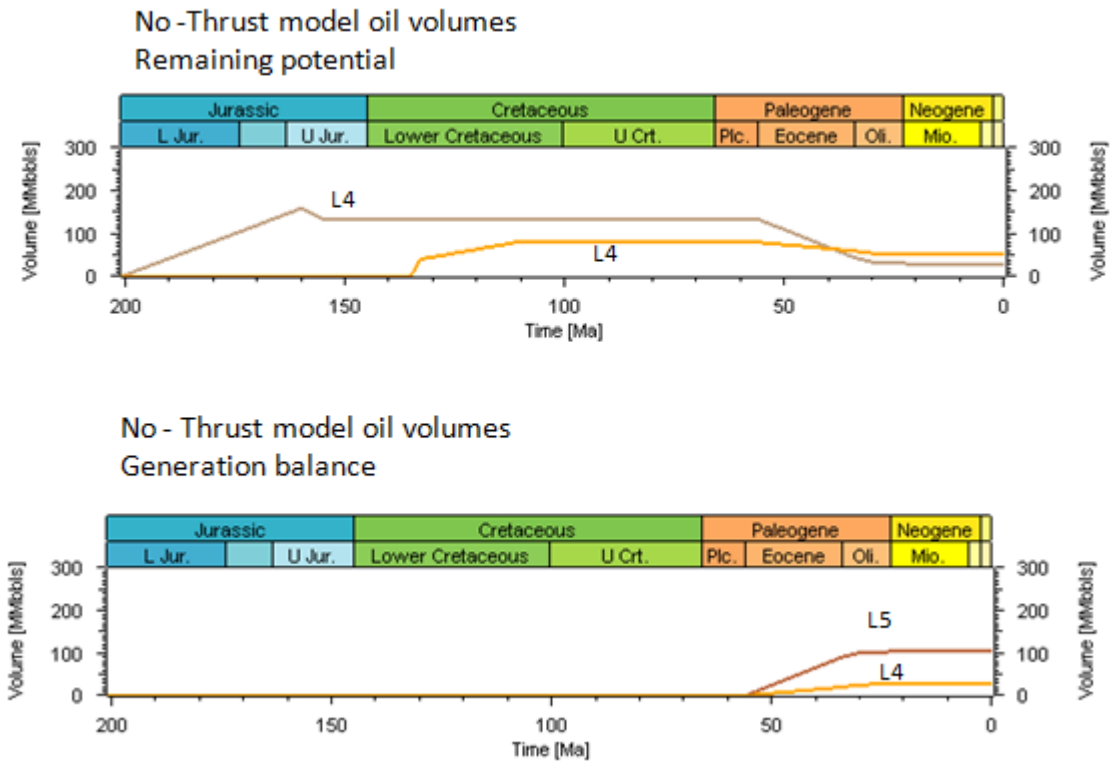


Figure 6.2.8 Generation balance and volumes accumulated in source for Tmax-derived vitrinite model. Layer 5 contributes most of the volumes.

The Thrust model oil volumes (million barrels)

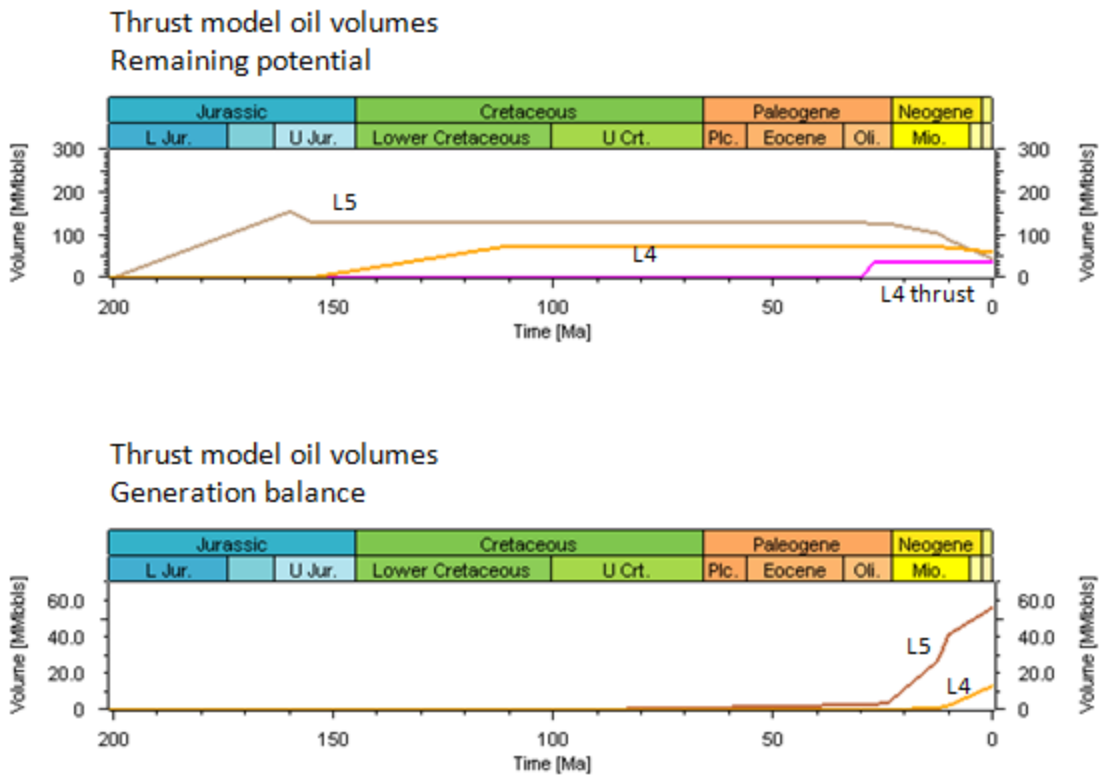


Figure 6.2.9 Thrust model volumes. Layer 5 contributes the most to the generated and accumulated hydrocarbons.

Figures 6.2.8 and Figure 6.2.9 show that the Layer 5 source rock contributes the most to the hydrocarbons as most of the heat is accumulated in Layer 5, acting on the available kerogen in that layer.

Modelling of the F_well petroleum system was possible after taking into account the geological constraints such as the lithologies, erosion effects and salt tectonics, and setting boundary conditions that closely as possible approximates those inferred for the zone where the F_well was drilled. Due to lack of data the main constrain on the modelling was the geology log and the geochemical data while the validation data was the vitrinite reflectance data. Vitrinite reflectance provides the most reliable kinetic data. The measurements are expected to have a range of uncertainties stemming from measurements from different sources induced by factors other than temperature and time during burial, (Makhous and Galushkin, 2005). The geological log should be supported by well-known regional geology information. Having as much real data as possible will reduce uncertainties in modelling. There are already uncertainties stemming from the subjectivity surrounding thermal modelling as it depends on the individual performing the modelling and their interpretation of geologic data as well as on the basin modelling program they use. Additional discrepancies can result from heat flow equations, thermal parameters, boundary conditions and as well as calibrations to well data. Ultimately the results presented above represents the best approximation to the F_well petroleum accumulations based on a single well data.

Conclusion

Geochemical analysis results indicate Layer 4 and Layer 5 rocks as potential source rock material. The TOC (%) range of the source rocks, Layer 4 and Layer 5, is wide from 0.19-3.83 with an average of 1.35% indicating poor to fair source rocks. However, the geochemical analysis places some parts of these source rocks in the mature oil window zone with high to very high productivity index. Layer 4 samples indicated the presence of both Type II and Type II/III kerogens. Half of Layer 5 samples indicate Type II kerogen while the other half indicates Type III kerogen. Early maturity was indicated for Layer 4 rocks while Peak maturity was indicated for the Layer 5 source rock.

The work to model a hypothetical petroleum system with the aim to scrutinize the hydrocarbon potential of the F_well (.) source rocks indicates the presence of hydrocarbon generative kerogen type II and Type III source rocks as was determined from analysis of Rock_Eval pyrolysis data. The resulting model after simulating in PetroMod 1D software indicates that the thrust model has more generative potential than the no-thrust scenario. Both scenarios required almost the same geological constraints except the need for thrusting to repeat some of the higher %Ro values in shallower layers. This was not overly pursued as the vitrinite model fits perfectly to the source data in the source layers. The limited geological knowledge of the petroleum system to constrain the geology limits the accuracy of the model. Rock - Eval pyrolysis and vitrinite reflectance data were used to control the thermal history modeling. However, the small data set was made even smaller when outliers were removed from %Ro data to produce a better fit. The combined effects of the burial history and thermal history conditions applied to simulate the petroleum generation potential of the sediments surrounding F-well show that the generation balance of the no-thrust scenario is higher than the thrust scenario at 134.09 million barrels while the thrust model produces 99.01 million barrels. However, the remaining potential balance of the no thrust is lower at 80.16 million barrels compared to 138.94 million barrels. Both the no thrust model and the thrust model produced a zero balance for hydrocarbons accumulated in the reservoir. These results are corroborated by the earlier workers findings of no shows and no hydrocarbons found in the drilled well. Waples (1980) warned against modeling without a clear conceptual model of geologic history from the start of maturity modeling, indicating that this could likely show weaknesses when closely investigated. He however added that errors and incorrect assumptions could be expected despite the amount of attention given to construction of the initial geologic model. Any errors and incorrect assumptions incorporated in this model will be unknown until the thermal history of this area is modeled with adequate data to constrain the model.

Recommendation

Further modeling could be carried out with 2D and or 3D modeling with increased geological knowledge, a lot more model validation that could include bottom-hole temperatures, regional geothermal gradients, measured heat flow values etc. The 2D and 3D models incorporate the use of seismic sections and maps among others; that if used with the above listed controls would significantly increase the confidence in the modeled results.

Acknowledgements

I would like to thank Schlumberger for awarding us the PetroMod version 2017 licence to be able to carry out this project. I would like to thank my professor for his patience and trust in me. My thanks also go to Vasilliki for her advice. No words can ever express my gratitude to my parents and partner for all their support and patience while I had to work in the course and all through the project time. Last by not least I am thankful to the friends I made during this course.

Appendices

Appendix A

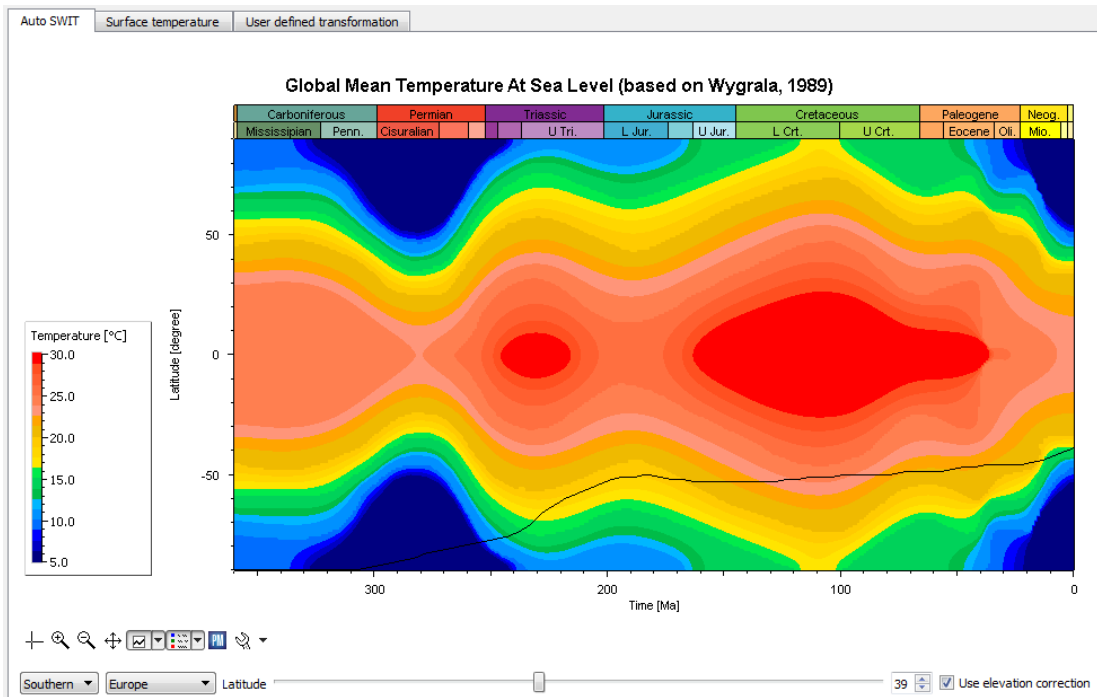
The Lithologies created for Layer 1, Layer 2 and Layer 3 in the PetroMod lithology editor.

	Lithology	Percent	
1	Sandstone (typical)	25.00	
2	Sandstone (clay rich)	15.00	
3	Siltstone (organic rich, 2-3% TOC)	45.00	
4	Marl	15.00	
5			

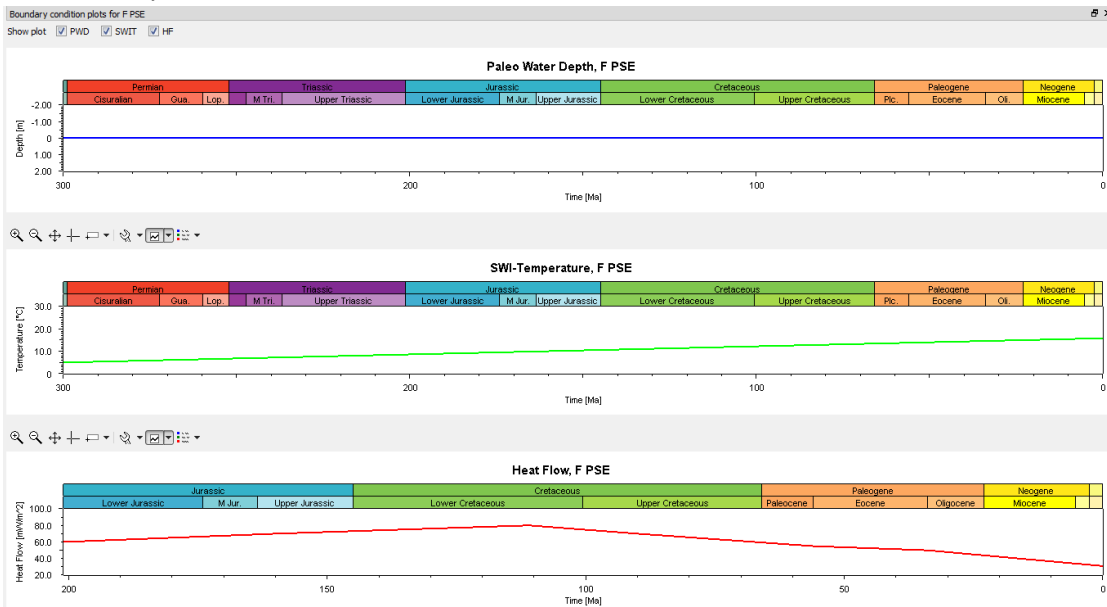
	Lithology	Percent	
1	Conglomerate (typical)	85.00	
2	Quartz	15.00	
3			
4			
5			

	Lithology	Percent	
1	Dolomite (organic lean, sandy)	65.00	
2	Shale (organic rich, 8% TOC)	35.00	
3			
4			
5			

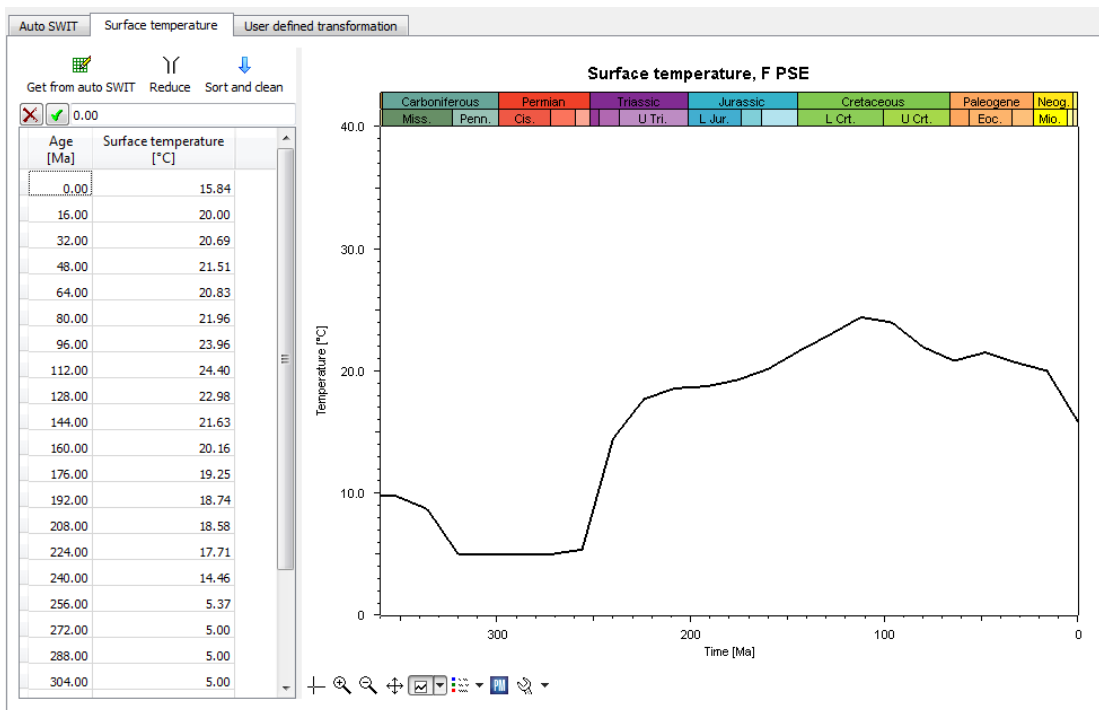
Appendix B



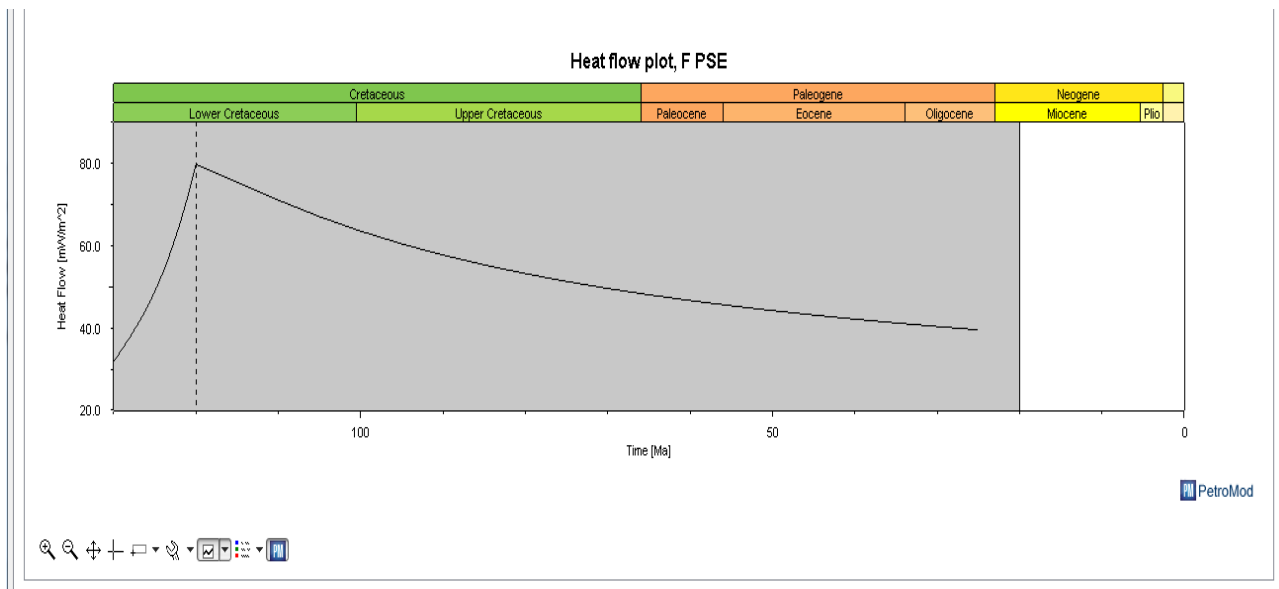
a) Global mean temperature at Sea level trend used for the F_{well} (.) petroleum system



b) Boundary conditions



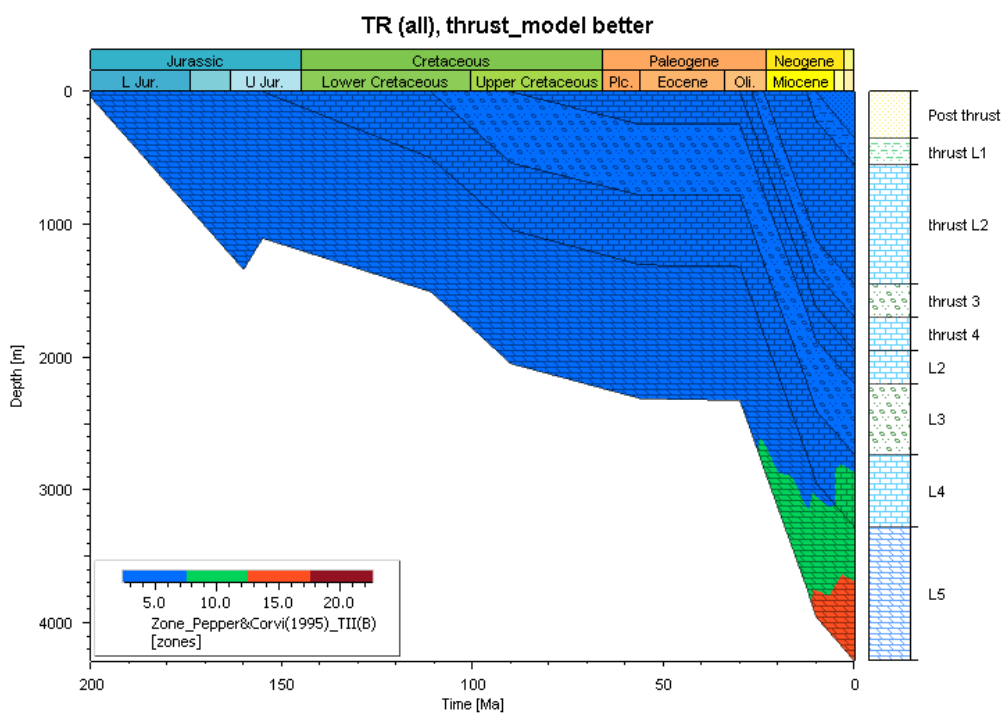
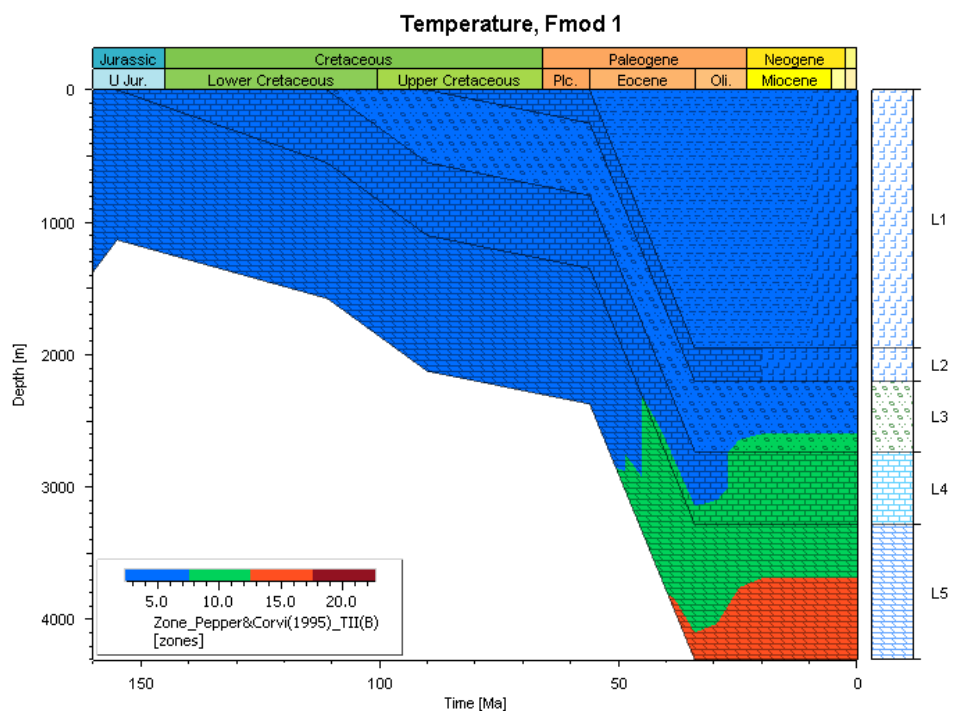
c) The surface flow trend calculated by the McKenzie Model.



d) Heat Flow trend

Appendix C

Hydrocarbon zones results of the three scenarios for the no thrust scenario (a) and the thrust scenario (b)



References

- Al-Hajeri, M. M., & Al Saeed, M. (2009). Basin and Petroleum System modelling. *Oilfield Review Summer 2009*: 21, no. 2. Copyright © 2009 Schlumberger. [online]
https://www.slb.com/~media/Files/resources/oilfield_review/ors09/sum09/basin_petroleum.ashx.
- Barker Collin. (1996). *Thermal modelling of Petroleum Generation: Theory and Applications*. Tulsa, OK, USA: Elsevier Ltd.
- Barker, C. E., (1989). Temperature and time in the thermal maturation of sedimentary organic matter: p. 75-98 in, "Thermal History of Sedimentary Basins - Methods and Case Histories," (Edited by N. D. Naeser and T. H. McCulloh), Springer-Verlag, New York.
- Bordenove, M.L., Espitalie, J., Leplat, P., Oudin, J.L., Vandenbrouke, M., (1993). Screening techniques for source rock evaluation. in: Bardenove (ed.), *Appl. Petrol. Geochem*, ParisEds. Technip. pp. 217–278.
- Connan, J., (1974). Time-temperature relation in oil genesis: *Am. Assoc. Petrol. Geol. Bull.*, v. 58, p. 2516-2521
- Higley, K.D., Lewan, M., Roberts, N. R. L., & Henry, E. M., (2006). *Petroleum System Modeling Capabilities for Use in Oil and Gas Resource Assessments: U.S. Geological Survey Open-File Report 2006-1024*
- Dembicki, J. H. (2016). *Practical petroleum geochemistry for exploration and production*. Elsevier Ltd.
- Dueppenbecker, S. J. (1991). Rocks-insights from geology , geochemistry and computerized numerical modelling. rocks-insights f r o m geology , geochemistry and computerized numerical modelling.
- Falvey, D.A., Middleton, M.F., 1981. Passive continental margins: evidence for a prebreakup deep crustal metamorphic subsidence mechanism. In: *Oceanologica Acta, Proceedings of 26th IUGG SP*, pp. 103–114.
- Hantschel, T., & Kauerauf, A. I. (2009). *Fundamentals of Basin and Patroleum systems modeling*. Springer.
<https://doi.org/10.1007/978-3-540-72318-9>
- Hunt M. J, Paul, P. P., & Kvenvolden A. K. (2002). Early development in Petroleum geochemistry. *Early Development in Petroleum Geochemistry*, 33, 1025–1052.
- Hunt, J.M., (1996). *Petroleum Geochemistry and Geology*, second ed., W.H. Freeman and Company.
- Huvaz, O., & Thomsen, O. R. (2005). A Simplistic Inversion Method for Sensitivity and Uncertainty Analysis in Basin Modeling: The Resolution Limits of Easy Ro,
http://webapp1.dlib.indiana.edu/virtual_disk_library/index.cgi/2870166/FID3366/PDF/482.PDF.
- Lerche, I., and Petersen, K. (1995). *Salt and Sediment Dynamics*, CRC Press, Boca Raton.
- Longford , F.F., Blanc-Valleron, (1990). Interpreting Rock–Evalpyrolysis data using graphs of pyrolyzable hydrocarbons vs.total organic carbon, *AAPG Bull.* 74 799–804.

- Magoon, L. B., & Dow, W. G. (1994). *The Petroleum System - From Source to Trap*. (L. B. Magoon & W. G. Dow, Eds.), *The Petroleum System - From Source to Trap*. Tulsa, Oklahoma: The American Association of Petroleum Geologists. <https://doi.org/10.1306/M60585>
- Nemcok, M., Schamel, S., & Gayer, R., (2009). *Thrustbelts: Structural Architecture, Thermal Regimes and Petroleum Systems*. Googlebooks.
- Nielsen, S.B, Clausen, O. R, McGregor, E., (2015). Basin% R_o : A vitrinite reflectance model derived from basin and laboratory data. *Basin Research*, Volume 29, Issue S1 February 2017 Pages 515–536in. DOI: 10.1111/bre.12160.<http://onlinelibrary.wiley.com/doi/10.1111/bre.12160/full>
- North, F. K. (1985). *Petroleum geology*: Boston, Allen and Unwin, 553 p.
- Parsons, B., & Sclater, J. G. (1977). An analysis of the variation of ocean floor bathymetry and heat flow with age. vol. 82, no. 5. https://www.depts.ttu.edu/gesc/Fac_pages/Yoshinobu/5362-Tectonics-Web/pdfs%202012%20Tectonics/parsons-sclater77.pdf
- Pepper, S. A., & Corvi, J. P. (1995). Simple kinetic models of petroleum formation. Part I: oil and gas generation from kerogen. *Marine and Petroleum Geology*, Vol. 12, No. 3, pp. 291-319, 1995 Copyright © 1995 Elsevier Science Ltd.
- Peters, K.E. (1986). Guidelines for evaluating petroleum source using programmed pyrolysis, *AAPG Bull.* 70 318–329.
- Schmoker, J.W. (1994). Volumetric calculation of hydrocarbons generated. In: Magoon, L.B., Dow, W.G. (Eds.). *The Petroleum System – from Source to Trap*, 60. American Association of Petroleum Geologists Memoir, pp. 323–326
- Sclater, J.G., Christie, P.A.F. (1980). Continental stretching: an explanation of post Mid-Cretaceous subsidence of the Central North Sea. *Journal of Geophysical Research* 85, 3711–3739.
- Sheplev, V. S. & Reverdatto, V. V. (1998). A Contribution to the Further Investigation of McKenzie's Rifting Model. *Geophysica*, 34(1-2), 63-76. http://www.geophysica.fi/pdf/geophysica_1998_34_1-2_063_sheplev.pdf
- Sluijk, D., Parker, J.R., (1988). Comparison of predrilling predictions with post drilling outcomes, using Shell's prospectappraisal system. In: Association of Petroleum Geologists Studies in Geology. Oil and Gas Assessment, vol. 21.
- Sweeney, J. J. & Burnham, K.A. (1990). Evaluation of a simple model of vitrinite reflectance based on Chemical kinetics. *The American Association of Petroleum Geologists Bulletin*, V.74, No. 10. P.1559-1570<https://www.researchgate.net/publication/255005110>
- Tissot, B.P., Espitalie, J. (1975). L'évolution thermique de la matière organique des sédiments: applications d'une simulation mathématique. *Revue de l'Institut Français du Pétrole* 30, 743–777.
- Ungerer, P., Burrus, J., Doligez, B., Chenet, P.Y., and Bessis, F. (1990). Basin evaluation by integrated two-dimensional modelling of heat transfer, fluid flow, hydrocarbon generation and migration. *American Association of Petroleum Geologists Bulletin* 74, 309–335

Ungerer, P., Pelet, R. (1987). Extrapolation of oil and gas formation kinetics from laboratory experiments to sedimentary basins. *Nature* 327, 52–5

Ungerer, P., Behar, F., & Discamps, D. (1983). Tentative calculation of overall volume of organic matter: implications for primary migration: p. 129-135 in "Advances in Organic Geochemistry 1981" (Edited by M. Bjoroy et al), Wiley, Chichester.

Van Krevelen, D.W. (1985). *Coal: Typology–Chemistry–Physics Constitution*, Elsevier Science, Amsterdam, 1961.
J. Espitalie, G. Deroo, F. Marquis, *Rock–Eval pyrolysis and its application*, *Inst. Fr. Petrol.* 72

Waples, D.W. (1980). Time and temperature in petroleum formation: application of Lopatin's method to petroleum exploration. *American Association of Petroleum Geologists Bulletin* 64 (6), 916–926.

Waples, D.W. (1992). Recent developments in petroleum Geochemistry. *Geol. Soc. Malaysia, Bulletin* 28, November 1991; pp. 107 - 122.

Wilkinson, D., & Willemsen, J.F. (1983). Invasion percolation: a new form of percolation theory. *Journal of Physics A: Mathematical and General* 16, 3365–3376

Wood, A. D. (1988). Relationships Between Thermal Maturity Indices Calculated Using Arrhenius Equation and Lopatin Method: Implications for Petroleum Exploration. <https://www.researchgate.net/publication/>

Yu. I. Galushkin, M. Makhous. (2005). Contribution of erosion and intrusive-hydrothermal activity to the depth profile of organic matter maturation in sedimentary basins, Volume 44, [Issue 12](#), pp 1225–1236

Yu, Z., R. O. Thomsen, I. Lerche. (1974). Crystalline basement focusing of heat versus fluid flow/compaction effects: a case study of the I-1 well in the Danish North Sea: *Petroleum Geoscience*, v. 1, no. 1, p. 31-35.